In Vitro Study of Two Virulence Factors of Listeria monocytogenes: Cytolysin LLO and Metalloenzyme PC-PLC

Author: Qiongying Huang

Boston College

The Graduate School of Arts and Sciences

Department of Chemistry

IN VITRO STUDY OF TWO VIRULENCE FACTORS OF LISTERIA MONOCYTOGENES: CYTOLYSIN LLO AND METALLOENZYME PC-PLC

a Dissertation

by

QIONGYING HUANG

submitted in partial fulfillment of the requirements

for the degree of

Doctor of Philosophy

May 2014

Abstract

The research reported in this thesis focused on three proteinaceous virulence factors of the intracellular bacterial pathogen *Listeria monocytogenes*: listeriolysin O (LLO), broad-range phospholipase C (PC-PLC), and phosphatidylinositol-specific phospholipase C (PI-PLC). Based on sequence homology of LLO with other cholesterol-dependent cytolysins (CDC), the protein has four domains of which domain 4 is thought to anchor the protein to cholesterol-containing surfaces while domain 3 mediates protein-protein binding on the membrane and contributes α-helices that convert to two β-strands that form the large β-barrel pore. It was previously assumed that the sequential and cooperative behaviors of domain 3 in each LLO monomer required D4 to bind to cholesterol-enriched membranes. By cloning and expressing a separate protein containing domains 1, 2, and 3 (D123) and the isolated domain 4 (D4) of LLO, I could uncouple some of the events in its membrane binding and pore-formation. Flow cytometry, used to investigate protein binding to vesicles and to red blood cells, showed that D123 had no membrane affinity on its own, but became membrane-bound when sub-lytic amounts of LLO were added. D123, not membrane-lytic by itself, became hemolytic when trace amounts of LLO were present to provide a membrane anchor for D123 proteins. FRET and fluorescence correlation spectroscopy were used to show that D123 and LLO formed oligomers at nanomolar concentration and could also associate with one another in the solution. These results suggest that D4 provides an initial membrane attachment but need not be present on all monomers to trigger the cooperative conformational change that leads to membrane insertion and pore formation.

The gene for *L. monocytogenes* PC-PLC was obtained, expressed in *E. coli* and the product protein purified and characterized. The zinc content of this metalloenzyme was analyzed with ICP-MS. The dissociation constants of the three zinc ions proposed as necessary for PC-PLC activity ranged from 0.05 to 60 μM. Enzymatic activities of PC-PLC were analyzed for various substrates, include long-chain phospholipid in vesicles (LUVs, SUVs) and micelles (Triton X-100), and short-chain lipids (diC_4PC, diC_6PC, diC_7PC) mono-dispersed in solutions. Key results include the following: (1) the *L. monocytogenes* PC-PLC has an acidic pH optimum (in contrast to other bacterial PC-PLC enzymes) consistent with its role in vacuole lysis upon acidification; (2) the preference of PC-PLC for longer chain monomeric substrates is not because of a higher k_{cat} but a reduced K_m suggesting some amount of hydrophobicity is important for substrate binding in the active site; (3) the apparent K_d of PC-PLC for Zn^{2+} derived from kinetics at pH 6.0 (1.94 ± 0.22 μM) is lower that that from ICP-MC; and (4) PC-PLC enzymatic activity is not enhanced by added LLO that generates pores in vesicles (likewise, PC-PLC does not affect the membrane lytic activity of LLO) indicating no synergism between the two virulence factors. These results should aid in understanding the function of PC-PLC in *L. monocytogenes* pathogenicity.

The *L. monocytogenes* PI-PLC and a variant with reduced catalytic activity were expressed and are currently used in a collaborative project with the Portnoy laboratory at the University of California at Berkeley.

Table of Contents

List of Figures

List of Tables

Chapter 1 Introduction

1.1 *Listeria monocytogenes*

Listeria monocytogenes is a Gram-positive, facultative, food-borne, intracellular bacterial pathogen of human and animals. It is the causative agent of listeriosis, a severe illness that affects immunocompromised individuals and pregnant women [Vazquez-Boland et al., 2001].

L. monocytogenes can invade a wide variety of cells through phagocytosis or pathogen-induced endocytosis. Upon initial entry, bacteria are immediately trapped in single-membrane vacuoles. Under normal circumstances, the vacuole will progressively acidify and eventually fuse with a host cell lysosome, where the foreign contents will be digested. *L. monocytogenes* is unable to replicate in the phagosomal compartment of mammalian cells but is exquisitely adapted to life in the host cell cytosol. The bacteria have evolved to escape from the vesicles after acidification and prior to digestion. Following phagosomal escape, *L. monocytogenes* cells end up in the host cell cytosol, where they proliferate. The bacteria can reach high numbers (>200 bacteria) in the cytosol without causing host cell toxicity [Schnupf and Portnoy, 2007]. These cytosolic bacteria hijack the host cell's machinery for actin polymerization and use actin-based motility to spread from cell to cell without entering the extracellular milieu, causing infections in more distant tissues [Figure 1.1; Tilney and Portnoy, 1989; Cameron et al., 1999; Cossart and Bierne, 2001].

The pathogenicity of *L. monocytogenes* is associated with the production of virulence factors, most of which are proteins that are either surface-associated or secreted into the growth medium [Cossart and Bierne, 2001; Vazquez-Boland et al., 2001; Cabanes et al.,

2002]. The genes encoding the major virulence factors of *L. monocytogenes* are clustered mainly in two distinct chromosomal loci: the virulence locus that comprises the *hly* gene encoding listeriolysin O (LLO), controlled by the pleiotropic regulatory activator, *PrfA*; and the *inlAB* locus, also partially controlled by *PrfA* [Milohanic et al., 2003].

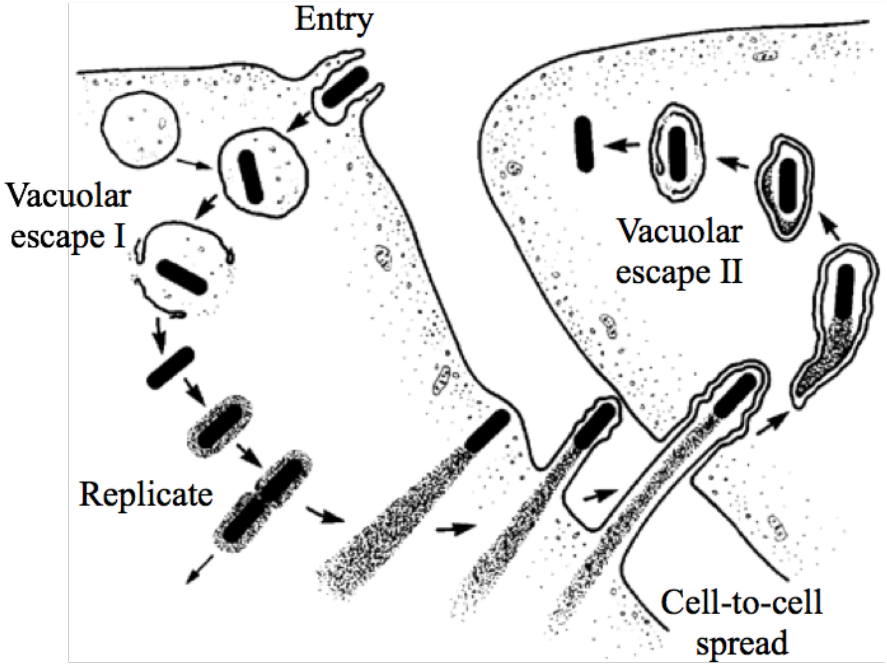

Figure 1.1 Major events in the life cycle of the intracellular pathogen *L. monocytogenes* [picture was adapted from Tilney and Portnoy, 1989].

1.1.1 Vacuolar escape of *L. monocytogenes*

One remarkable feature of *L. monocytogenes* pathogenesis is its prompt escape from two distinct vacuoles: (1) the single-membrane vacuoles that surround the bacteria after initial host cell invasion, and (2) the double-membrane vacuoles resulting from cell-to-cell spread. Failure in vacuolar escape results in an abortive and avirulent infection [Cossart et al., 1989]. Multiple virulence factors of *L. monocytogenes* have been

identified to be responsible for mediating phagosomal escape. Three of them have been studied in my work: listeriolysin O (LLO), encoded by the *hly* gene, is a pore-forming cytolysin [Geoffroy et al., 1987; Mengaud et al., 1988]; a phosphatidylinositol-specific phospholipase C (PI-PLC) [Camilli et al., 1991; Leimeister-Wachter et al., 1991; Mengaud et al., 1991], and a broad-range phospholipase C (PC-PLC) [Vazquez-Boland et al., 1992; Smith et al., 1995], encoded by the *plcA* and *plcB* genes.

1.2 Listeriolysin O (LLO)

Listeriolysin O (LLO) is essential to promote the escape of *L. monocytogenes* from a phagosome into the cytoplasm [Portnoy et al., 1988; Gedde et al., 2000; Dancz et al., 2002]. In the absence of LLO, *L. monocytogenes* bacteria remain trapped in the acidified phagosome in most cell types and are unable to replicate [Portnoy et al., 1988; Beauregard, K., 1997; Henry, et al., 2006]. Similarly, neutralizing antibody to LLO inhibits phagosomal escape of wild-type *L. monocytogenes* [Edelson and Unanue, et al., 2001]. In addition, LLO is sufficient to allow escape of *Bacillus subtilis* and *E. coli* from phagocytic vacuoles [Bielecki et al., 1990].

LLO also mediates membrane disruption of the secondary vacuole after cell-to-cell spread. When LLO transcription was put under an IPTG-inducible promoter, the size of the plaque resulting from cell-to-cell spread was found to correlate with IPTG in a dose-dependent fashion [Dancz et al., 2002].

In a murine model of infection, LLO activity is absolutely required. In *L. monocytogenes* producing inactive LLO, virulence was diminished more than five logs in the mouse model of listeriosis [Portnoy et al., 1988].

1.2.1 LLO is a pore-forming virulence factor

LLO is a member of the family of cholesterol-dependent cytolysins (CDCs). CDCs are β-barrel pore-forming toxins that require high concentrations of cholesterol to insert into cell membranes [reviewed in Tweten et al., 2001; Bayley, 1997; Heuck, 2010]. Other examples include streptolysin O, perfringolysin O (PFO), and pneumolysin. LLO is the only CDC that is made by an intracellular pathogen; it also has a pronounced acidic pH optimum for insertion and membrane rupture [Glomski et al., 2002].

Early work of Jones and Portnoy [Jones and Portnoy, 1994] showed that expression of the *pfo* gene (encoding PFO) under p*hly* promoter control, in an *hly*-negative mutant of *L. monocytogenes*, restored hemolytic activity and promoted partial phagosomal escape (~50%) in the mouse macrophage-like J774 cell line. However, *L. monocytogenes* secreting PFO killed the host cell after entry into the cytosol and therefore did not restore virulence. The cytotoxicity of PFO is due in part to the lack of a PEST-like sequence in PFO, which targets LLO for phosphorylation and/or degradation in the cytosol [Decatur and Portnoy, 2000]. More importantly, PFO does not have the pronounced acidic pH optimum like LLO [Portnoy et al, 1992], which could be a way to compartmentalize LLO activity in the vacuoles and then allow release as the vacuoles become acidified.

Crystal structures of the soluble monomers have been solved for three of the CDCs: perfringolysin O (PFO) from *Clostridium perfringens* [Rossjohn et al., 1997], intermedilysin (ILY) from *Streptococcus intermedius* [Bourdeau et al., 2009], and anthrolysin O (ALO) from *Bacillus anthracis* [Polekhina et al., 2005] revealing a four domain structure, Domain 1 to Domain 4 (D4). Based on the degree of sequence identity (>28%) and similarity (>45%) among CDC members, the three-dimensional structure and

modes of action are assumed to be similar [Heuck et al., 2000]. The structure of LLO was estimated via SWISS-MODEL [Arnold et al., 2006] based on homology with perfringolysin (Figure 1.4) and is shown in Figure 1.2.

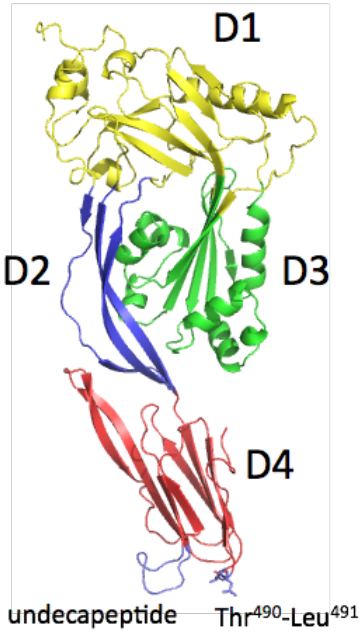

Figure 1.2 Model structure of LLO based on sequence homology of PFO. Domains 1 to 4 are labeled as D1 (yellow), D2 (blue), D3 (green), and D4 (red). The undecapeptide and the Thr^{490}-Leu^{491} are in purple. The two residues Thr^{490}-Leu^{491} critical for pH-sensitivity are represented in sticks.

1.2.2 Cholesterol-dependent cytolysins (CDC)

CDCs are secreted by a large number of pathogenic Gram-positive bacteria [Bayley, 1997]. Generally, these toxins are produced as water-soluble proteins that specifically recognize and bind cholesterol in the target mammalian membranes. On the target membrane, CDC monomers aggregate and oligomerize, forming arc- and ring-like architectures. With a concerted conformational change of each monomer, CDC oligomers penetrate the membrane bilayer, forming a giant β-barrel pore [Giddings et al., 2005; Olofsson et al., 1993; Czajkowsky et al., 2004; Dang et al., 2005; Tilley et al., 2005]. The dimensions of the pore range up to nearly 300 Å [Heuck et al., 2010].

PFO is the prototypical CDC, from which most of the general mechanism of pore-formation for the CDC has been revealed. Specifically, the C-terminal domain 4 (D4) of PFO encounters the membrane first (Figure 1.3, step I). The binding of D4 triggers the structural rearrangements required to initiate the oligomerization of PFO monomers and formation of a prepore complex on the membrane surface (step II). Pore formation commences when two amphipathic β-hairpins from each PFO molecule insert and span the membrane (step III). The concerted insertion of two transmembrane β-hairpins from up to 50 monomers then creates the large transmembrane β-barrel that penetrates the membrane. While the formation of a prepore complex has been demonstrated, it is still controversial whether incomplete toxin rings also undergo the structural changes of prepore-to-pore transition [Gilbert, 2005].

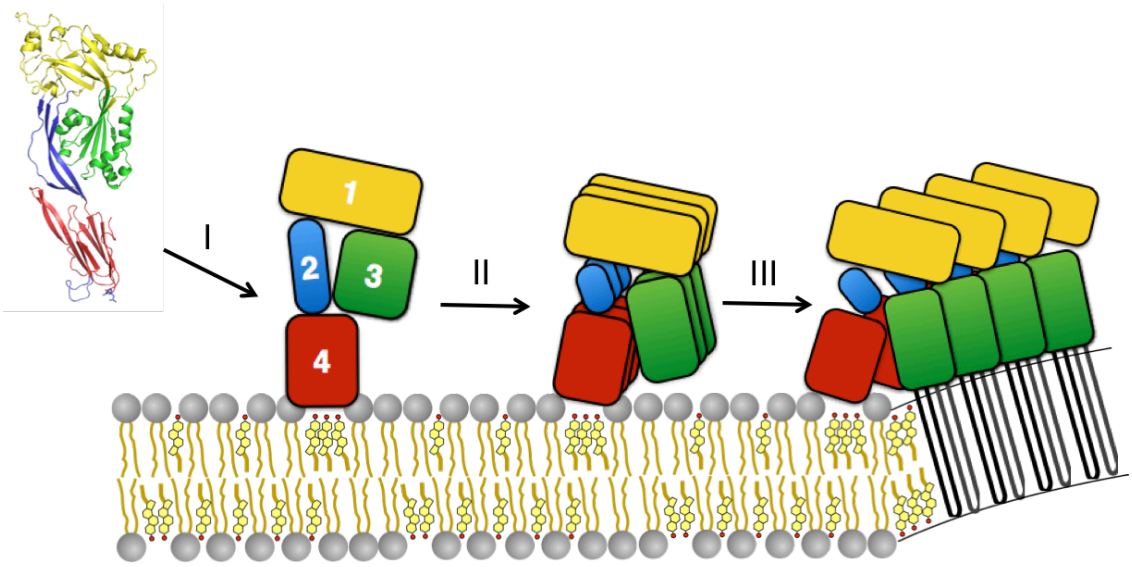

Figure 1.3 Model of the pore-forming mechanism of CDCs on a target membrane. Defined domains of CDCs are numbered. The pore formation occurs in three steps. Step I, membrane binding; step II, oligomerization; step III, membrane penetration. The membrane bilayer is depicted with cholesterol molecules intercalated between the phospholipid constituents.

1.2.3 D4 and membrane binding

From the sequence similarity between LLO and other CDCs (as shown in sequence alignment of LLO and PFO in Figure 1.4), it is notable that conservation is generally higher in the D4 domain than in the other portions of the molecule. The sequence identity between LLO and PFO is 64% in the D4 but only 38% in the rest of the molecule (42% for the whole sequence) [Kayal and Charbit, 2006]. This is understandable since domain 4 is the region in all CDCs that mediates the cholesterol-dependent membrane binding, which is the essential character of CDC family proteins that they are named after.

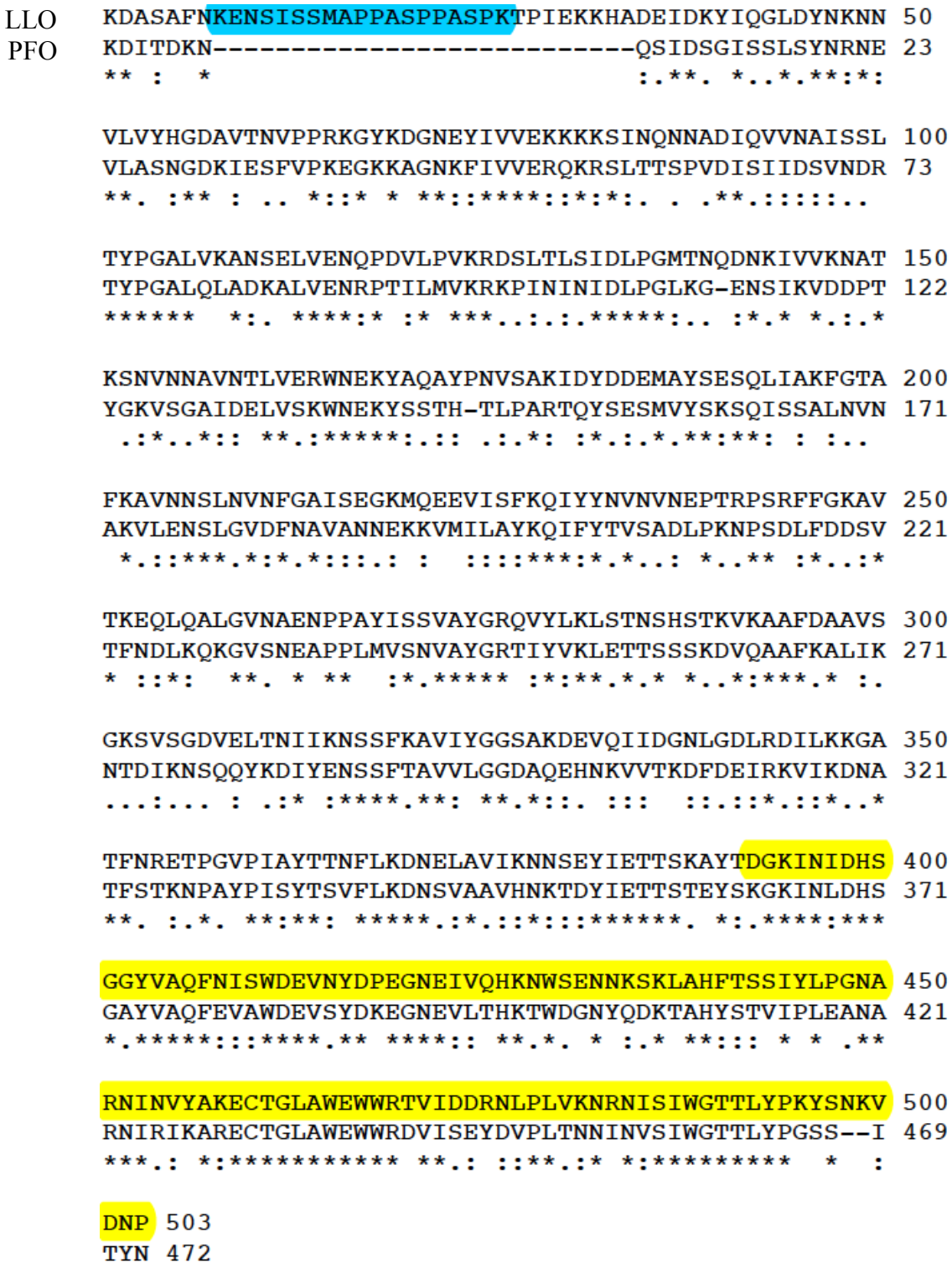

Figure 1.4 Amino acid sequence alignment of LLO with PFO, produced by online program T-coffee [Di Tommaso et al., 2011]. "*": identical; ":": conserved substitutions; ".": semi-conserved substitutions. The sequence of the PEST-like motif is highlighted in blue and that of domain 4 (D4) is in yellow.

Cytolysis starts when the C-terminal D4 first contacts the target membrane. Domain 4 has a β-sandwich structure with an undecapeptide and three other short loops at the tip [Figure 1.2]. These loops do not penetrate deeply into the membrane and do not directly participate in the architecture of the transmembrane pore, rather they help in the initial anchoring of a monomer on the membrane. It has been shown that D4 is oriented perpendicular to the membrane interface and the bulk of it is surrounded by the aqueous milieu, even in the oligomeric state [Ramachandran et al., 2002; Soltani et al., 2007a]. One of these loops, an 11 amino acid-residue sequence, ECTGLAWEWWR also known as the Trp-rich loop, is highly conserved among the CDCs [Alouf et al., 2005; purple loop in Figure 1.2]. Modifications in this conserved undecapeptide typically inhibit the hemolytic activity of the toxin by blocking the conformational changes that are required to allosterically trigger the insertion of the transmembrane β-barrel [Michel et al., 1990; Ramachandran et al., 2004; Soltani et al., 2007b]. The correlation between this highly conserved amino acid sequence and the absolute cholesterol dependence led researchers to hypothesize that this undecapeptide represented the cholesterol-binding site for the CDCs [Rossjohn et al., 2007]. However, it has been shown that cholesterol recognition and toxin binding are mediated by three other loops, while the insertion of the undecapeptide may be coupled to the insertion of the transmembrane β-barrel [Soltani et al., 2007b]. More specifically, two residues Thr^{490}-Leu^{491} in D4 have been identified as essential for specifically recognizing cholesterol in the membrane and initiating the cholesterol-dependent interaction of CDCs with membranes [Farranda et al., 2010].

There is also an important Cys residue in the undecapeptide whose modification inhibits pore-forming activity. Previously, the CDCs were designated as thiol-activated

toxins since CDC activity could be inhibited by oxidation or thiol-reacting compounds and reactivated by thiol-reducing agents [Smyth and Duncan, 1978]. It was also thought that this residue was essential for activity, presumably by interacting with membrane cholesterol. However replacement of this residue with Ala in LLO [Michel et al., 1990] and in other CDCs [Pinkney et al., 1989; Saunders et al., 1989] did not significantly affect activity, although it did remove the sensitivity to oxidation or thiol-alkylation agents. Replacement with Gly or bulkier amino acids, however, abolished most of the activity, indicating that the mechanism underlying Cys-mediated reversible inhibition of cytolytic function probably involves steric hindrance due to formation of toxin dimers or heterodimers with other proteins via disulfide bridges.

1.2.4 PEST motif and LLO stability

The PEST-like motif is any protein sequence rich in proline, glutamate, serine, and threonine residues [Rechisteiner and Rogers, 1996]. PEST-like sequences are thought to target eukaryotic proteins for phosphorylation and/or rapid degradation by the proteasome. A putative PEST-like motif has been identified close to the N-terminus of LLO (highlighted sequence in Figure 1.2.3) and its role in pathogenesis studied [Decatur and Portnoy, 2000; Lety et al., 2001].

Deletion of the PEST-like motif in *L. monocytogenes* LLO led to increased cytotoxicity and lower virulence. When the sequence was introduced in PFO and the chimeric toxin was expressed in *L. monocytogenes*, bacteria were less cytotoxic than those expressing wild-type PFO and were able to replicate intracellularly. These data suggest that adoption of a PEST motif in LLO is one strategy to restrict the activity of the

toxin to the host cell vacuole, thereby preserving the intracellular niche for bacterial proliferation [Decatur and Portnoy, 2000]. It has also been shown that *L. monocytogenes* mutants expressing a PEST-deleted *hly* allele, although fully hemolytic, are strongly impaired in the ability to escape from the phagocytic vacuole. This suggests that the PEST motif in LLO may also play a specific role in the disruption of the phagosomal membrane, for example, by serving as a ligand for targeting other factors required for its efficient disruption to that membrane [Lety et al., 2001].

1.2.5 Cholesterol: membrane receptor?

As do many other bacterial and viral proteins, the CDCs take advantage of a distinguishing feature of mammalian membranes, in this case the presence of cholesterol [Palmer, 2004; Umashankar et al., 2008]. Among all the different lipids in cell membranes, the presence of cholesterol is a distinguishing feature of mammalian cells.

It was long thought that cholesterol functioned as a membrane receptor for CDCs. This paradigm was established based on two phenomena: (1) pre-incubation of cholesterol with the toxins inhibited hemolytic activity [Cowell and Bernheimer, 1978; Duncan and Schlegel, 1975; Howard et al., 1953; Shany et al., 1974]; and (2) some CDCs could bind directly to cholesterol [Iwamoto et al., 1987; Johnson et al., 1980]. Because of its ability to directly bind to cholesterol-containing membranes, PFO has been used as a probe for membrane cholesterol [Nakamura et al., 2003; Waheed et al., 2001]. However, recent findings have challenged this long-standing paradigm, as not all CDCs require cholesterol to bind to the membrane. For example, intermedilysin recognizes and binds

the human CD59 protein [Giddings et al., 2004]. However, cholesterol is still required for the cytolytic activity of intermedilysin [Giddings et al., 2003].

In liposomal membranes containing only phosphatidylcholine and cholesterol, more than 50 mole % cholesterol is required for CDCs such as tetanolysin (Alving et al., 1979), SLO (Rosenqvist et al., 1980), and PFO (Heuck et al., 2000; Ohno-Iwashita et al., 1992), to bind and create a pore in the bilayer. This is an amount of cholesterol well above what is stable in model membrane systems. Interestingly, it has been shown that the transition from little or no binding to full binding to liposomes occurs in a narrow range of cholesterol concentration [Heuck et al., 2000; Rottem, et al., 1982], indicating a function of cholesterol more complex than a simple membrane receptor of CDCs.

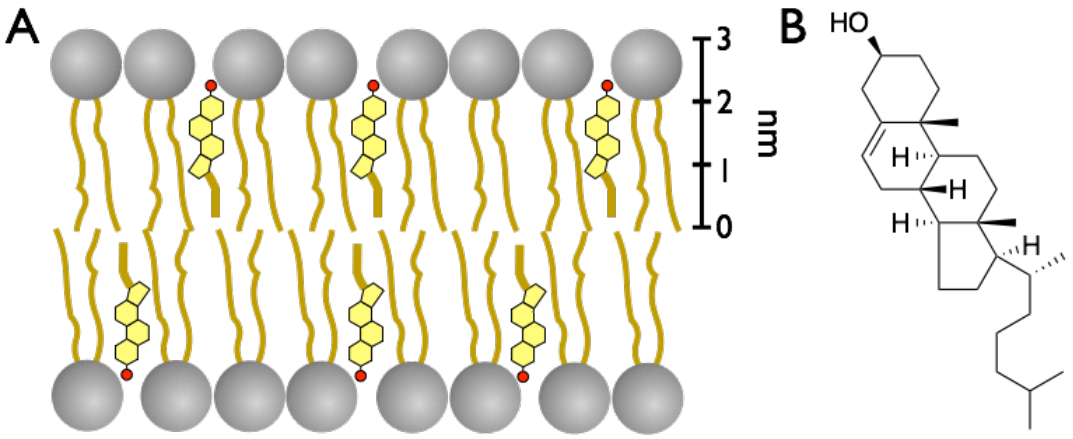

Figure 1.5 (A) Model of membrane bilayer with phospholipids and cholesterol molecules; (B) molecular structure of cholesterol.

Cholesterol-rich micro-domains in eukaryotic cell membranes are termed lipid rafts. Lipid rafts are dynamic assemblies of proteins and lipids that are distinct from the liquid-disordered bilayer regions of cellular membranes [Simons et al., 2002]. Cholesterol is

thought to serve as a spacer between the hydrocarbon chains of the sphingolipids and to function as a dynamic glue that keeps the raft assembly together [Figure 1.5]. These specialized membrane micro-domains compartmentalize cellular processes by serving as organizing centers for the assembly of signaling molecules. This in turn influences membrane fluidity membrane protein trafficking, and regulates neurotransmission and receptor trafficking. The fact that CDCs could go from virtually no binding to maximal binding within such a narrow range of cholesterol suggests that they might interact with the target membrane via binding to lipid rafts instead of individual cholesterol molecules. PFO has been shown to preferentially associate with lipid rafts in cells [Shimada et al., 2002; Waheed et al., 2001]. The ability to target lipid rafts may enable the bacterial pathogen to disrupt essential functions of the cell by disrupting the structure of the lipid rafts, a cellular feature where it is increasingly evident that a significant number of essential cellular processes, such as signaling and endocytosis, occur.

1.2.6 Acidic pH optimum of LLO activity

In spite of significant amino acid sequence similarity with the other members of the CDC family, LLO possesses unique biological properties that prevent it from being cytotoxic when released by *L. monocytogenes* into the cytosol. One of the characteristics of LLO that contributes to that is its acidic pH optimum (~ pH 5.5).

By swapping dissimilar residues from a pH-insensitive orthologue, PFO, a single residue in D4, Leu^{461}, was found to be responsible for the acidic pH optimum of LLO action. Mutation of Leu to Thr (present in PFO) resulted in an almost 10-fold increase in the hemolytic activity of LLO at a neutral pH. However, *L. monocytogenes* synthesizing

L461T displayed a 100-fold virulence defect in the mouse listeriosis model. These bacteria escaped from acidic phagosomes and initially grew normally in cells and engaged in cell-to-cell spread, but they prematurely permeabilized the host membrane and killed the cell [Glomski et al., 2002]. These results suggest that the acidic pH optimum of LLO results from an adaptive mutation that limits cytolytic activity to acidic vesicles and prevents damage to the host.

More recently, it was shown that rapid LLO aggregation at slightly alkaline pH is responsible for LLO inactivation [Schuerch et al., 2005], while no reduction in hemolytic activity was detected for PFO under the same conditions. A structural basis for pH-dependent aggregation of LLO was proposed, arguing that acidic residues located on the α-helices of domain 3 (D3) determine pH sensitivity. In the major conformational change of pore-formation, the α-helices of D3 from each monomer transform into a β-hairpin that penetrates the target membrane. However, at alkaline pH and at temperatures above 33 °C, these helices would prematurely unfurl to β-hairpins, leading to the exposure of core hydrophobic residues to the aqueous milieu [Schuerch et al., 2005; Nomura et al., 2007]. These results suggest that the acidic cytolytic activity of LLO is caused by a pH-dependent loss of function, and not by pH-dependent activation.

1.2.7 LLO and autophagy

It has been recently suggested that host cells may utilize autophagy as a defense against intracellular pathogens [Colombo, 2007; Orvedahl and Lavine, 2009; Swanson, 2006]. Autophagy is a mechanism by which cytoplasmic components, including long-lived proteins and damaged organelles (peroxisomes, ER, and mitochondria) are

enveloped within specialized double-membrane-bound vesicles that deliver their cargo to the lysosome for degradation [Mizushima et al., 2002; Levine and Kroemer, 2008]. Recent data suggest that autophagy plays an essential role in both acquired [Paludan et al., 2005] and innate immune responses.

L. monocytogenes has been shown to interact with the host autophagic machinery [Rich et al., 2003]. Py et al. (2007) and Birmingham et al. (2007) reported that under normal intracellular conditions, *L. monocytogenes* is targeted by autophagy and that this process efficiently limits bacterial growth. Additionally, LLO was found as the bacterial agent necessary and sufficient to induce autophagy subsequent to infection by *L. monocytogenes* [Meyer-Morse et al., 2010].

1.3 Broad-range phospholipase C (PC-PLC)

In addition to LLO, two phospholipases have been implicated in the virulence process: a broad-range phospholipase C (termed as PC-PLC since it exhibits a high rate of hydrolysis of that phospholipid) and phosphatidylinositol-specific phospholipase C (PI-PLC). PC-PLC and PI-PLC, encoded by genes *plcB* and *plcA* respectively, also play important roles in the escape of *L. monocytogenes* from vacuoles.

PC-PLC is involved in the lysis of the double-membrane vacuoles after cell-to-cell spread [Vazquez-Boland et al., 1992]. The mutant lacking PC-PLC activity was found to be 20-fold less virulent in mice and was defective in cell-to-cell spread [Smith et al., 1995]. Interestingly, in some cases of human cell lines, LLO has been shown to be dispensible for vacuolar lysis. Under this situation, in the absence of LLO, a critical role of PC-PLC in membrane dissolution of primary and secondary vacuoles has been

recognized [Portnoy et al., 1988; Marquis et al., 1995; Gründling et al., 2003; Alberti-Segui et al., 2007].

1.3.1 Folding and activation of PC-PLC

PC-PLC is synthesized and secreted as an inactive proenzyme of 33 kDa. The proenzyme translocates across the cell membrane after the cleavage of the N-terminal signal peptide. The secreted proenzyme accumulates at the membrane-cell wall interface [Marquis and Hager, 2000; Snyder and Marquis, 2003]. The compartmentalization and activity of PC-PLC is regulated by its propeptide and the proteolytic activity of a metalloprotease (Mpl) of *L. monocytogenes* [Marquis and Hager, 2000; Slepkov et al., 2010; Brian et al., 2011].

Mpl is a member of the thermolysin family of metalloproteases that contains a Zn^{2+} ion in the active site [Hase and Finkelstein, 1993]. Mpl is also synthesized as a proenzyme of 55-kDa, with an N-terminal propeptide of 30 kDa and a catalytic domain of 35 kDa [Mengaud et al., 1991a]. Like PC-PLC, Mpl is secreted and is an associated virulence factor of *L. monocytogenes*. The compartmentalization of Mpl is dependent on the propeptide. Removal of the propeptide occurs exclusively by intramolecular autocatalysis [Bitar et al., 2008] upon a decrease of environmental pH.

With the activation of Mpl proteolytic activity, the N-terminal 26-residue propeptide of the PC-PLC proenzyme is removed, producing a mature enzyme PC-PLC of 29 kDa, as shown in Figure 1.6 [Vazquez-Boland et al., 1992; Geoffroy et al., 1991; Raveneau et al., 1992; Poyart et al., 1993; Marquis et al., 1997; O'Neil et al., 2009]. The mature PC-PLC is then rapidly released into the environment.

Figure 1.6 Schematic diagrams of *L. monocytogenes* PC-PLC sequence. PC-PLC is translated as preproenzyme. The inactive proform of PC-PLC encompasses the propeptide and the catalytic domain. With the proteolytic cleavage of Mpl, the catalytic domain of 27.7 kDa protein is released to across the cell wall.

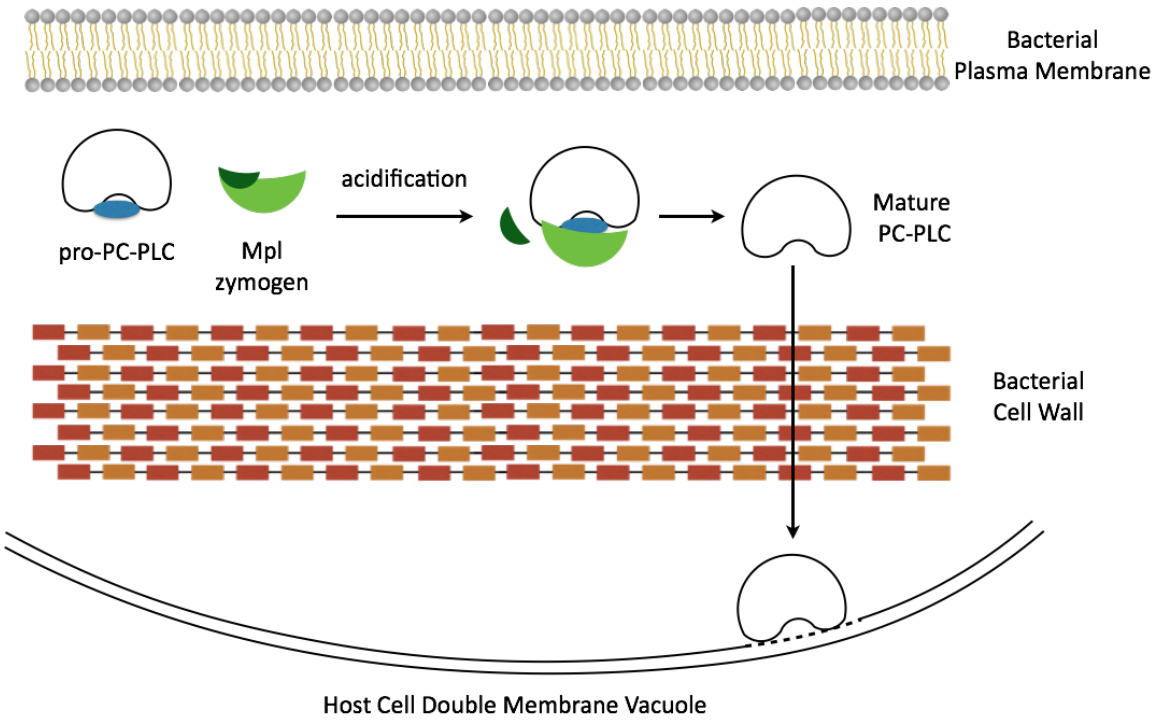

Figure 1.7 Schematic representation of the behavior of PC-PLC and Mpl when *L. monocytogenes* is entrapped in a secondary vacuole upon cell-to-cell spread. Pro-PC-PLC and pro-Mpl remain at the membrane-cell wall interface until a decrease in pH triggers Mpl autocatalysis and Mpl-mediated maturation of PC-PLC. The mature proteins are then secreted across the cell wall where PC-PLC can hydrolyze membrane phospholipids. [Forster et al., 2011]

The mechanism by which the propeptide inhibits PC-PLC activity is unclear thus far. The propeptide could interfere with folding of the catalytic domain or block the entrance

of the active site of PC-PLC. It is noteworthy that even a single residue from the propeptide at the N-terminus is sufficient to prevent PC-PLC activity, presumably due to the critical role of the first residue Trp in coordinating zinc ions in the enzyme active site [Slepkov et al., 2010].

1.3.2 PC-PLC as a phospholipase

Phosphatidylcholine hydrolysis, or lecithinase activity, by *L. monocytogenes*, had been recognized as early as 1962 [Fuzi and Pillis, 1962] in egg yolk agar opacification assays. Together with hemolytic activity, which is caused by LLO, lecithinase activity was one of the two major phenotypes used to identify the pathogen *L. monocytogenes*. As a lecithinase/phospholipase, PC-PLC catalyzes cleavage at the glycerol side of the phosphodiester bond to give diacylglycerol (DAG) and a phosphorylated head group (Figure 1.8).

In previous studies, PC-PLC, secreted by the *L. monocytogenes* into the medium, had been isolated and purified [Geoffroy et al., 1991; Goldfine et al., 1993]. The purified enzyme had activity over a broad spectrum of substrates, including phosphatidylcholine (PC), phosphatidylethanolamine (PE), phosphatidylserine (PS), and sphingomyelin (SM), but had only minimal activity towards phosphatidylinositol (PI). The order of specificity among the substrates had been identified as PC>PE>PS>SM>>PI [Goldfine et al., 1993]. It was also suggested that PC-PLC was active over a broad pH range, from 5.5 to 8.0 [Goldfine et al., 1993].

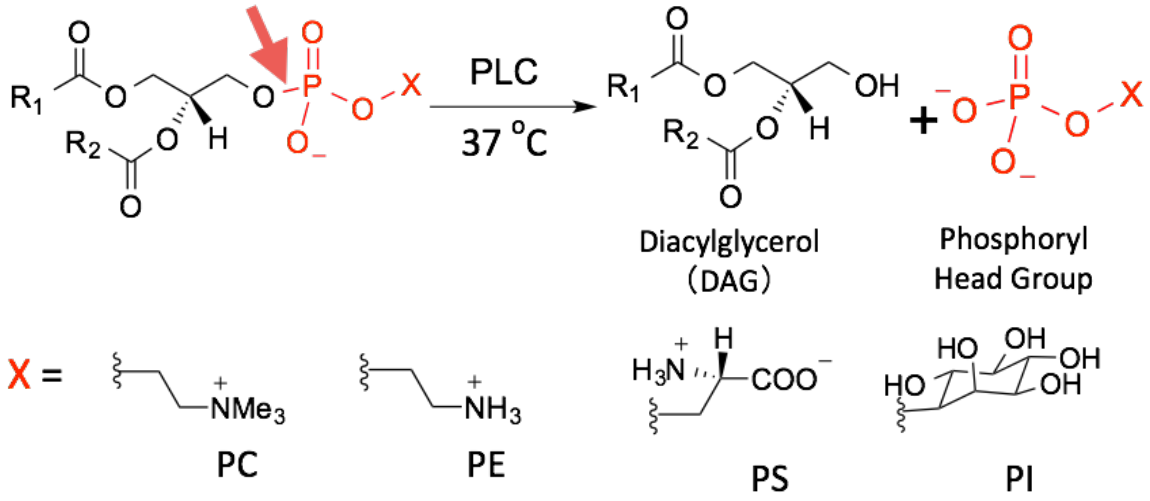

Figure 1.8 Reactions catalyzed by PC-PLC producing diacylglycerol (DAG) and phosphorylated head group as products. The red arrow points to the bond to be broken by the hydrolysis of phospholipase C. The phospholipid substrates differ in the head group (-X) and can be phosphatidylcholine (PC), phosphatidylethanolamine (PE), phosphatidylserine (PS). The phosphatidylinositol (PI) head group is also shown, although this is not a substrate for the PC-PLC.

1.3.3 Structure of PC-PLC

A crystal structure of the *L. monocytogenes* PC-PLC awaits solution. However, homologues to this PC-PLC have been identified in other Gram-positive bacteria, including the phospholipase C from *Bacillus cereus* (PLC_{Bc}) which has 38.7% identity over 253 amino acids [Johansen et al., 1988; Gilmore et al., 1989] (Figure 1.9) and α-toxin from *Clostridium perfringens* (22.4% identity over 223 amino acids) [Titball et al., 1989; Titball et al., 1999]. *L. monocytogenes* PC-PLC shares considerable sequence and function identity with PLC_{Bc} [Titball, 1993]. Therefore, it is likely that PC-PLC has similar molecular architecture to PLC_{Bc}.

Figure 1.9 Sequence alignment of *L. monocytogenes* PC-PLC and its homologue from *B. cereus*, PLC_{Bc}, produced by online program T-coffee [Di Tommaso et al., 2011]. "*": identical; ":": conserved substitutions; ".": semi-conserved substitutions. The residues that coordinate Zn^{2+} ions are highlighted in yellow. Point mutations made in my work are lighlighted in red.

Using the online program SWISS-MODEL [Arnold et al., 2006], I generated a homology model structure for the *L. monocytogenes* PC-PLC (Figure 1.10). This suggests that the PC-PLC protein, like PLC_{Bc}, is a monomeric helical metalloprotein, with three Zn^{2+} ions in the active site [Hough et al., 1989].

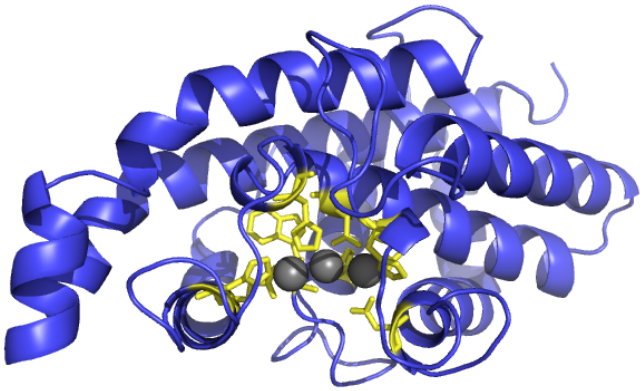

Figure 1.10 Modeled structure of PC-PLC based on sequence homology to PLC_{Bc}. Three zinc ions are shown in grey spheres. All the nine residues coordinated with zinc ions are represented in yellow sticks.

1.3.4 PC-PLC as a metalloenzyme

The high homology of PC-PLC to PLC_{Bc} (38.7% sequence identity, Figure 1.9) allows many critical residues to be identified. Notably, all the nine amino acids, namely, Trp-1, His-14, Asp-55, His-69, His-118, Asp-122, His-128, His-142, and Glu-146 (residues highlighted in yellow in Figure 1.10) that bind to the three Zn^{2+} atoms in PLC_{Bc} are found in identical positions in *L. monocytogenes* PC-PLC. This is consistent with PC-PLC as a metalloenzyme like PLC_{Bc}, whose activity is dependent on the presence of Zn^{2+} ions [Geoffroy et al., 1991].

There are two major roles that the zinc ions play in metalloenzymes: (1) coordination with the substrate that renders it more susceptible to nucleophilic attack; and (2) coordination with an active site water molecule that facilitates its nucleophilic attack. However, little is known about the zinc ions in *L. monocytogenes* PC-PLC, except that the activity of PC-PLC is zinc-dependent [Geoffroy et al., 1991].

From the structure of the metalloenzyme PLC_{Bc}, all of the zinc ions are pentacoordinate adopting the trigonal-bipyramidal geometry. Crystal structures of PLC_{Bc} in complex with various ligands have been obtained, and they are shown schematically in

Figure 1.11 in comparison [Hansen et al., 1992, 1993a]. A structure exists with PLC_{Bc} bound with an inorganic phosphate (Pi) at the active site; Pi is a weak competitive inhibitor of the enzyme (50% of inhibition of the enzyme at 50 mM [Hansen et al., 1992]). Another structure shows the enzyme with a phosphonate inhibitor, 3(S), 4-dihexanoylbutyl-1-phosphonylcholine, bound; this inhibitor has a K_i of 1.15 mM [Hansen et al., 1993a]. Interactions of the inhibitor with the protein provide crucial information for the catalytic mechanism.

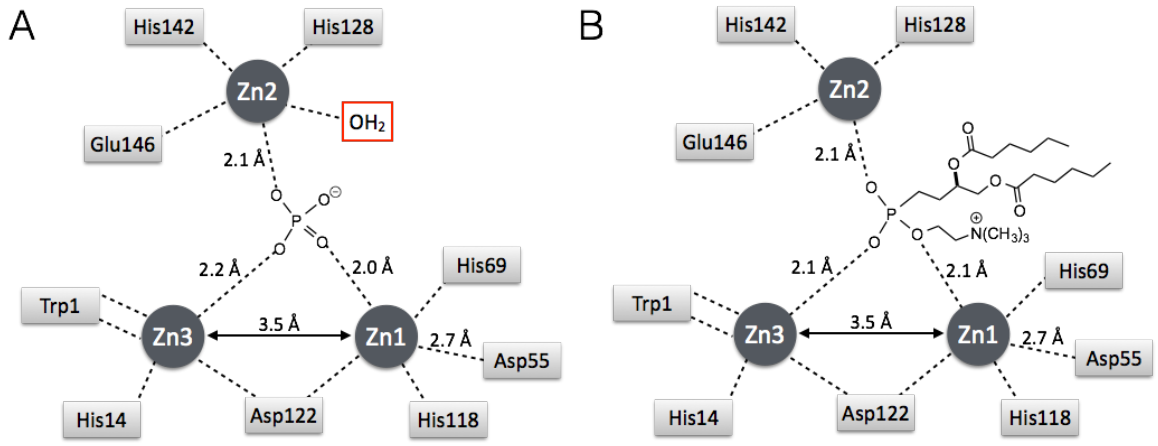

Figure 1.11 Active site of PLC_{Bc} with three zinc ions and all the coordinating residues. Distances between Zn^{2+} and residues were found in structure of PLC_{Bc} in complex with (A) inorganic phosphate [Hansen et al., 1992]; (B) binding of a phosphonate inhibitor in the active site [Hansen et al., 1993a].

1.3.5 General base/general acid catalytic mechanism – a lesson from PLC_{Bc}

There is not much consensus on the detailed catalytic mechanism of non-specific phospholipase C. One of the few commonly accepted points is the mechanism uses general base/general acid catalysis. A water molecule must be activated by a general base so that it can attack the phosphodiester linkage. A general acid then provides a proton to the leaving group (DAG) so that it can exit the enzyme active site (Figure 1.12).

However, whether a bound Zn^{2+} contributes to nucleophilic water polarization and which of many possible side chains acts as the general base are debated.

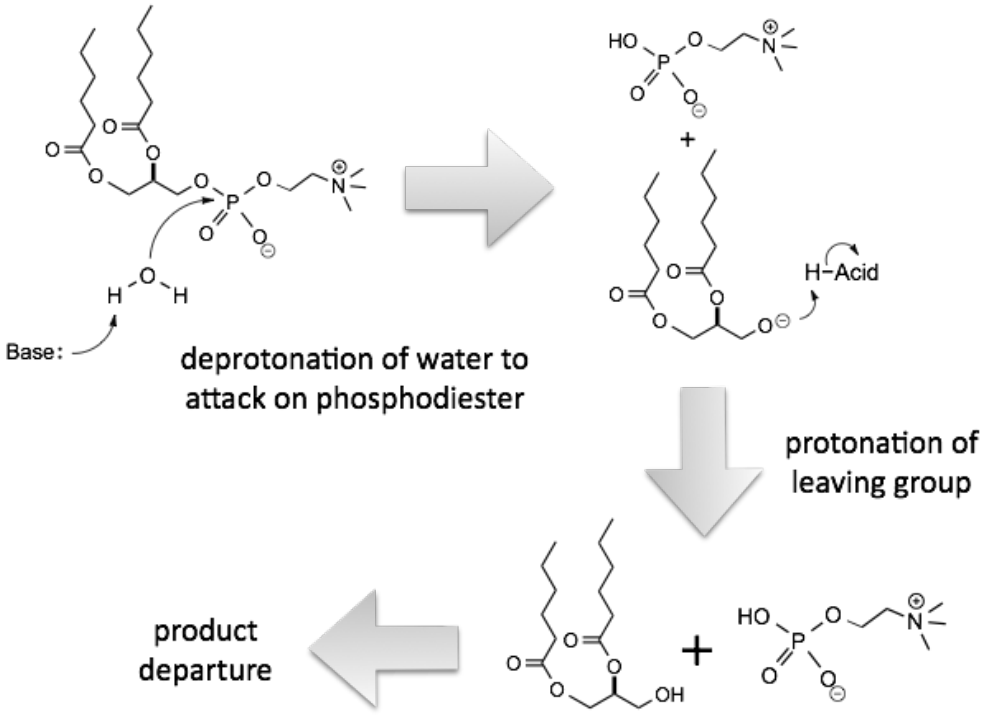

Figure 1.12 General acid/general base mechanism proposed for phospholipid hydrolysis catalyzed by PC-PLC.

1.3.6 Enzymatic characteristics of PC-PLC

The mechanistic aspects of metalloenzyme-catalyzed hydrolysis of phospholipids have been extensively studied with PLC_{Bc} [Hergenrother and Martin, 2000]. However, the candidate for the general base in PLC hydrolysis remains to be resolved. Usually, with three zinc ions in the active site, any zinc bound water is routinely invoked as the nucleophile for zinc peptidases, amidases, and zinc phosphoryl transfer enzymes [Strater et al., 1996]. However, in the crystal structure of PLC_{Bc} complexed with a phosphonate substrate analogous inhibitor, there is no such zinc bound water molecule available in the

active site as shown in Figure 1.13 [Hansen et al., 1993], which leaves the identity of general base a subject of speculation.

In the complex structure, both Glu4 and Asp55 are in a position to serve as the general base in the PLC_{Bc}-catalyzed reaction by activation of W2, an active site water molecule (although it should be noted that W2 is fairly far from the phosphorus atom). Between them, Asp55 was suggested as a better candidate for the general base, since even the analogous mutant D55N resulted in about ~ 4000-fold decrease of enzyme efficiency while mutations of Glu4 led to more modest effects [Martin and Hergenrother, 1998], and PC hydrolysis was reduced but not abolished [Tan and Roberts, 1998]. However, Asp55 is also a Zn^{2+} ligand.

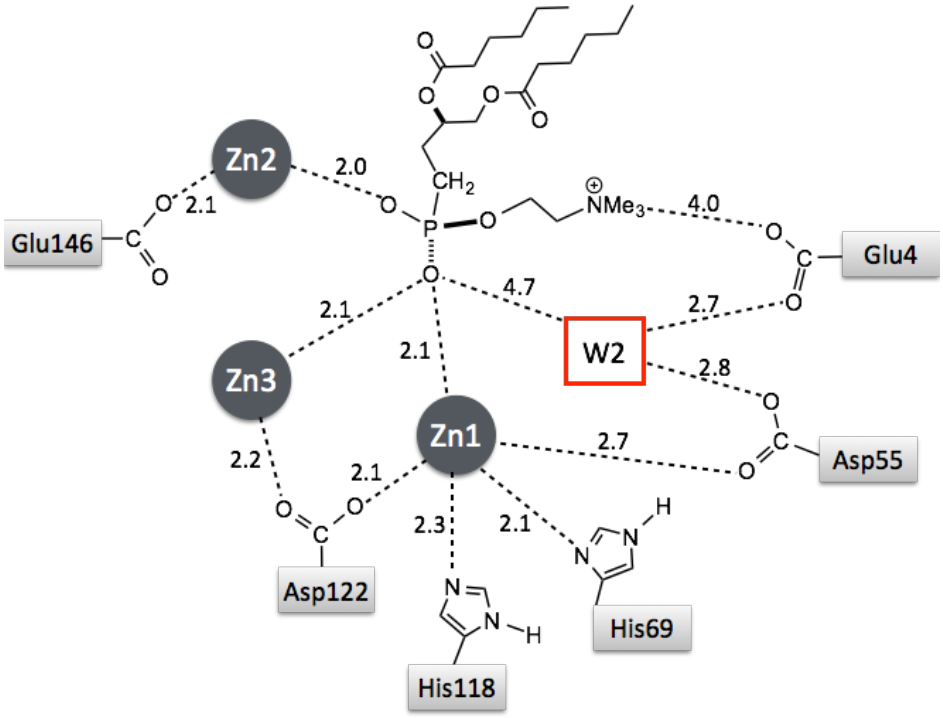

Figure 1.13 Distances (Å) of selected active site residues of PLC_{Bc} from a phosphonate substrate analogue inhibitor [Hansen et al., 1993a]. The active site water as putative general base is in red box.

1.3.7 Choline binding pocket

As suggested by characterization of the E4A enzyme [Tan and Roberts, 1998], Glu4 plays a role in substrate binding, particularly in the binding of the choline head group [Martin et al., 2000]. The substrate-binding cleft of PLC_{Bc} that accommodates the choline head group is lined with residues Glu4, Tyr56, and Phe66 (Figure 1.14). Along with Glu4, Tyr56 and Phe66 were also found critical for the specific recognition of choline containing substrates [Martin et al., 2000]. Presumably, the carboxyl group on the side chain of Glu4 helps neutralize the choline positive charge and Tyr56 and Phe66 provide aromatic rings to stabilize the positive charge via π-cation interaction. Systematic mutation studies of PLC_{Bc} activity on different monomeric substrates diC_6PC, diC_6PE, diC_6PS were consistent with that hypothesis [Martin et al., 2000]. Of the three residues, Glu4 is most critical for the hydrolysis of PC and PS, the head groups of which contain a positive charge. The aromatic properties of Tyr56 and Phe66 were essential for optimal catalytic efficiency. Interestingly, the largest changes in the kinetic parameters for the mutant enzymes were in k_{cat}, which varied over nearly three orders of magnitude, whereas changes in K_m varied by less than a factor of ten. Therefore the contributions of the choline binding pocket were more than simple substrate recognition. The chemistry carried out by the enzyme was significantly impacted.

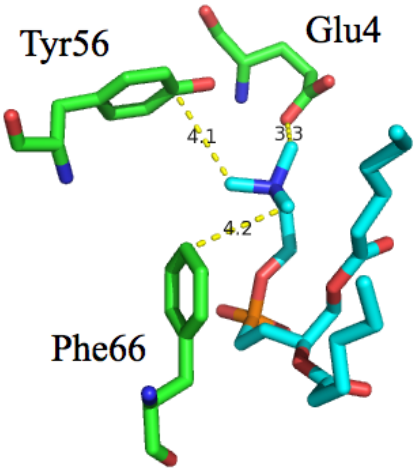

Figure 1.14 Residues lining the choline-binding pocket in the structure of PLC_{Bc} in complex with the substrate mimic inhibitor (PDB code: 1P6D). The distances of the hydrogen in the trimethylammonium moiety to the closest atom of the aligning residues (Glu4, Tyr56, and Phe66) are labeled in Å.

1.3.8 Rate-determining step (RDS)

Enzyme catalyzed hydrolysis reactions proceed through the steps of substrate binding, hydrolysis, product release, and enzyme rearrangement to the unbound conformation. Of particular interest in the PC-PLC catalytic cycle is the identity of the rate-determining step (RDS). The rate-determining step may involve substrate binding or product release, which is external to the hydrolysis reaction, or the hydrolysis itself, which is internal.

Studies on the RDS of PLC_{Bc} using various viscosity buffers, wherein the diffusion coefficient of the enzyme was different [Martin and Hergenrother, 1999], indicated that there was little change in reactivity, and hence a diffusion-controlled process, such as substrate binding or product release is not rate limiting in PLC_{Bc} catalysis.

A hydrolysis reaction involves breaking an O-H bond in the transition state. If the chemistry of hydrolysis is the rate-determining step of a reaction, the reaction rates would be affected by the contents of D_2O in the buffer, as the activation energy is higher for breaking a D-O bond compared to an H-O bond. A deuterium isotope effect was indeed

observed in the PLC_{Bc} catalyzed reaction [Martin and Hergenrother, 1999], indicating proton transfer was involved in the rate-determining step.

Most of the structure and mechanism studies were only tested on PLC_{Bc}. It is likely that PC-PLC chemistry is similar to that of PLC_{Bc}. However, it is also possible it has some unique properties that help facilitate its function as a virulence factor of an intracellular pathogen.

1.4 Phosphatidylinositol-specific phospholipase C (PI-PLC)

L. monocytogenes PI-PLC is a 33 kDa polypeptide similar to the PI-PLC from *B. thuringiensis, B. cereus*, and *Staphylococcus aureus* (around 30% primary sequence identity) and eukaryotic PI-PLCs, such as that produced by *Trypanosoma brucei* [Mengaud et al., 1991]. PI-PLC enzymes cleave PI in two discrete steps: (1) an intramolecular phosphotransferase reaction that generates DAG and inositol 1,2-(cyclic)-phosphate, followed by (2) hydrolysis of the cyclic water-soluble intermediate to inositol-1-phosphate. The chemical reaction is shown in Figure 1.15.

The structure of the *L. monocytogenes* PI-PLC has been solved [Moser et al., 1997]. As shown in Figure 1.16, this monomeric protein is an $(\beta\alpha)_8$-barrel with the active site located at the C-terminal side of the β-barrel. The purified PI-PLC is highly specific for PI, with a pH optimum that depends on the substrate. For example, with PC solubilized in Triton X-100 micelles, the pH profile was broad with a maximum between pH 5.5 and 6.5; however, the cIP hydrolysis reaction was optimal at pH 7. The observation of acidic optimum with micellar substrate suggests that, like LLO, it would be active in acidified phagocytic vesicles. No hydrolysis of PC, PS, PE, PI-4-phosphate, or PI-4,5-biphosphate

was observed with PI-PLC [Goldfine and Knob, 1992]. Unlike other bacterial PI-PLC enzymes, the *L. monocytogenes* PI-PLC is much less efficient at catalyzing the hydrolysis of glycosylphosphatidylinositol (GPI)-anchored eukaryotic membrane proteins [Goldfine and Knob, 1992; Mengaud et al., 1991; Gandhi et al., 1993]. This would fit with its secretion by an intracellular pathogen.

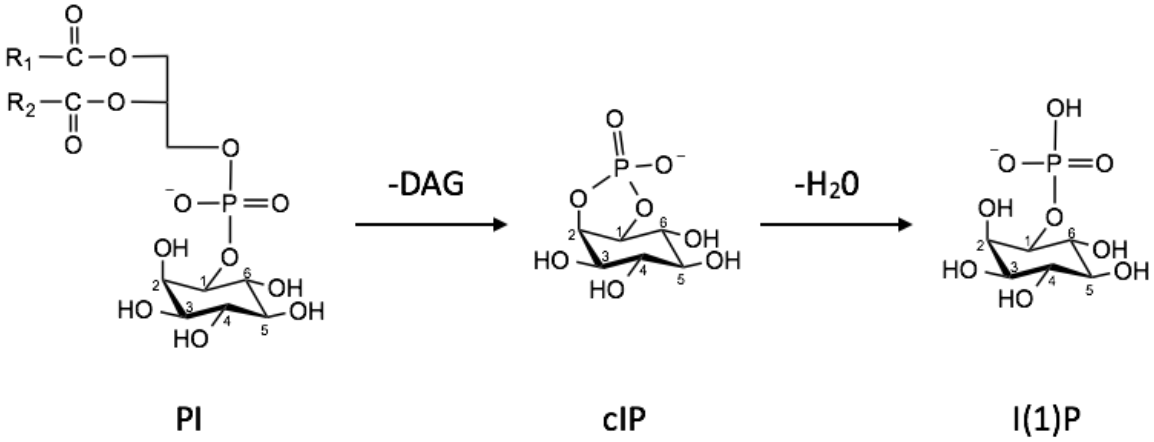

Figure 1. 15 Reaction catalyzed by *L. monocytogenes* PI-PLC.

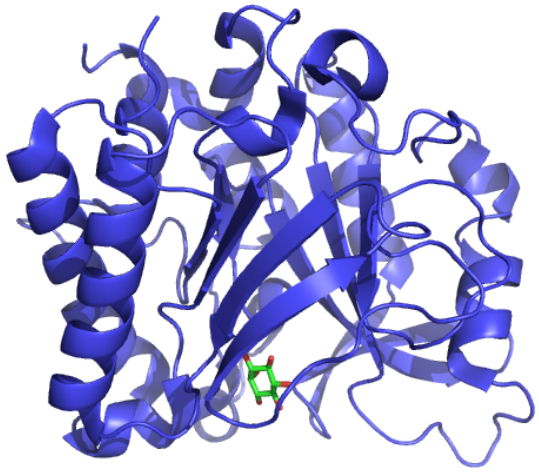

Figure 1.16 Crystal structure of PI-PLC from *L. monocytogenes* (PDB code: 1AOD) with inositol (green) bound in the active site.

The detailed role of PI-PLC in *L. monocytogenes* virulence is still unclear. Studies with a *plcA* deletion mutant revealed only a slight reduction in virulence and in the ability

of the bacterium to escape from the primary phagosomes of murine bone marrow macrophages [Smith et al., 1995]. The absence of PI-PLC led to only a small defect in infection in mouse models (threefold increase in LD_{50}) and the cell-to-cell spread was unaffected [Smith et al., 1995; Camilli et al., 1991, 1993]. However, a double mutant lacking both PI-PLC and PC-PLC is more than 500-fold less virulent than the wild-type strain [Smith et al., 1995; Camilli et al., 1991, 1993]. Overall, it seemed that PI-PLC has a minor individual role in virulence, but acts synergistically with PC-PLC and LLO, to achieve the most efficient vacuolar escape.

1.5 Issues addressed in the thesis

The research reported in this thesis focused on three proteinaceous virulence factors of the intracellular bacterial pathogen *Listeria monocytogenes*: listeriolysin O (LLO), broad-range phospholipase C (PC-PLC), and phosphatidylinositol-specific phospholipase C (PI-PLC). All three of the proteins contribute to the successful escape of the bacteria from acidifying vacuoles that immediately surround them upon entering the host cells or cell-to-cell spread. My two major projects concerned LLO and PC-PLC; a third project was a collaboration with Dr. Gabe Mitchell from the laboratory of Prof. Daniel Portnoy, University of California, Berkeley, on a relatively new function for PI-PLC in *L. monocytogenes* pathogenicity. In this third project, my role has been to supply *L. monocytogenes* PI-PLC (and selected variants with minimal activity) and PC-PLC for testing in an *in vitro* autophagy assay. I also prepared PI-PLC enzymes from other Gram-positive bacteria. Prior to the work with *L. monocytogenes* virulence factors, I also collaborated with Dr. Chris Pace from the laboratory of Prof. Jianmin Gao, Boston

College, on a project in developing a fluorescent assay to probe transmembrane α-helix association. However, this thesis will present details only of my two major projects on LLO and PC-PLC.

(1) *The roles of D123 and D4 domains in LLO pore-formation*

LLO is essential in mediating disruption of vacuole membranes. For an intracellular pathogen as *L. monocytogenes*, failure in the vacuolar escape results in abortive and avirulent infection. The current model is that C-terminal domain 4 (D4) recognizes and engages the target membrane, where on-membrane oligomerization is prompted by hydrogen bonding between residues in domain 3 from each monomer. Once triggered, each monomer within the oligomer unfurls the α-helices in domain 3 and transforms them into two β-strands. It has been assumed that the sequential and cooperative behaviors of domain 3 were initiated by D4 binding cholesterol-enriched membranes. However, I found that pores could form without all LLO molecules bearing a D4 domain. I cloned and expressed a separate protein containing domains 1, 2, and 3 (D123) and the isolated domain 4 (D4) of LLO, aiming to isolate the events in its membrane binding and pore-formation. D123, even though not membrane-lytic by itself, became hemolytic when trace amounts of LLO were present.

FRET and FCS assays showed that D123 homooligomerizes but also forms heterooligomers with LLO in solution. Flow cytometry, used to investigate protein binding to POPC/cholesterol vesicles and to red blood cells, showed that D123 has no membrane binding affinity on its own, but becomes membrane-localized with sub-lytic amounts of LLO.

My results indicate that the cooperative conformational change that leads to membrane insertion and pore formation can occur in some monomers in the absence of the D4 anchor. Thus, this change does not use D4 as an intramolecular trigger. This is a new and intriguing insight into LLO membrane penetration mechanism.

(2) *Characterization of metalloenzyme PC-PLC.*

The gene of *L. monocytogenes* PC-PLC was obtained from Prof. Helene Marquis, Cornell University; the metalloprotein was for the first time, cloned, recombinantly expressed, and purified into a homogeneous and active form. The kinetic features and mechanism of PC-PLC were systematically studied through my work. While a homology structure for the protein could be constructed based on the crystal structure of the *B. cereus* PC-PLC, I showed that there are significant differences in the enzymatic activities of these two proteins that are likely important for their pathogenicity.

PC-PLC is a metalloenzyme, however, the content and association properties of zinc ions has been little characterized. These issues were addressed in my work. The dissociation constants of the three zinc ions from PC-PLC were estimated to range between 0.05 to 60 μM. However estimations of the K_d for Zn^{2+} from kinetics (with 5 mM diC_6PC as substrate at pH 6.0), suggest a much tighter binding of Zn^{2+}, perhaps suggesting a cooperative binding of the last zinc ion and substrate.

The enzymatic activity of PC-PLC towards a wide variety of substrates was examined. Substrates included long-chain phospholipid (PC, PE, PG, PS, SM) in vesicles (LUVs, SUVs) and micelles (Triton X-100), and short-chain PC molecules (diC_4PC, diC_6PC, diC_7PC) mono-dispersed in solutions. I found that PC-PLC from *L. monocytogenes* has an acidic pH optimum (5.5~6.5), for all substrates. Some amount of hydrophobicity is

needed for the substrate since PC-PLC prefers long-chain lipids over short-chain lipids - a preference due to the improved substrate affinity (K_m) instead of turnover rate (k_{cat}). In evaluating binding studies of the enzyme to vesicles (using FCS), I show that the peripheral membrane association is pH-independent with the presence of 50 μM of Zn^{2+} and that the apparent K_d of PC-PLC to POPC/POPG SUVs was very close to the K_m for monomeric diC_7PC.

I also attempted to look for potential synergistic interactions of LLO and PC-PLC in their membrane disruption activity. However, under my experiment conditions little to no such synergism was found. Specifically, there were little effects in membrane lytic activity of LLO from the addition of PC-PLC, and PC-PLC enzymatic activity experienced no significant augment with the presence of LLO.

In summary, the zinc coordination and enzyme activity of PC-PLC were characterized, providing knowledge for the community to better analyze its function in pathogenicity *in vivo*. Synergism of LLO and PC-PLC was not found, suggesting they have independent roles in vacuolar escape.

Chapter 2 Materials and Methods

2.1 Materials

1-Palmitoyl-2-oleoyl-*sn*-glycero-3-phosphocholine (POPC) and 1,2-dioleoyl-*sn*-glycero-3-phosphoethanolamine-N-(lissamine rhodamine B sulfonyl) (ammonium salt) (DOPE-rhodamine), 1,2-dibutyryl-*sn*-glycero-3-phosphocholine (diC_4PC), 1,2-dihexanoyl-*sn*-glycero-3-phosphocholine (diC_6PC), 1,2-diheptanoyl-*sn*-glycero-3-phosphocholine (diC_7PC) and 1,2-dioleoyl-*sn*-glycero-3-phospho-(1'-*rac*-glycerol) (sodium salt) (DOPG), 1,2-di-(9Z-octadecenoyl)-sn-glycero-3-phospho-L-serine (sodium salt) (DOPS), 1,2-dioleoyl-sn-glycero-3-phosphoethanolamine (DOPE) were obtained from Avanti Polar Lipids (Alabaster, AL) and used without further purification. Most of the phospholipids were purchased as dry powders. *n*-Dodecylphosphocholine (DPC) was purchased from Affymetrix (Santa Clara, CA). Alexa Fluor 488 (Alexa488) and Alexa Fluor 555 (Alexa555) succinimidyl esters and Alexa Fluor 488 C_5 maleimide were obtained from Molecular Probes (Eugene, OR). Isopropylthio-β-galactoside (IPTG), ampicillin, and kanamycin were obtained from American Bioanalytical (Natick, MA). Human red blood cells (RBC) were obtained from Research Blood Components (Boston, MA). Other chemicals were reagent grade from Sigma-Aldrich (St. Louis, MO) unless specifically stated.

Escherichia coli strains XL-1 Blue (Stratagene, La Jolla, CA) were used for cloning. *E. coli* strains BL21-AI (Life Technologies, Carlsbad, CA) were used for protein PC-PLC expression and strains BL21(DE3)PlysS were used for protein LLO and PI-PLC expression. All *E. coli* strains were grown in Luria-Bertani broth (LB; Fisher, Hampton, NH).

2.2 Production and fluorescent labeling of recombinant proteins

2.2.1 Plasmids and gene isolations

The pET29a-*hly* plasmid containing the gene for LLO was a generous gift from Professor Daniel A. Portnoy, University of California, Berkeley. The LLO gene in this plasmid served as the template for PCR to obtain the coding regions specifically for D123 and D4; Phusion Hot Start High-Fidelity DNA Polymerase (Fisher Scientific, Pittsburgh, PA) was used for the PCR.

The gene for the PC-PLC from *L. monocytogenes* encoded in a pET vector (pET-*plcB*) was obtained from Dr. Helene Marquis, Cornell University.

The gene for expression of *L. monocytogenes* PI-PLC, in the vector pTYB11-*plcA,* was previously generated by Dr. Wei Chen in the Roberts Laboratory [Chen et al., 2009].

2.2.2 Expression and purification of LLO

Overexpression and purification of recombinant protein LLO was done following published protocols [Glomski et al., 2002]. Specifically, expressing strains were grown to stationary phase and inoculated into 1 L fresh LB media. After 90 min of shaking at 30 °C, expression was induced by the addition of 1 mM of IPTG and maintained for another 6 hr. The bacterial suspension was centrifuged and the pellet resuspended in 35 ml cold lysis buffer (50 mM sodium phosphate, pH 8.0, 1 M NaCl, 20 mM imidazole, 10 mM 2-mercaptoethanol, 1 mM PMSF). Cells were lysed by ultrasonication. The lysate was centrifuged for 30 min at 17000 g. The supernatant was mixed with 5 ml of Ni-NTA resin (QIAGEN, Venlo, Netherlands) equilibrated in lysis buffer. The mixture was mildly stirred at 4 °C for 1 hr to ensure protein binding. Afterwards, the resin was packed in a

column and unbound protein was washed with lysis buffer until the UV absorbance of the eluate reached baseline. The column was then washed with lysis buffer, pH 6.0, containing 10% glycerol and 0.1% Tween 20. The desired protein was eluted from the column with lysis buffer, pH 6.0, containing 800 mM imidazole. The eluate was dialyzed against storage buffer (lysis buffer, pH 6.0, with 1 mM EDTA). This procedure yielded ~20 mg protein per liter of media.

Expression and purification of D123 and D4 are reported in detail in Chapter 3.

2.2.3 Expression and purification of *L. monocytogenes* PI-PLC

pTYB11-*plcA* was transformed into *E. coli* strain BL21(DE3)pLysS. The bacteria were cultured overnight and inoculated into fresh LB media, until the OD_{600} reached 0.7. Expression of protein PI-PLC was induced with addition of IPTG to the final concentration of 0.4 mM. After 6 h of shaking at 20 °C, cells were harvested. The bacterial suspension was centrifuged and the cell pellet resuspended in column buffer (20 mM HEPES, 1 M NaCl, pH 8.5). After cell lysis, the supernatant was applied to a chitin resin column (New England Biolab, Ipswich, MA). Nonspecifically bound protein was washed off with up to 1 L column buffer. The target protein was eluted after incubation of the resin with 50 mM DTT to initiate cleavage of the PI-PLC from the chitin-containing intein. Excess DTT was removed by dialysis in column buffer containing 2 mM DTT. All steps were performed at 4 °C.

2.2.4 Expression and purification of *S. aureus* PI-PLC

A plasmid containing the gene for the *S. aureus* PI-PLC (PI-PLC$_{Sa}$) was previously constructed in the Roberts laboratory [Cheng et al., 2012]. After transformation of the

gene into *E. coli* expression strain BL21(DE3), a single colony was picked from plate for overnight culture. The resultant overnight culture was inoculated into 1 L of fresh LB media; the cells were incubated at 37 °C until the OD_{600} reached 0.7~0.8. At that point, protein expression was induced with 0.4 mM IPTG. The bacterial suspension was shaken at 225 rpm at 30 °C for 6 h later and then harvested.

Cells were lysed by ultrasonication, and the supernatant containing PI-PLC_{Sa} was separated from cell debris by centrifugation. 5 mL of Ni-NTA resin was used for the supernatant resulting from 1 L of cell culture. Protein was purified following the manufacturer's suggested batch protocol. The eluate from the resin was dialyzed against 20 mM Tris, pH 8.3 to remove imidazole.

After dialysis, the protein was further purified by anion exchange chromatography with Q Sepharose Fast Flow (QFF) resin using an increasing salt gradient from buffer A (20 mM Tris, pH 8.0) to buffer B (20 mM Tris, 0.6 M NaCl, pH 8.0). Target protein eluted at 10~15 mM NaCl. The three most concentrated fractions (5 mL each) were collected and stored at 4 °C until use.

2.2.5 Expression and purification of *B. thuringiensis* PI-PLC

A plasmid containing the gene for the *B. thurngiensis* PI-PLC (PI-PLC_{Bt}), previously produced in the Roberts laboratory, was transformed into the same *E. coli* strain used for PI-PLC_{Sa}. The expression protocol was the same as that of PI-PLC_{Sa}.

Cells were lysed with ultrasonication and lysate were centrifuged. Supernatant was collected for dialysis in 4 L of buffer 20 mM Tris, pH 8.9. After dialysis, the protein was purified first through anion exchange chromatography with QFF resins through an

increasing salt gradient from buffer A (20 mM Tris, pH 8.0) to buffer B (20 mM Tris, 0.6 M NaCl, pH 8.0). Target protein eluted at about 0.25 M NaCl. The three most concentrated fractions (5 mL each) were collected and stored at 4 °C until use.

The pooled fractions of PI-PLC$_{Bt}$ were then applied to a hydrophobic column (Phenyl Sepharose CL-4B) pre-equilibriated with 20 mM Tris, 1 M NaCl, pH 8.0. After protein loading, the column was thoroughly washed until the UV signal no longer decreased. The target protein was eluted with decreasing salt gradient (1 M to 0 M added NaCl in 20 mM Tris, pH 8.0). The eluted protein was concentrated and stored at 4 °C.

2.2.6 Protein concentration and SDS-PAGE

Protein concentration was determined by measuring the absorbance at 280 nm on a Nanodrop 2000c UV/Vis spectrometer. Extinction coefficients, ε_{LLO} = 75,000 $M^{-1}\bullet cm^{-1}$, ε_{D123} = 43,430 $M^{-1}\bullet cm^{-1}$, $\varepsilon_{PIPLC(Sa)}$ = 32,000 $M^{-1}\bullet cm^{-1}$, $\varepsilon_{PIPLC(Bt)}$ = 43,000 $M^{-1}\bullet cm^{-1}$, were calculated based on protein sequences with ProtParam in the ExPASy web site.

Concentrations of PC-PLC were determined using the BCA assay following the manufacturer's protocol [Smith et al., 1985].

The purity of all protein samples in this study were analyzed with 12.5% SDS-PAGE.

2.2.7 Fluorescent labeling of recombinant proteins

LLO and D123 were labeled with Alexa Fluor 488- or 555- succinimidyl ester (Molecular Probes, Eugene, Oregon) on the N-terminal amine. The manufacturer's protocol was employed in labeling, except that the pH for labeling was pH 7 to preferentially react with the N-terminal amine. Protein PC-PLC mutant C143S has only

one cysteine at residue 168. Therefore, C143S was fluorescently labeled with the thiol-reactive dye Alexa Fluor 488 C_5 maleimide [Hermanson, G., 1996].

2.3 Methods

2.3.1 Circular dichroism (CD)

Far UV CD spectra of the proteins, covering the wavelength range 200 ~ 250 nm (1 nm step size with integration time of 10 s), were recorded at 22 °C with a 2 mm light path-length cuvette on an AVIV Circular Dichroism Spectrometer Model 420 (Biomedical Inc., Lakewood, NJ).

Thermal melting data were collected at 222 nm over the temperature range 20 to 100 °C. The ellipticity data were collected in 2 ° steps after a 90 s equilibration time followed by 30 s integration.

2.3.2 Inductively coupled plasma mass spectrometry (ICP-MS)

The ICP-MS analysis of Zn content of *L. monocytogenes* PC-PLC was performed on a Perkin-Elmer NexION 300X ICP mass spectrometer (PerkinElmer, Waltham, MA). The instrument is located at the University of Massachusetts, Amherst, Department of Chemistry, in the Vachet Laboratory. Protein samples were subjected to acid digestion with a mixture of nitric acid and hydrogen peroxide. After digestion, samples were diluted to 10 mL. Triplicate measurements were made for each sample. Both ^{63}Zn and ^{65}Zn were measured under kinetic energy discrimination (KED) mode. ICP-MS operating conditions were as followed: nebulizer flow rate: 0.95 L/min; rf power: 1600 W; plasma Ar flow rate: 18 L/min; dwell time: 50 ms; KED cell gas: 4.6 mL/min.

2.3.3 Nuclear magnetic resonance spectroscopy (NMR)

Specific activity of PC-PLC or PI-PLC towards lipid substrates in the form of monomer, micelle, or liposomes could be measured using ^{31}P NMR spectra acquired on an Agilent Direct Drive 600 MHz spectrometer at 242.9 MHz (Santa Clara, CA). NMR parameters for the different phospholipids were based on previous reports. [Zhou et al., 1997; Qian et al., 1998] At this high field, ^{31}P dipolar relaxation is minimal so there is no appreciable NOE; furthermore, relaxation rates for all species are less than 1 s^{-1} so that there was no saturation of substrate or product resonances under standard acquisition conditions.

For the PC-PLC reaction, enzyme and liposomes were incubated for fixed time at 37 °C, then the reaction was stopped by addition of quenching buffer (2 M Tris, 0.4% g/mL SDS, pH 8.0) to one third of the reaction volume and immediate boiling of the sample for 5 min. PI-PLC reactions were quenched by addition of glacial acetic acid (one third the volume of the reaction). In each reaction, the substrates (phospholipids) and the products (phosphorylated head groups) of the phospholipases have distinct ^{31}P chemical shifts in the NMR spectrum, as shown in Figure 2.1. The relative concentration of each species is proportional to the integrated area of its ^{31}P resonance. A comparison of the product peak to the substrate one allows us to calculate the rate of conversion from substrate to product. All the activity measurements were taken before the conversion reached 10% of substrate so that initial rate conditions applied.

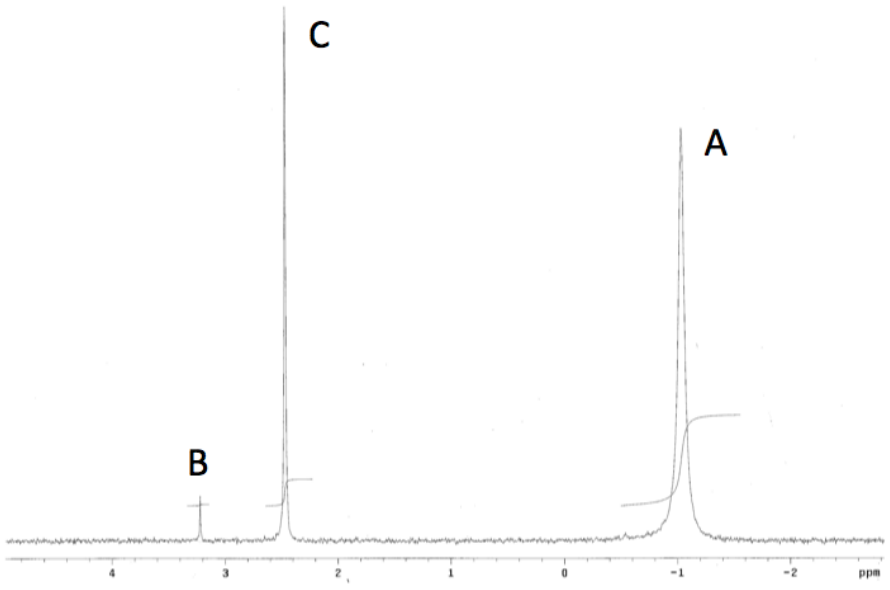

Figure 2.1 ^{31}P NMR spectrum of the hydrolysis reaction of POPC catalyzed by PC-PLC. Substrate POPC and product phosphorylcholine are represented in the spectrum as peak A and B, respectively. Inorganic phosphate was added as an external standard; the Pi is labeled C. The relative ratio of each species could be calculated by integrating the area of each peak.

2.3.4 Fluorescence correlation spectroscopy (FCS)

Fluorescence correlation spectroscopy (FCS) uses a fluorescent microscope and optics that can detect fluorescence intensity fluctuations in a very small volume (Figure 2.2). The typical size of the laser focus is sub-femtoliter (~1 μm^3). Therefore, diffusion behavior of fluorescent molecules can be monitored down to a single molecule level. With the analysis of the cross-correlation curve, important information such as concentration and diffusion coefficient of the fluorescent particles can be obtained. The diffusion coefficient is related to the size of the particles in the solution. In the experiment where protein associates with liposomes, the two particles have drastically different sizes. By monitoring the variation of diffusion coefficient in the solution, we

can deduce the fraction of protein bound in the liposomes, f, and thereby follow the process.

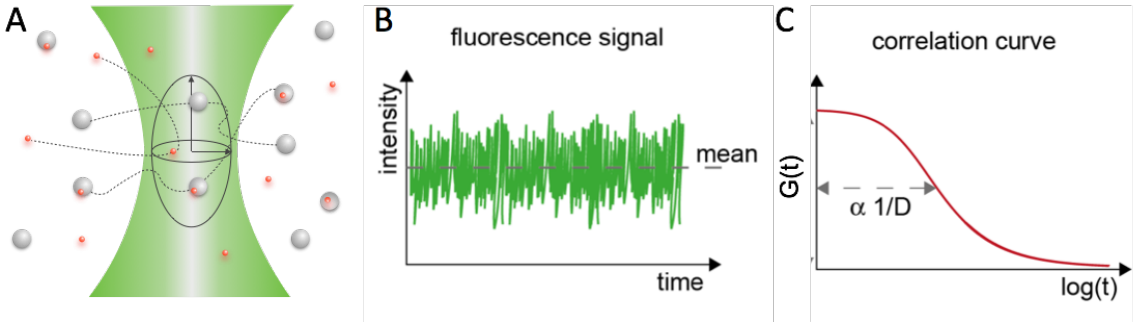

Figure 2.2 Analysis of diffusion behavior of fluorescent particles by FCS. (A) Only a few particles were observed via the tiny laser focus (~μm^3) in FCS device. Red particles: fluorescently labeled protein; grey particles: non-fluorescent vesicles. (B) Fluorescence intensity fluctuation curve recorded with time. (C) Correlation curve derived from fluctuation curve, the width of which is related to the diffusion coefficient (D) of the fluorescent particles.

The FCS instrument was a home-built confocal setup based on an IX-70 inverted microscope (Olympus) as previously described [Pu et al., 2009a, 2009b]. Experiments were carried out at 20 °C with samples in chambered cover glass wells. Prior to use, the chambers were coated with 10 mg/mL of BSA and rinsed with reaction buffer with 1 mg/mL of BSA to prevent protein adhesion to the sides of the wells. Protein samples (250 μL) were in MES-buffered saline (20 mM MES, 150 mM NaCl, pH 5.5) or HEPES-buffered saline (20 mM HEPES, 150 mM NaCl, pH 7.4) with 1 mg/mL of BSA. The averaged diffusion coefficients, D, of fluorescent species were calculated as described previously [Pu et al., 2009a, 2009b]. Specifically, the relationship of the autocorrelation or cross-correlation, G (τ), with fraction bound f, is shown in the equation 2.1, where <N> is the time-averaged number of protein molecules in the detection volume, τ_{free} and

τ_{bound} are the diffusion times for free and vesicle-bound protein, respectively, and S is the ratio of the axial (z) to the radial (x-y) dimension for the effective volume. The diffusion time is given by $\tau_{species}=\omega_o^2/4D_{species}$, where $D_{species}$ is the diffusion coefficient for each species (free or bound) and ω_o is the radius of the observation volume in the x-y plane. The values of S and ω_o were determined at the beginning and end of each day of experiments using the calibration dye rhodamine 119 with a reported D=280 $\mu m^2/s$ [Magde et al., 1974].

Eq 1
$$G(\tau) = \frac{1}{\langle N \rangle}\left((1-f)\left[\left(1+\frac{\tau}{\tau_{free}}\right)\sqrt{1+\frac{\tau}{S^2\tau_{free}}}\right]^{-1} + f\left[\left(1+\frac{\tau}{\tau_{bound}}\right)\sqrt{1+\frac{\tau}{S^2\tau_{bound}}}\right]^{-1}\right)$$

2.3.5 Fluorescence resonance energy transfer (FRET)

Steady-state fluorescence experiments assessing interactions of LLO and D123 were carried out on a Fluorolog-3 Spectrometer (Edison, NJ). Fluorescently-labeled D123 (D123-Alexa488) serving as the donor was added to phosphate buffer (10 mM sodium phosphate, 100 mM sodium chloride), at either pH 5.5 or pH 7.4, to a final concentration of 0.2 μM. LLO labeled with a fluorophore acceptor (LLO-Alexa555) was titrated into the solution. The fluorescence of donor D123-Alexa488, measured at 515 nm upon excitation at 485 nm, decreased as the concentration of acceptor LLO-Alexa555 increased, indicating FRET between the two labeled proteins. The FRET efficiency was evaluated as $(I_D–I_{DA})/I_D$, where I_D is the fluorescence of donor in the absence of acceptor, and I_{DA} is the fluorescence in the presence of different concentrations of acceptor protein.

2.3.6 Trypsin digestion

Trypsin digestion was used to investigate the accessibility of the LLO D4 domain when it was incubated in solution with or without liposomes. D4 (50 μM) in Tris buffer, pH 8.0, in the absence or presence of 20 mM LUVs (lipid/protein ~ 400:1), was mixed with trypsin (0.1% mass of D4) and incubated at 22 °C. At different time points (0, 10, 30, 60, 100 min), 20 μl of each reaction was taken out, and the digestion reaction was terminated by addition of 10 μl of SDS gel loading buffer, followed by boiling at 95 °C for 10 min. Proteolysis products as a function of time were analyzed by SDS-PAGE using 12.5 % gels.

2.3.7 Liposome preparation

Dry lipids were dissolved in chloroform and mixed in the desired ratio. Chloroform was removed with a rotary evaporator and the resultant film was dried under vacuum overnight. The dry lipid films were re-suspended in buffers, producing multilamellar vesicles (MLVs). Large unilamellar vesicles (LUVs) were prepared by extrusion of MLVs through polycarbonate membranes with 100 nm pores using an Avestin lipid extruder (Avestin, Ottawa, ON); the extrusion was repeated more than 30 times to generate a fairly homogeneous population of LUVs. Small unilamellar vesicles (SUVs) were prepared by ultrasonication of MLVs until solutions became optically clear. This generates small, curved vesicles with most diameters between 200-300 Å.

2.3.8 Calcein leakage assay

The membrane lytic activity of LLO and its domain D123 was measured with calcein-containing vesicles. In the experiment, large unilamellar vesicles (LUVs) were made with concentrated fluorescent dye calcein (40 mM) in the corresponding buffers. Any free calcein in the solution was removed by buffer exchange via gel filtration on an ÄKTA FPLC with Hiload 16/60 Sephacryl S-500 HR prep grade column. Calcein is an interesting fluorophore that is self-quenched when concentrated in solution. Therefore, the calcein encapsulated vesicles had minimal fluorescence. When the membrane integrity of the vesicles is disrupted by a membrane lytic agent, such as LLO, the entrapped fluorescent dye leaks out into bulk solution. Upon this dilution of the dye, the fluorescence is significantly enhanced. The fluorescence increase is a measure of the vesicle membrane leakage. The addition of 0.1% Triton X-100 to the vesicle solution is used as positive control (the detergent lyses all the vesicles), while the addition of buffer serves as negative control. The difference in fluorescence between the positive and negative controls is a measure of maximum (total) leakage. The fluorescence observed with LLO can then be linked to the amount of total calcein released into solution. LLO, D123, or D4 was serially diluted into a solution of 20 mM HEPES/sodium acetate, 150 mM NaCl, pH 5.5 or pH 7.4 buffer, containing LUVs (100 μM phospholipid) encapsulating 40 mM calcein. Fluorescence of the calcein in the samples was monitored at 525 nm (excitation at 485 nm) using a SpectraMax M5 Microplate reader (Molecular Devices, Sunnyvale, CA). Fractional leakage, measured after 2 h incubation at 22 °C, was calculated as $(I_{protein} - I_{buffer})/(I_{+TX\text{-}100} - I_{buffer})$, where I_{buffer} is the fluorescent intensity when the liposomes were mixed with buffer without any added proteins and $I_{+TX\text{-}100}$ is the

intensity after the addition of 0.1 % Triton X-100 to the buffer containing calcein loaded vesicles.

2.3.9 Hemolytic assay

Human red blood cells were washed three times in phosphate buffered saline (PBS, 10 mM Na_2HPO_4, 1.8 mM KH_2PO_4, 137 mM NaCl, 2.7 mM KCl), pH 7.4, and resuspended to 2% (v/v) in PBS at pH 7.4 or pH 5.5 (adjusted with HCl). Proteins were diluted to various concentrations in the appropriate pH buffer and mixed 1:1 (v/v) with the red blood cell solution. Three samples were prepared and monitored for each protein concentration. The resulting mixtures were gently shaken and incubated at 37 °C for 1 h, followed by centrifugation. Aliquots of the supernatant from each sample were transferred to a 96-well plate for absorbance measurement at 545 nm using the SpectraMax M5 Microplate reader. The fractional hemolysis was calculated from the absorbance as $(A_{protein} - A_{buffer})/(A_{+TX\text{-}100} - A_{buffer})$. PBS buffer at pH 5.5 or pH 7.4 was mixed with cells (no LLO or other recombinant protein) to yield A_{buffer}, and complete hemolysis was achieved by the addition of 0.1 % Triton X-100 to the buffer.

2.3.10 Induction of eryptosis (red blood cell apoptosis)

Fresh erythrocytes were washed three times in PBS, pH 7.4. Cells were stimulated with 5 μM Cu^{2+} in Ringer buffer as previously described [Lang et al., 2007] for 16 h. Phosphatidylserine exposure on the apoptotic cell membrane was assessed through the binding of annexin V [van Engeland et al., 1998]. After copper incubation, cells were washed in PBS and resuspended in annexin-binding buffer: 10 mM HEPES, 140 mM

NaCl, 2.5 mM $CaCl_2$, pH 7.4. The cells were mixed with 3 μl of annexin V, R-phycoerythrin conjugate (Life Technologies, Grand Island, NY) or D123-Alexa555 at a final concentration of 10 nM. The mixtures (cell density ~ 5×10^6 cells/mL) were incubated for 15 min in the dark at room temperature before flow cytometry analysis.

2.3.11 Flow cytometry

This technique was used to assess the binding of the recombinant LLO and D123 proteins to liposomes and to human erythrocytes. In the liposome binding experiment, LUVs composed of POPC/cholesterol (2:1) with 0.1 mol% DOPE-rhodamine were mixed with Alexa488 labeled proteins. To assess binding to human erythrocytes, the cells were resuspended in PBS, pH 5.5, at a concentration of 5×10^6 cells/mL, and incubated with proteins labeled with Alexa488 or Alexa555 for 10 min. Alexa488 was detected using the FITC channel (530±15 nm band pass filter), and Alexa555 and rhodamine were detected using the PE channel (585±21 nm band pass filter). Flow cytometry experiments were carried out on a BD FACSAria cell sorter (BD Biosciences, San Jose, CA). Data analysis was performed with Flowjo (Tree Star, Ashland, OR).

2.3.12 Phosphate colorimetric assay for PC-PLC activity

PC-PLC activity on monomer-dispersed substrates diC_4PC, diC_6PC, and diC_7PC in solution was measured with a phosphate colorimetric assay using slight modifications of a published protocol [Hergenrother et al., 1997]. Hydrolysis of the PC substrates yields DAG and a phosphomonoester. The addition of alkaline phosphatase converted the

phosphomonoester to inorganic phosphate (Pi) and an alcohol. The Pi produced was quantified with a malachite green colorimetric assay [Lanzetta et al., 1979].

Reactions (100 μL) were carried out in various buffers: 20 mM of buffering agent (MES for pH 5.0, 5.5, 6.0, MOPS for pH 6.5, 7.0, HEPES for pH 7.5, 8.0, 8.5), 150 mM NaCl, 0.1 mg/mL bovine serum albumin (BSA), 50 μM $ZnSO_4$, and the desired concentration of substrate. The reaction temperature was 37 °C. Buffers were pre-warmed for at least 20 min before the reaction was initiated by the addition of PC-PLC. After 5, 10, 15, 20, 25, 30 min of each reaction, 15 μL of reaction mixture was removed and quenched by mixing with 5 μL of quenching buffer (2 M Tris, 0.4% g/mL SDS, pH 8.0) and boiling for 10 min. The phosphomonoester was then dephosphorylated by addition of 40 unit/ml of alkaline phosphatase (APase), producing inorganic phosphate (Pi) stoichiometric to the released phosphomonoester. The Pi was then quantified with a malenchite green assay, in which the inorganic phosphate forms a strong complex with molybdate. [Lanzetta et al., 1979] The complexed Pi was quantified by its absorbance at 650 nm. The absorbance measurement was carried out in triplicate in the microplate reader.

2.3.13 Transmission electronic microscopy (TEM)

Before TEM, 1 mM of LUVs with POPC/cholesterol ratio of 2:1 was incubated with 1 μM of LLO at room temperature for 1 h. 2 μl aliquots of the liposome-LLO suspension were taken and attached to glow discharge-treated carbon support films, washed rapidly by touching to one 2-μl droplet of distilled water, and stained by touching to a 2-μl droplet of negative staining solution (2% phosphotungstic acid, pH adjusted to pH 7.0 by

NaOH). Specimens were examined and photographed in a JEOL 200CX transmission electron microscope, operated at 200 kV.

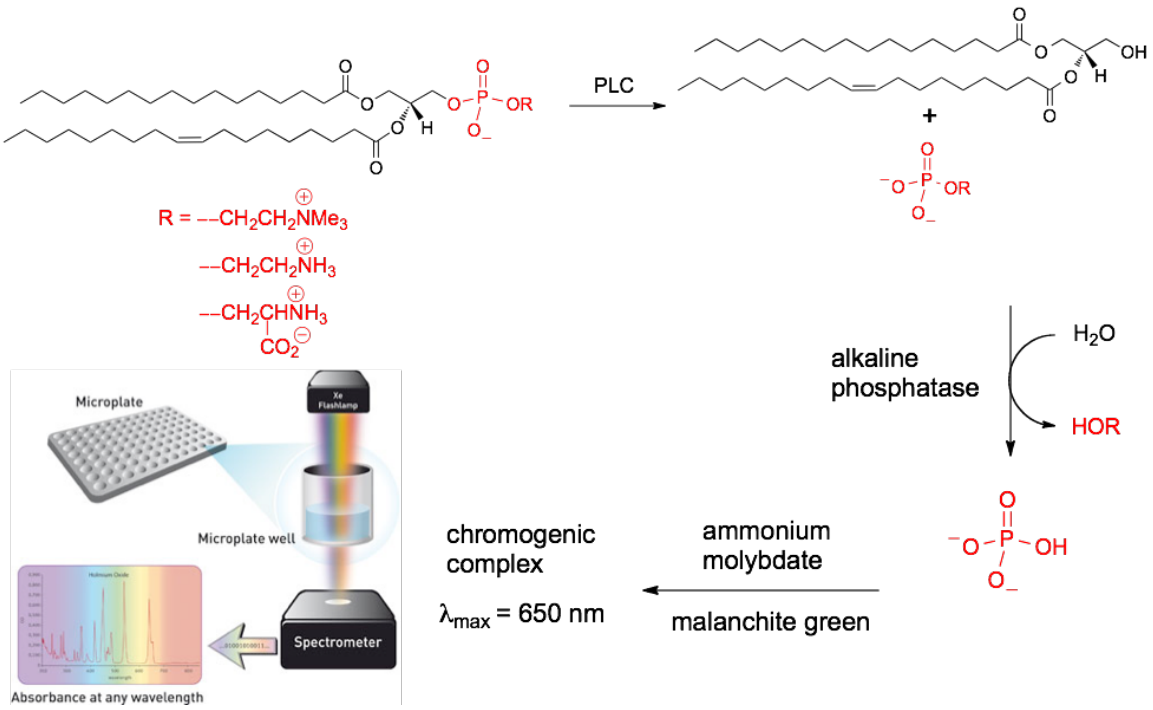

Figure 2.3 Schematic representation of the phosphate colorimetric assay for phospholipase activity. Substrates (various phospholipids with different head groups, shown in red) were hydrolyzed to produce diacylglycerol and a phosphomonoester (in red). The latter was dephosphorylated by alkaline phosphatase (APase) producing inorganic phosphate (Pi) that was complexed with ammonium molybdate and malanchite green. The absorbance of the complex at 650 nm was used to quantify product.

Chapter 3 Listeriolysin O and Domains

This part of my research set out to separate the functional units of LLO and to explore their membrane binding and hemolytic activity individually, as well as their interactions with the full-length cytolysin LLO. Proteins consisting of domain 1 through 3 (D123) or domain 4 (D4) were separately cloned and expressed. D123 is a soluble protein (although it aggregates at low concentrations in solution) that does not bind to membranes, although it contains the sequence that becomes the pore-forming β-strands. Even though D123 has no membrane-lytic activity on its own, D123 could bind to membranes and aid in hemolysis by associating with low concentrations of full-length LLO. This shows that not all LLO molecules need D4 cholesterol recognition domain to participate in pore formation. In contrast to D123, D4 is very hydrophobic and tends to associate with interfaces irrespective of the presence of cholesterol. When solubilized in micelles, D4 adopts a predominantly β-structure conformation likely reflecting its membrane binding conformation.

3.1 Protein preparation

3.1.1 Gene construction

The genes coding for D123 and D4 were obtained through polymerase chain reaction (PCR) amplification of pET29a-*hly* using Phusion Hot Start High-Fidelity DNA Polymerase. Primers for D123 included 5'-CGTCG**CATATG**AAGGATGC-3' (to introduce the *Nde*I site) and 5'- CAT**CTCGAG**TCATGAAGTTGTTTCAA-3' (*Xho*I

site). The D4 primers were 5'- ATGC**CATATG**AAAGCTTATACAGATGGAAAA-3' (the *Nde*I site) and AATG**GGATCC**TTATTAGTGGTGGTG (the *Bam*HI site). After the restrictive digestion, the amplified fragment of gene of D123 was ligated into a pET-28a plasmid and that of D4 into a pET-30a plasmid. DNA constructs were sequenced to confirm the correct DNA was generated.

3.1.2 D123 and D4 protein expression and purification

Recombinant D123 has an N-terminal His_6-tag, and D4 has a C-terminal His_6-tag (as does LLO). D123 was expressed and purified using the protocol for full-length LLO [Glomski et al., 2002]. The same expression protocol for D4 led to packaging of the protein in inclusion bodies. Inclusion bodies often contain almost exclusively the over-expressed protein. The protein is thought to aggregate because proper folding of the proteins lags behind the super fast translation. Segregation into inclusion bodies could also indicate the aggregation of a fairly hydrophobic protein.

If the target protein in inclusion bodies can be converted into a soluble and native form, it would be a relative convenient way to obtain abundant target protein. Therefore the D4 protocol was modified to purposely express and purify D4 in inclusion bodies. For this, the culture temperature was kept at 37 °C after induction with 1 mM of IPTG, and the expression lasted for 4 h. After cell harvest and lysis, the pellet was extensively washed with Tris storage buffer (10 mM Tris 150 mM NaCl, pH 8.0), 1 % Triton X-100 in Tris buffer, and then Tris buffer again. This treatment removed most of the membrane components and other proteins from the pellet. The remaining pellet, consisting largely of D4, was solubilized with Tris buffer containing 1 mM sodium dodecyl sulfate (SDS). The

SDS was partially removed by overnight dialysis at 4 °C against Tris buffer containing 5 mM DTT. Dialysis to remove all the SDS caused the protein to precipitate.

D4 was purified (and detergent exchanged) via size-exclusion chromatography using Sephadex G-150 pre-equilibrated with Tris storage buffer containing 2 mM dodecylphosphocholine (DPC). DPC is a mild non-ionic detergent with a phosphocholine head group. The dialyzed D4 was loaded on the column, and fractions containing D4 were pooled and dialyzed against Tris storage buffer with 5 mM DTT. In contrast to LLO and D123, D4 was found to aggregate at low pH (< 6) as assessed by dynamic light scattering (data not shown), hence it was stored in 10 mM Tris storage buffer, pH 8.0, with 5 mM DTT.

An example of the protein purity achievable is shown in Figure 3.1.

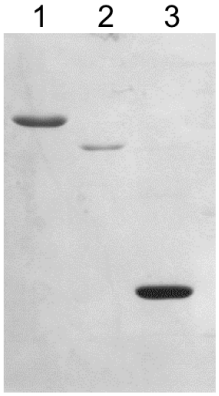

Figure 3.1 SDS-PAGE analysis of purified recombinant proteins LLO (lane 1: 57 kDa), D123 (lane 2: 44 kDa), and D4 (lane 3: 14 kDa).

Recombinant LLO, D123, and D4 were purified to over 95% purity as analyzed by SDS-PAGE (Figure 3.1).

3.2 Protein characterization

3.2.1 Circular dichroism

A circular dichroism spectrum showed that D123 had a mixture of α- and β-structures (Figure 3.2) in 50 mM sodium phosphate buffer, 150 mM NaCl, 5 mM DTT, pH 6.0. This balance of secondary structure for D123 is consistent with the crystal structures of CDC proteins [Rossjohn et al., 1997; Boudeau et al., 2009; Polehina et al., 2005].

D4 was initially solubilized in SDS micelles and then exchanged to milder nonionic and phospholipid-mimic dodecylphosphocholine (DPC) micelles. In DPC micelles the D4 exhibited secondary structure dominated by β-sheets (Figure 3.2), consistent with the structure of the D4 domain in other CDCs. In the thermal melting experiment, protein was slowly heated up to 100 °C in the CD cuvette, and the ellipticity at 217 nm was monitored as function of temperature (Figure 3.3 filled squares). For DPC micelle-solubilized D4, the transition in secondary structure was quite sharp, indicating an initial well-folded structure for the domain. In contrast, in SDS micelles (Figure 3.3 empty squares), the CD signal of D4 became less negative tracking the initial part of the thermal curve for the domain in DPC micelles. The lack of a cooperative unfolding transition in the heating process suggests a different unfolding mechanism for the D4 in SDS micelles, where only partial local unfolding of the D4 occurs over the same temperature range. The strong anionic detergent SDS often binds to membrane proteins allowing them to stay folded (at least until heating to high temperatures).

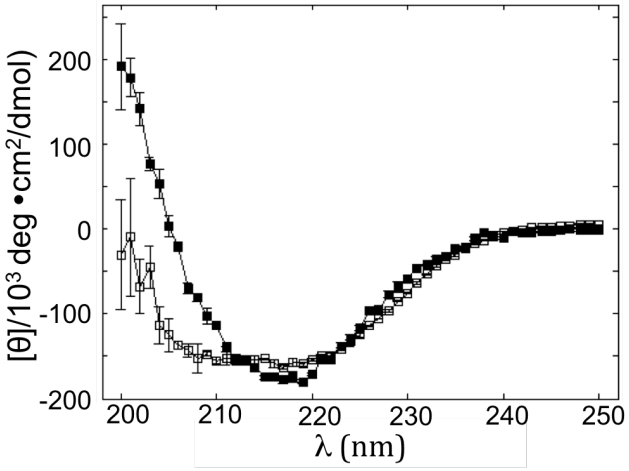

Figure 3.2 CD spectra of D123 (empty squares) in 50 mM phosphate buffer, 150 mM NaCl, 5 mM DTT, pH 6.0, and D4 (filled square) in 2 mM DPC micelles, 10 mM Tris buffer, 150 mM NaCl, pH 8.0.

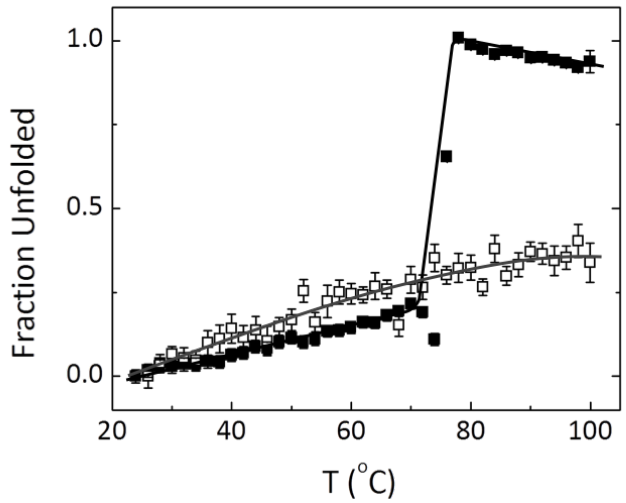

Figure 3.3 Thermal denaturation curve of D4. Fraction of unfolded D4 protein (f_U) solubilized in 2 mM DPC micelles (filled square) and D4 in 2 mM SDS micelles (empty square), with Tris storage buffer, as a function of increasing temperature. f_U at each temperature was calculated from the CD signal at 217 nm.

3.3 Vesicle and cell membrane binding

3.3.1 Binding of LLO and domains to LUVs

Flow cytometry was utilized to study protein binding to liposomes. In the experiment, the liposomes were made with POPC and cholesterol in the molar ratio of 2:1, and were fluorescently labeled with 0.1 mol% of 1,2-dioleoyl-sn-glycero-3-phosphoethanolamine-N-(lissamine rhodamine B sulfonyl). All proteins of interests were labeled with Alexa Fluor 488 at the N-terminus. The fluorescence of both dyes, rhodamine (on LUVs) and

Alexa Fluor 488 (on protein), could be monitored with flow cytometry via distinct channels; these are displayed as the y-axis and x-axis in the plots (Figure 3.4). Panel A and B show protein LLO binding to liposomes at pH 5.5 and pH 7.4. This experiment shows that LLO bound efficiently to LUVs with 33 mol% cholesterol at both pH 5.5 (Figure 3.4 A) and pH 7.4 (Figure 3.4 B), as most of the particles, which were rhodamine fluorescence positive (y-axis) were also detected as Alexa Fluor 488 positive (x-axis). These "double-positive" particles indicated association of proteins with liposomes. In each plot (A and B), there are two noticeable distinct particle populations (*a* and *b*). The maximized fluorescence intensities of each population are summarized in Table 1. From the data in the table, we can see the fluorescence intensities of the lipids in the two populations are comparable, indicating these vesicles are of similar sizes. However, the protein fluorescence and the ratio of protein-to-lipid fluorescence are different, and both are higher at pH 5.5 (Table 1), indicating enhanced binding at the acidic pH. It is not entirely clear what these two populations of liposomes are, but their detection by the cell sorter indicates these particles are probably fairly large size in comparison with normal LUVs (100~200 nm). These large particles are likely to be aggregated lipid vesicles of two different protein/vesicle populations arising from membrane lysis of LLO, as seen in the TEM images of liposomes with LLO (Figure 3.5).

In contrast to LLO, D123 does not bind to the vesicles (Figure 3.4 C). However, about 30% of the D123 could be detected in association with the LUVs when an equal amount of unlabeled LLO was added (Figure 3.4 D), suggesting D123 may associate with the target membrane through interactions with the full-length protein.

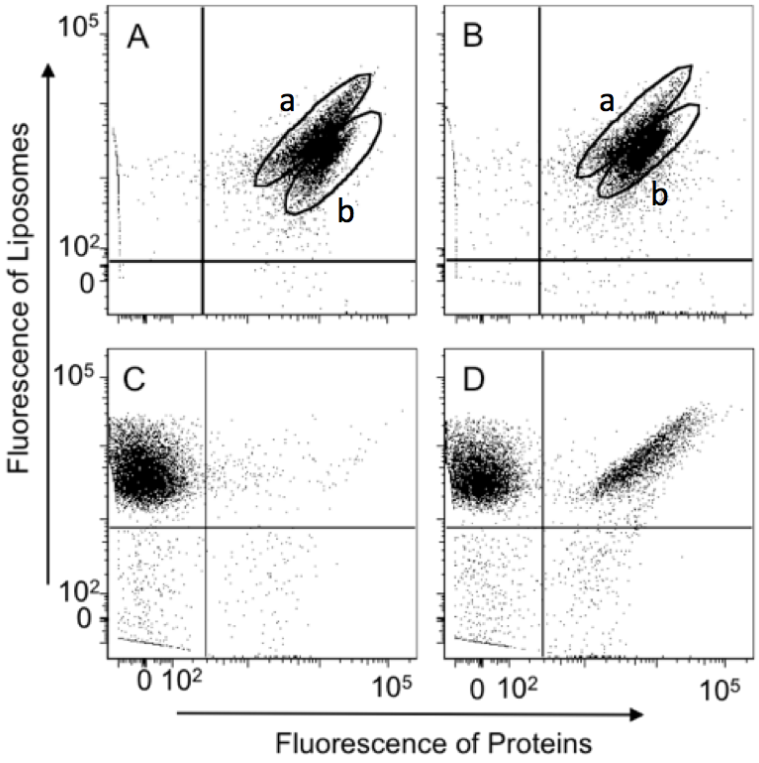

Figure 3.4 LLO and D123 binding to 100 μM of POPC/cholesterol (2:1) LUVs monitored using flow cytometry. LUVs were mixed with (A) 100 nM LLO-Alexa488 at pH 5.5, (B) 100 nM LLO-Alexa488 at pH 7.4, (C) 50 nM D123-Alexa488 at pH 5.5, and (D) 50 nM D123-Alexa488 and 50 nM of LLO at pH 5.5.

Table 1. Population percentage and peak fluorescence of particle species *a*, *b* in LLO binding to POPC/cholesterol (2:1) LUVs.

	Population	**Percentage**	**Peak protein fluorescence (I_P)**	**Peak lipid fluorescence (I_L)**	**I_P/I_L**
pH 5.5	*a*	40.9	8619	3319	2.6
	b	40.8	12344	1815	6.8
pH 7.4	*a*	21.8	4508	3822	1.2
	b	59.8	6652	2210	3

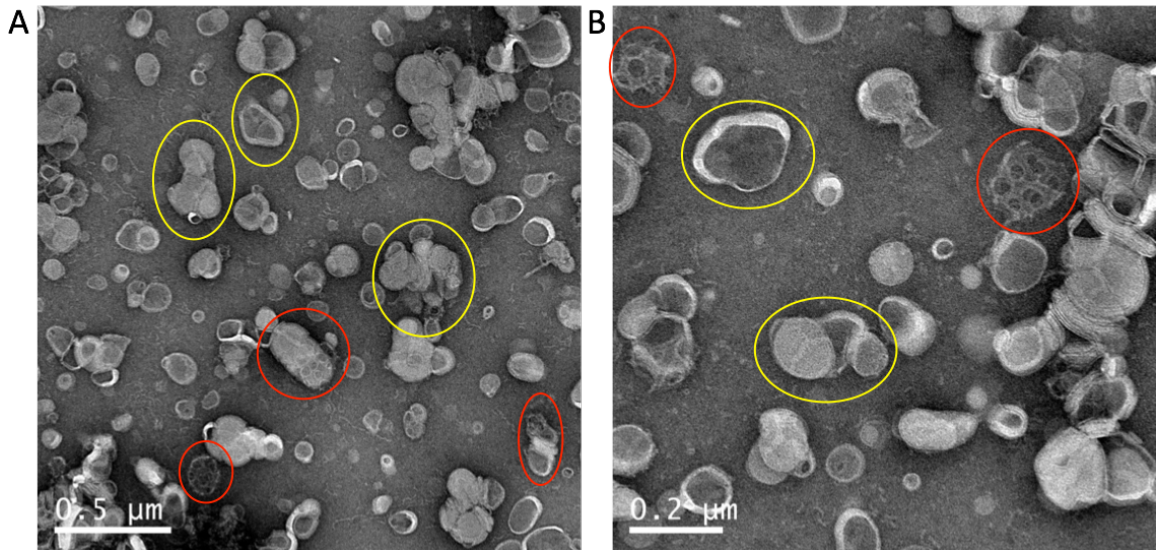

Figure 3.5 TEM images of POPC/Cholesterol (2/1) LUVs after 1 h of incubation with LLO (lipid/protein ratio: 1000) in phosphate buffer pH7.4 at room temperature. Representative liposome aggregates with significant LLO binding are shown in red circles; and the ones with less protein aggregates are in yellow circles.

3.3.2 Binding of LLO and domains to human red blood cells

To test whether the interaction between LLO and D123 on liposomes translates to binding to live cells, we explored the binding of LLO and D123 to human red blood cells. LLO is known to bind to human red blood cells, causing severe damage to the cells, and inducing apoptosis at low (nanomolar or subnanomolar) concentrations [Carrero et al., 2004]. Induction of apoptosis by LLO is rapid, and occurs through both caspase-dependent and -independent pathways. I checked the disruption of red blood cells induced by incubation with various amount of full-length LLO through the flow cytometry light scattering. The results were consistent with the apoptogenic characteristic of LLO, as shown in Figure 3.6. With increasing amounts of LLO, from 0.1 to 0.5 nM, a second population, indicated by *b*, is detected; this population is distinct from that of the

live cells (labeled *a*), as shown in Figure 3.6 A. The second population of cells, *b*, appeared higher in the side scattering cross-section and lower in the forward scattering, indicating diminished size and higher complexity inside the cells - typical features of apoptotic cells. The second population increased with clear apoptotic features as the LLO concentration increased (from Figure 3.6 B to D). At 0.5 nM, LLO had the most dramatic effects on cell morphology while 0.1 nM of LLO caused no detectable change.

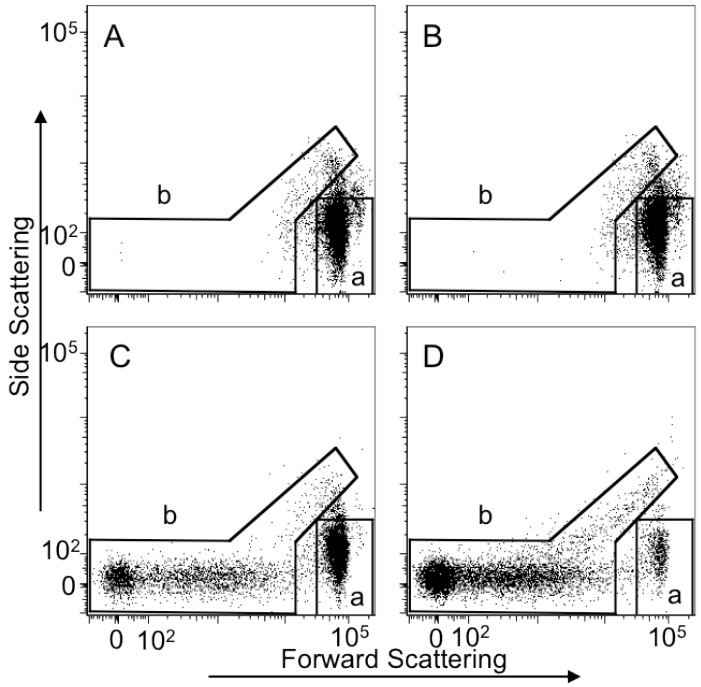

Figure 3.6 LLO binding leads to apoptosis of human red blood cells. Cell density maps of 10^7/ml human red blood cells after incubation for 15 min at room temperature with various amount of LLO: (A) 0 nM; (B) 0.1 nM; (C) 0.2 nM; and (D) 0.5 nM. Live cells show (region *a*) show higher forward scattering than apoptotic cells (region *b*). The pH of the suspended cells was 7.4.

Protein binding to the red blood cells was investigated via flow cytometry with fluorescently labeled proteins. The results are summarized in Figure 3.7. The panel on the

left shows the cell density maps of batches of red blood cells incubated with various proteins including (A) LLO, (B) D123, (C) LLO and D123. The panel on the right displays the mass histograms of the particles chosen from specific cell populations in the corresponding cell density map on the left, based on the fluorescent intensity. As expected, LLO associated with the cells in a dose dependent fashion (Figure 3.7 A, i). Upon incubation with 1 nM LLO, most of the red blood cells were converted to an apoptotic population, as shown in the cell density map in (A). With more protein added, more protein was bound, as indicated in the histogram (i).

In contrast to full-length protein LLO, D123 neither bound to cells (Figure 3.7 B and ii) nor caused any noticeable variation in the morphology of the red blood cells, at concentrations up to 100 nM. Population *a* had little to no association with fluorescent D123. The histogram showed 0.21% of the cells were fluorescently labeled. However, when non-labeled LLO was added at a lower, non-lytic concentration (~0.2 nM) in conjunction with D123, the situation was quite different. There was a second, apoptotic population, *b*, in the cell density map (Figure 3.7 C). Furthermore, 24.5% of the cells in population *b* were now fluorescently labeled, indicating association with D123 (Figure 3.7 iii). One should keep in mind that in this experiment only D123 was labeled with fluorescent dye, while LLO was unlabeled.

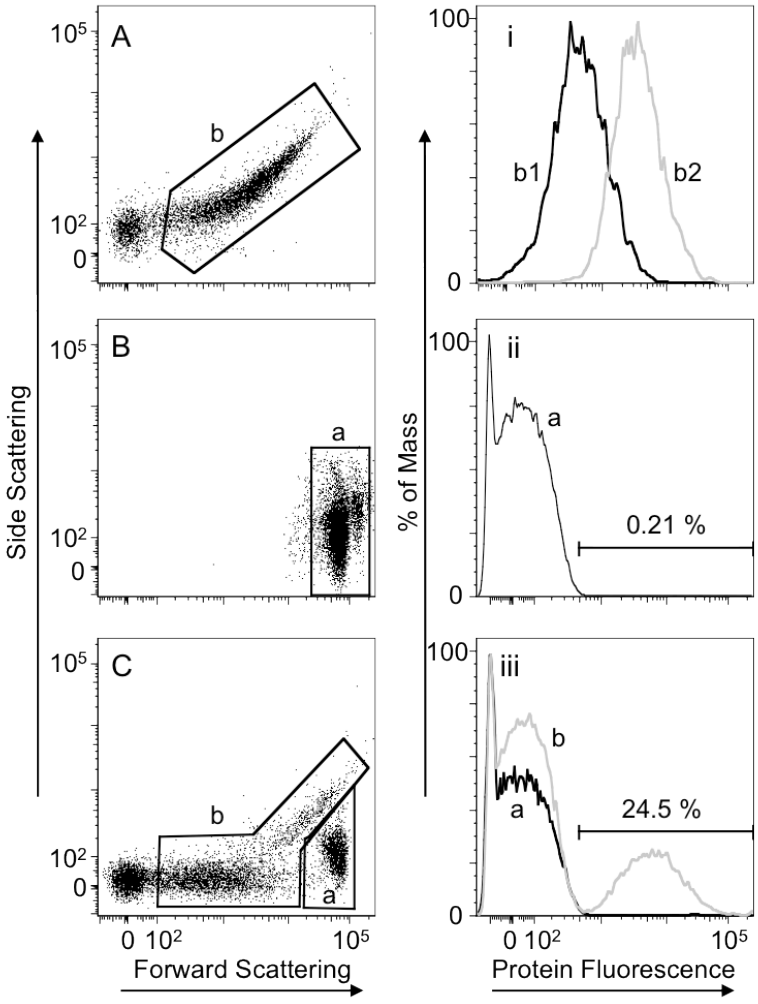

Figure 3.7 D123 binds to human red blood cells only in the presence of full-length LLO. Left panel: cell density maps of 10^7/ml of red blood cells incubated with (A) 1 nM of LLO-Alexa Fluor555, (B) 100 nM of D123-Alexa Fluor555, (C) 100 nM of D123-Alexa Fluor555 and 0.2 nM of unlabeled LLO in phosphate buffered saline (PBS) pH 7.4. Right panel: the correlated fluorescence histogram of the gated cell populations via the PE-channel when the cells were passing through the cell sorter. The fluorescence of the cell population *a, b* in cell maps A, B, C is summarized in histograms i, ii, and iii, respectively. (i) *b1* (the black curve) is the fluorescence histogram of cell population *b* gated in A with 1 nM of LLO-Alexa Fluor555; *b2* (the grey curve) is the histogram of a similar cell population *b* in a cell map after incubation with 2 nM of LLO-Alexa Fluor555. (ii) Fluorescence histogram of population *a* in B, when cells were incubated only with 100 nM of D123-Alexa555: only 0.21% of cells in population *a* had D123 fluorescence. (iii) Fluorescence histogram of populations *a* (black) and *b* (grey) in C, when cells were incubated with 100 nM of D123 as well as 0.2 nM of non-fluorescent LLO: in population *a*, only 0.45% of cells had D123 fluorescence, but in population *b,* a significant 24.5% of cells had D123 fluorescence, indicating D123 binding to the cells with LLO.

3.4 Does D123 bind to apoptotic cells?

LLO incubation can lead to apoptosis of the cells, and D123 association occurred almost exclusively in the apoptotic population of the cells (*b* in Figure 3.8), rather than with healthy cells (*a* in Figure 3.8). One possible explanation is that D123 is bound to the cells only because they are undergoing apoptosis, where a significant portion of the cell membrane properties are altered [Demchenko, 2012]. To investigate this possibility, I induced apoptosis in human red blood cells (termed 'erythropsis') via an approach that did not involve LLO. The association of D123 with these apoptotic cells was studied with flow cytometry.

To induce apoptosis in human red blood cells, we utilized the protocols by Lang et al. [2007]. Red blood cells were incubated overnight with 10 μM Cu^{2+}. The development of apoptosis in the cells was confirmed by both the cell morphology and the externalization of phosphatidylserine (PS) on the cell surface. As shown in Figure 3.8, the red blood cells developed a second population, *b* (Figure 3.8 A, C), whose smaller size was monitored by the forward scattering. Staining of the cell preparations with fluorescent annexin V, showed that 22.6% of this population was annexin V positive (Figure 3.8 B), indicating the migration of PS to the cell surface and the onset of the apoptotic process [van Engeland et al., 1998]. However, fluorescent D123 did not bind to these apoptotic cells, as shown in Figure 3.8 D; only 2.2% of population *b* had D123 fluorescence associated with it. Therefore we exclude the possibility that D123 binds to apoptotic cells due to varied membrane permeability. D123 binds to the cell membranes in a mechanism dependent on LLO, but not on apoptosis.

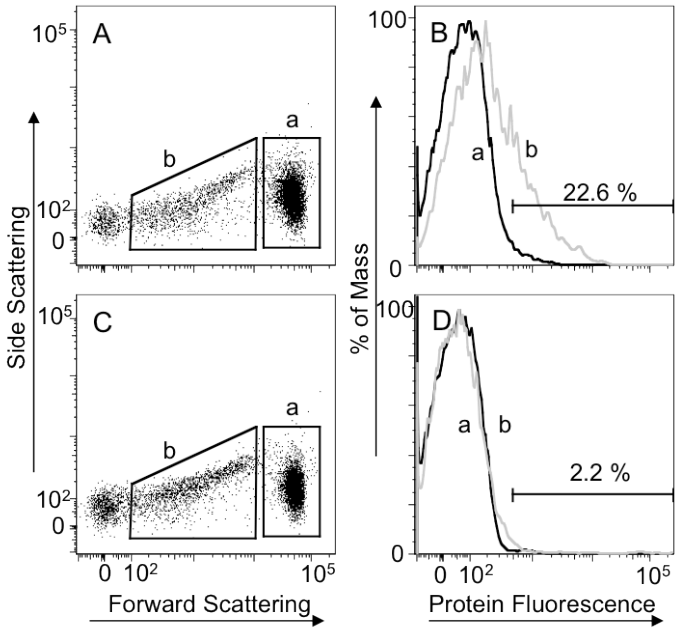

Figure 3.8 Cu^{2+} induced apoptotic cells bind annexin V, the R-phycoerythrin conjugate, but not D123-Alexa Fluor 555. Cell density maps of 2×10^6/ml red blood cells labeled with (A) annexin V-PE and (C) 100 nM of D123-Alexa 555 after the overnight incubation of red blood cells with 10 μM of Cu^{2+} to induce erythropsis. Live cell and apoptotic cell populations were gated in *a* and *b*, respectively, for protein detection. Plots B and D summarize the fluorescence histograms of the gated cell populations (*a, b*) from A and C, respectively.

3.5 Membrane lytic activity

3.5.1 Binding of LLO and D123 can enhance hemolysis

The membrane lytic activity of LLO and the construct of domains D123 was measured with calcein-loaded vesicles. In the experiment, large unilamellar vesicles (LUVs) were made with the concentrated fluorescent dye calcein (40 mM) in the corresponding buffers. Any exterior calcein was removed by gel filtration. Calcein is an interesting fluorophore that is self-quenched when concentrated in solution. Therefore, the calcein encapsulated vesicles had minimal fluorescence. When the membrane integrity of the vesicles is disrupted by a membrane lytic agent, such as LLO, the entrapped fluorescent

dye leaks out into bulk solution. Upon this dilution of the dye, the fluorescence is significantly enhanced. The fluorescence increase is a measure of the vesicle membrane leakage. The addition of 0.1% Triton X-100 to the vesicle solution is used as a positive control (the detergent lyses all the vesicles), while the addition of buffer serves as negative control. The difference in fluorescence between the positive and negative controls is a measure of maximum (total) leakage. The fluorescence observed with LLO addition can then be linked to the amount of total calcein released into solution.

As a cytolysin, full-length LLO caused leakage of POPC/cholesterol (2:1) LUVs in a concentration- and pH-dependent fashion (Figure 3.9). These results were consistent with previous studies [Glomski et al., 2002; Schuerch et al., 2005]. LLO exhibited much better lytic activity at acidic pH. At pH 5.5, LLO caused significant calcein release, with 50% of liposome leakage achieved by adding approximately 100 nM of LLO (lipid/protein ratio = 1000). At pH 7.4, a much higher concentration of LLO was required for vesicle leakage. At the highest concentration tested (1 μM, lipid/protein ratio = 100), only about 20% of calcein was released. In contrast, up to 1 μM of D123 did not cause release of the LUV-entrapped calcein at either pH 5.5 or 7.4, indicating that the complete absence of D4 impairs the pore-formation ability of LLO, presumably by preventing initial binding of D123 to vesicles.

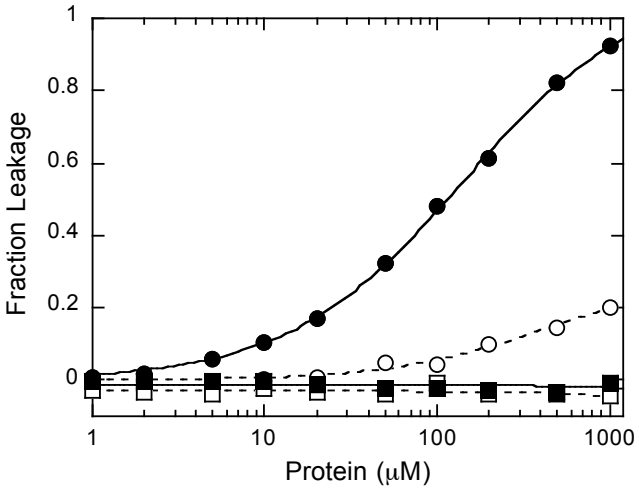

Figure 3.9 Full-length LLO, but not D123, induces vesicle leakage. Calcein leakage from POPC/cholesterol (2:1) LUVs: LLO alone at pH 5.5 (●) and pH 7.4 (○); D123 alone at pH 5.5 (■) and pH 7.4 (❐).

Results from the hemolytic assay paralleled those from the vesicle leakage assay. LLO exhibited optimal hemolytic activity at pH 5.5 and noticeably lower hemolytic activity at pH 7.4 (Figure 3.10 A). Isolated domain D123 had no noticeable hemolytic activity at either pH at concentrations up to 0.5 μM (Figure 3.10 B, squares). Intriguingly, even though on its own D123 had no hemolytic activity, co-incubation of D123 could significantly augment the cell lytic activity of LLO at pH 5.5, the optimal pH for LLO pore formation (Figure 3.10 B). The additional D123 boosted the total cell lysis from less to 20% (caused by 0.1 nM LLO) to over 80% at pH 5.5. I did notice that there was much higher concentration requirement (up to 0.2 μM) for the domain 123 to work in concert with sublytic LLO compared to what is required for lysis by full-length LLO. In contrast, at pH 7.4, co-incubation of D123 caused inhibition of LLO hemolysis. Specifically, 1 nM LLO on its own caused around 20% hemolysis of the red blood cells. When D123 was added along with this concentration of full-length LLO, there was a sharp drop in the total leakage. The prevention of LLO-induced lysis of the red blood cells suggests that LLO and D123 must interact, either in solution or on the target membrane.

These experiments showed that with sublytic amounts of full-length LLO, the addition of domain123 dramatically enhanced red blood cell hemolysis. Presumably the activity of D123 is enabled by association with full-length protein LLO and by participating in pore-formation together with it. From the knowledge of the pore-formation mechanism proposed for CDCs [Tweten et al., 2001], domain 1 through 3 physically possesses all the necessary components for membrane penetration, except the initial membrane anchor of domain 4. The absence of the membrane-binding segment necessitates some full-length protein LLO. A possibility is that clusters of LLO, even in a very small fraction, can recruit D123 in a membrane-bound aggregate that can then undergo the conformational change to pore-forming oligomers.

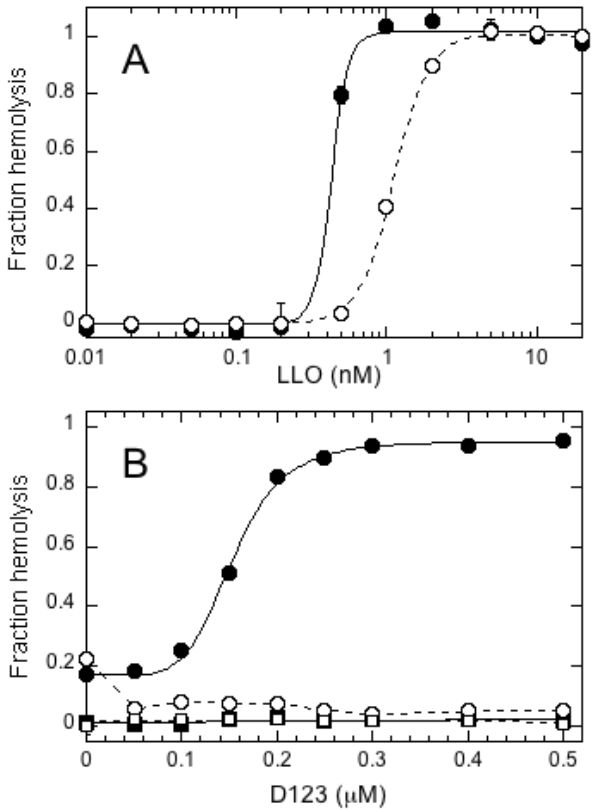

Figure 3.10 Sub-lytic levels of LLO facilitate cell lysis by D123. Lysis of 5×10^7/ml human red blood cells caused by (A) LLO at pH 5.5 (●) and pH 7.4 (○) or by (B) D123 in the presence of 0.3 nM of LLO at pH 5.5 (●) or 1 nM of LLO at pH 7.4 (○). In (B) the effects of D123 alone at pH 5.5 (■) or at pH 7.4 (□) are shown.

3.6 Protein interactions of LLO and D123

3.6.1 Fluorescence correlation spectroscopy

Both the vesicle and the human red blood cell data show that the presence of a small, sublytic amount of LLO enables D123 to bind to a cholesterol-containing membrane (Figure 3.4 D and 3.6 iii). This could be the result of a direct interaction of the two proteins in solution before interaction with a membrane or it could reflect recruitment of D123 by membrane-bound LLO. Of particular interest is whether LLO or D123 aggregate in solution at the concentrations used in the LUV binding and hemolysis assays. The protein aggregation status was examined via fluorescence correlation spectroscopy (FCS). This technique monitors the average translational diffusion coefficient (*D*) of the fluorescently labeled proteins. The *D* values of LLO and D123 in aqueous solution were measured to be 3.7×10^{-11} and 4.1×10^{-11} m^2/s, respectively. However, the theoretical *D* values of LLO and D123 were estimated to be 5.9×10^{-11} m^2/s and 7.1×10^{-11} m^2/s, respectively, using the program HYDROPRO and simulated structures of the proteins [Ortega et al., 2011]. For comparison, the *B. thuringiensis* phosphatidylinositol specific phospholipase C is a 34.9 kDa monomer in solution. The *D* for that protein measured by FCS using the same instrument and rhodamine reference is $5.8\pm0.5\times10^{-11}$ m^2/s; the *D* calculated by HYDROPRO is 6.1×10^{-11} m^2/s, consistent with experimental results [Pu et al., 2009]. For LLO and D123, the D values measured in FCS are considerably smaller than their theoretical values, indicating that both LLO and D123 form oligomers in solution at nM concentrations, typically what I used in liposome binding and hemolysis assays. Interestingly, if one of the unlabeled proteins was added to a nM solution of the other containing a fluorophore, there was no further change in *D*.

This occurred for proteins in both acidic and neutral buffers. This could indicate that the two proteins do not mix in solution but more likely indicates that the aggregates are quite heterogeneous and the averaged *D* cannot reflect subtle changes in aggregation state. The FCS experiment says LLO and D123 form homooligomers in solution. However, it doesn't address if they can form heterooligomers as well.

3.6.2 Fluorescence resonance energy transfer of LLO and D123

Fluorescence resonance energy transfer (FRET) is an excellent technique to explore protein-protein interactions. Therefore, I carried out a FRET experiment with labeled LLO and labeled D123 to assess their association in solution. As the effect of D123 on sublytic LLO hemolysis required much higher concentrations of D123, the donor protein was typically 0.2 μM while the accepter was added up to μM. Protein D123 and LLO were labeled with Alexa488 and Alexa555, respectively. As shown in Figure 3.11 A, the fluorescence intensity of donor D123-Alexa488 (λ_{max} ~520 nm), decreased as the acceptor LLO-Alexa555 (λ_{max} ~565 nm), was added into the solution. At submicromolar concentrations of protein, the association of D123 with LLO in solution occurred at both pH 5.5 and pH 7.4 (Figure 3.11 B). Based what we learned from FCS, that both proteins oligomerize by themselves in solution, the association between LLO and D123 undoubtedly produces hetero-oligomers instead of a simple 1:1 interaction. Therefore it was impossible for me to extract a dissociation constant from the plot. However, the extent of the FRET signal was smaller at pH 7.4 in comparison with that at pH 5.5, suggesting that the heterooligomers formed near neutral pH had either different stoichiometries of the two proteins or the spatial relationship of the two fluorophores in

the aggregate was different. Nonetheless, this indicates that in solution LLO and D123 can directly associate at both acidic and physiological pH.

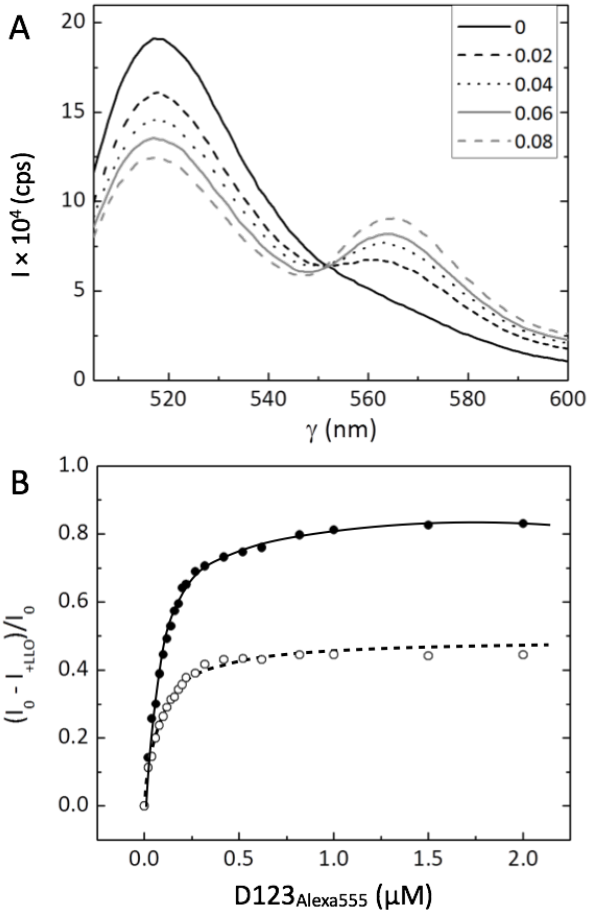

Figure 3.11 FRET of D123 and LLO in solution. (A) Titration of 0.2 μM of LLO-Alexa488 in phosphate buffer, pH5.5, with D123-Alexa555, shows decreased donor (Alexa488) intensity and increased acceptor (Alexa555) intensity with increasing concentration of D123-Alexa555 (indicated in μM on the figure). (B) Calculated FRET efficiency with increasing D123 (acceptor) concentrations is shown at pH5.5 (●) and pH7.4 (○).

3.7 Does D4 binding to micelles and vesicles depend on cholesterol?

Expressed and purified domain 4 (D4) had low solubility in the absence of detergent. This made binding studies problematic. However, I could assess how the protein behaved in comparison to LLO in binding to different interfaces. Initially, the effect of cholesterol presented in diC_7PC micelles on the intrinsic fluorescence of LLO and D4 was examined. As shown in Figure 3.12, there was a 30-40% increase in intrinsic fluorescence of LLO in the presence of diC_7PC micelles containing cholesterol. This increase in fluorescence

likely arises from the Trp-rich loop in D4. This domain of LLO contains four of the total five Trp residues in LLO. Changes in the intrinsic fluorescence of the homologous toxin perfringolysin O had been used to monitor its interaction with membranes [Nakamura et al., 1998]. If D4 alone is specifically activated by cholesterol, D4 interactions with diC_7PC/cholesterol micelles should yield a similar signal variation. However, when recombinant D4 was mixed with diC_7PC micelles containing cholesterol, the intrinsic fluorescence was the same as with diC_7PC alone. In its micelle soluble form (when the D4 is stored in DPC micelles), isolated D4 does not respond specifically to added cholesterol.

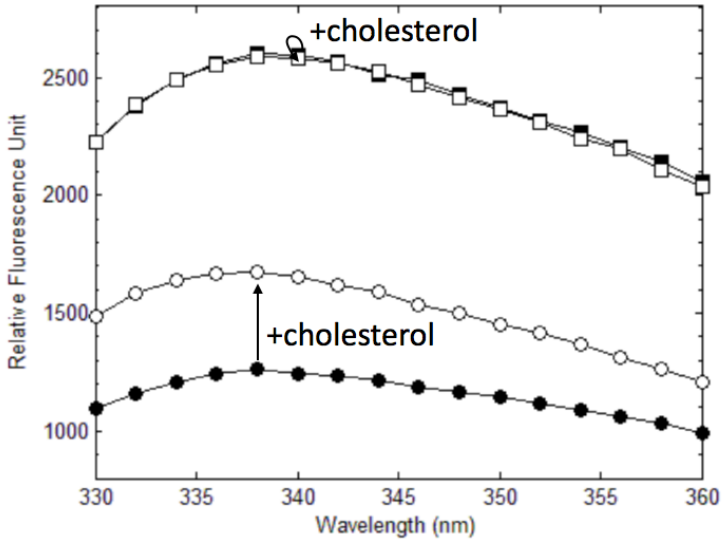

Figure 3.12 Intrinsic fluorescence spectra of 1 μM of recombinant LLO (circle) or 2 μM of D4 (square) mixed with 20 mM of diC_7PC micelles in the absence (filled) and presence (empty) of 6 mol% of cholesterol.

D4 binding to large unilameller vesicles (LUVs) with or without cholesterol was also investigated, in this cases using susceptibility of the protein to trypsin digestion. The digestion products were analyzed with SDS-PAGE, as shown in Figure 3.13. Compared with D4 diluted in the solution (lane *a* in Figure 3.13), which will aggregate and possibly misfold as detergent diffuses away leading to rapid proteolysis by trypsin, D4 incubated

with POPC (*b*) or POPC/cholesterol (*c*) small unilamellar vesicles (SUVs) was digested much more slowly. Presumably the membrane-anchored portion of D4, when bound is protected from the trypsin in the solution. Again, there was no difference between POPC and POPC/cholesterol SUV incubations either in the rate of trypsin digestion or in the identity of the digestion products (protein fragments were analyzed by LC/MS), suggesting that the recombinant D4, in the absence of D123, binds to lipid surfaces in a cholesterol independent fashion.

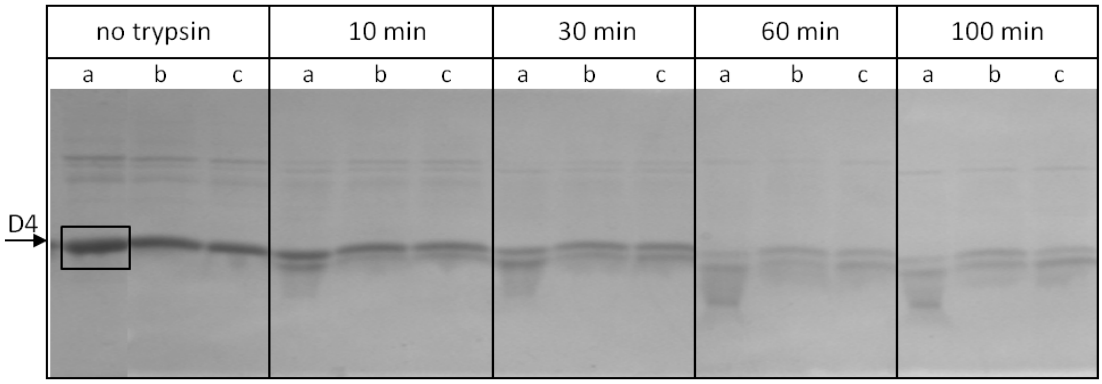

Figure 3.13 D4 liposome binding is unchanged by cholesterol. Trypsin digestion of D4 in 20 mM Tris, 150 mM NaCl, pH 8.0, monitored by SDS-PAGE: (*a*) D4 alone, (*b*) D4 incubated with POPC SUVs, and (*c*) D4 incubated with POPC/cholesterol SUVs at different time points (0, 10, 30, 60, 100 min).

D4 alone has no lytic activity either on vesicles or on red blood cells (data not shown), which is not surprising as it is not the membrane-penetrating domain in the full-length protein. Mixing D4 and D123 also did not recover any of the hemolytic ability of LLO. Furthermore, binding experiments using flow cytometry showed that D123 was not recruited by D4 to the target cell membrane, indicating that when D4 is bound to the membrane, it is not able to interact productively with D123.

3.8 Discussion

Based on the experimental results, I have suggested a model to account for interactions of D123 with LLO (Figure 3.14). D123 and LLO in solution are likely to follow an assembly mechanism similar to that of α-hemolysin [Thompson et al., 2011]: monomers in the solution constantly associate and dissociate with other monomers or small oligomers (i, ii, iii), forming transient complexes. The processes of complex association are likely to be reversible until the last step where the conformational rearrangement occurs and rapid membrane penetration ensues.

In FCS, we observed that both LLO and D123 are multimeric in solution. The association between D123 and LLO in solution is likely to be fairly weak but could be detected with tenths of μM proteins. FRET experiments showed D123-LLO association in the absence of membranes. In the hemolysis assay, D123 oligomers could bind to membranes and contribute to hemolysis with the presence of sub-lytic full-length LLO, but not isolated D4. However, with sublytic LLO, 1000-fold more D123 than LLO was needed to enhance red blood cell hemolysis, indicating that hetero-oligomer formation between D123 and LLO was much weaker than homo-oligomer association between LLO monomers.

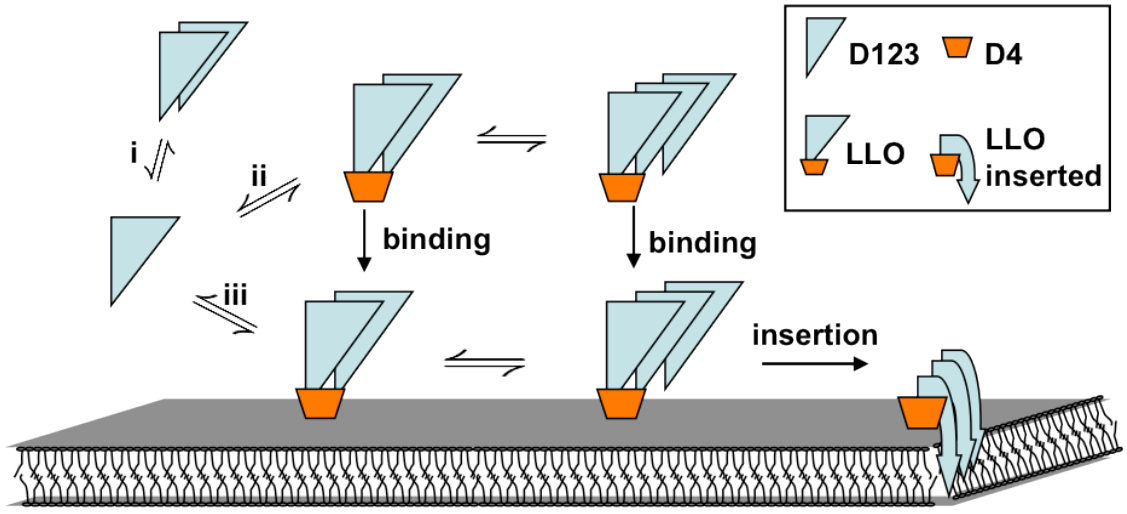

Figure 3.14 Model of D123 interacting with full-length LLO to cause pore formation. D123 monomers in solution reversibly associate with (i) D123, (ii) LLO, and (iii) LLO bound on the membrane. LLO binding and insertion to the membrane, both of which require a functional domain 4, finally enable D123-LLO complexes to form pores on the membrane.

As expected, D123 had no hemolytic activity on its own, since it is devoid of the membrane-anchoring domain and therefore the ability to bind membranes. However, mixing isolated D4, which could rapidly associate with membranes, with D123 did not lead to any membrane lysis. An explanation for this is that the connection loop between domain 2 and domain 4 is the lever. Movement of this lever (which should be pH sensitive) transmits the signal of membrane binding from D4 to induce the conformational change in D123 to form the pore. Flexible linkers have been shown to be important for allostery and conformational changes on other proteins (for example see [Ma et al., 2011]). When the connection is broken, isolated D123 and D4 cannot recreate the function of full length LLO. Therefore, D123 can only enhance hemolysis with full length LLO with a potency that is approximately three orders of magnitude lower than that of LLO. I propose that the limiting step is the transmission of the membrane-bound

LLO conformational change to the LLO-bound D123 monomers on the membrane surface, and that this change is triggered and transferred from D4 in full-length LLO. In LLO oligomers, the pore-formation signal is directly transduced from D4 in each monomer, resulting in a concerted action. For D123-LLO oligomers to work, the signal for the conformational change has to come from D4 in the limited number of LLO monomers. The ratio of LLO in the complex is unfortunately unclear from our experiments, but definitely much less than 1. Although the hetero-oligomers are much less effective (presumably because of relatively weak associations), this is the first experiment showing that concerted interactions between D123 protein and LLO can lead to active pore-formation.

Similar to LLO, D123 in concert with sublytic LLO only has membrane lytic activity at acidic pH. This is not just the result of decreased binding of the two proteins since D123 inhibited the small amount of lysis induced by LLO at neutral pH (Figure 3.9 B). This suggests that the conformational rearrangement needed for pore formation has some contribution from a titratable group that must be protonated. Schuerch et al. [2005] reported the inactivation of LLO aggregates at neutral pH *in vitro* and hypothesized it was due to the partial unfolding of α-helices in D3. It is very likely that D123 maintains the same labile fold of full-length LLO at neutral pH. Therefore when D123 is present in huge excess in the hemolysis assay, D123 complexed with the small amount of LLO leads to aggregated, inactive complexes.

My experiments show that D123 and LLO associate in solution, and that the complexes form active pores when bound to membranes. The molecular mechanism of how D123, without domain 4, cooperates with LLO and works as an active cytolysin is

still elusive. In mammalian systems, complex membrane lysins, such as membrane attack complex/perforin superfamily (MACPF) have been identified. These lysins consist of multiple complement components but they have similar structures and membrane-disruption mechanisms as CDCs [Hadders et al., 2007; Rosado et al., 2008]. The fundamental study of interactions between D123 and LLO may therefore provide insight into the working mechanism of more complex cytolysins as well as bacterial cytolysins.

Chapter 4 PC-PLC

Despite a number of studies investigating the contribution to virulence of PC-PLC [Vazquez-Boland et al., 1992; Raveneau et al., 1992; Poyart et al., 1993; Marquis et al., 1995, 1997; Gründling et al., 2003; Alberti-Segui et al., 2007], a specific role for this phospholipase in pathogenesis has not been established. There are even fewer studies on the enzymatic features and mechanism of the *L. monocytogenes* PC-PLC [Geoffroy et al, 1991; Goldfine et al., 1993] in comparison with well-studied homologous enzymes: phospholipase C from *Bacillus cereus* (PLC_{Bc}) [Hergenrother and Martin, 2001] and the α-toxin of *Clostridium perfringens* [Titball et al., 1999].

In this work, the *L. monocytogenes* broad-range PC-PLC was cloned, expressed in *Escherichia coli* as an intein-fused recombinant protein, purified and characterized in an active and homogeneous form. The zinc content and affinity of the metalloprotein were measured. Systematic kinetic studies were employed to probe substrate specificity and pH profile. Membrane partitioning of the protein onto POPC/cholesterol vesicles was examined by fluorescence correlation spectroscopy (FCS). In addition, mutations of residues homologous to active site residues in PLC_{Bc} were produced to test a structural model generated for *L. monocytogenes* PC-PLC from the crystal structure of PLC_{Bc}. The rate-determining step of PC-PLC catalysis was also investigated through assays assessing viscosity and deuterium effects.

4.1 Protein preparation and characterization

4.1.1 Gene construction and protein purification

Plasmid pET29-*plcB* containing the gene *plcB* for mature PC-PLC was a generous gift from Professor Helene Marquis, Cornell University. The PC-PLC gene was amplified via polymerase chain reaction (PCR) using HotStartTaq DNA Polymerase (Qiagen, Valencia, CA) and primers 5'-GGTT**GCTCTTC**CAACTGGTCCG-3' (to introduce the *Sap*I site) and 5'- GCTG**CATATG**TCAGTGGTGGTGG-3' (*Nde*I site). The amplified fragment was ligated into the pTYB21 with T4 DNA ligase (New England BioLabs, Ipswich, MA). The final gene construct was sequenced by Genewiz (Cambridge, MA). After the sequence confirmation, the plasmid was transformed into *E. coli* expression strain BL21-AI (Life Technologies, Grand Island, NY). Protein expression was induced with both 0.2% g/mL L-arabinose and 0.4 mM IPTG. Cells were shaken at 225 rpm at 20 °C for 6 h before harvesting. In this system the recombinant protein was expressed as a fusion protein with an N-terminal intein tag. The intein tag contains a chitin-binding domain that allows isolation of PC-PLC on a chitin resin. On-resin excision of the intein by incubation with dithiothreitol (DTT), following manufacturer's suggested protocol [Chong et al., 1999], yielded purified PC-PLC with its native N-terminus without any extra residues from the vector. The PC-PLC protein was precipitated from the solution by the addition of 40 % g/g ammonium sulfate powder. After 1 h of mild stirring, the precipitated protein was pelleted and re-dissolved in storage buffer (20 mM HEPES, 1 M NaCl, 2 mM DTT, pH 8.5) in a volume typically 0.05-0.1 of the original column eluate volume. Excessive ammonium sulfate was removed by dialysis against fresh storage buffer. Aliquots of purified proteins were stored at 4 °C or frozen with liquid nitrogen in 20% glycerol and stored in -80 °C. All of the purification procedures were performed at 4 °C. Site-directed point mutations of PC-PLC were made with the QuikChange Lightning

Site-Directed Mutagenesis Kit (Agilent Technologies, Inc., Santa Clara, CA). Mutant proteins were expressed and purified following the same protocol as the recombinant wild type PC-PLC. The protein concentrations of all samples used in this study were measured with a Pierce BCA protein assay kit (Pierce Biotechnology, Rockford, IL) [Smith et al., 1985].

4.1.2 Protein characterization and Zn^{2+} content

The theoretical isoelectric point (pI) of this PC-PLC is 7.37 calculated by ExPASy ProtParam tool [Gasteiger et al., 2005]. To prevent protein precipitation over time, a basic pH environment (~8.5) was more effective compared to an acidic pH (~6). Concentrated salt (1 M NaCl) also improved the long-term stability of PC-PLC. The CD spectrum of PC-PLC (Figure 4.1 A) indicated a secondary structure mostly of α-helices (~84.3 % as deconvoluted by online program K2D2 [Perez-Iratxeta and Andrade-Navarro, 2008]). The high helix content is consistent with the crystal structure of PLC_{Bc} [Hough et al., 1989]. The PC-PLC displayed very similar CD spectrum in the absence (no Zn^{2+} added in the purification) or presence of added Zn^{2+} (100 μM), suggesting that saturating the zinc ion sites did not involve significant alternations in secondary structure of the enzyme.

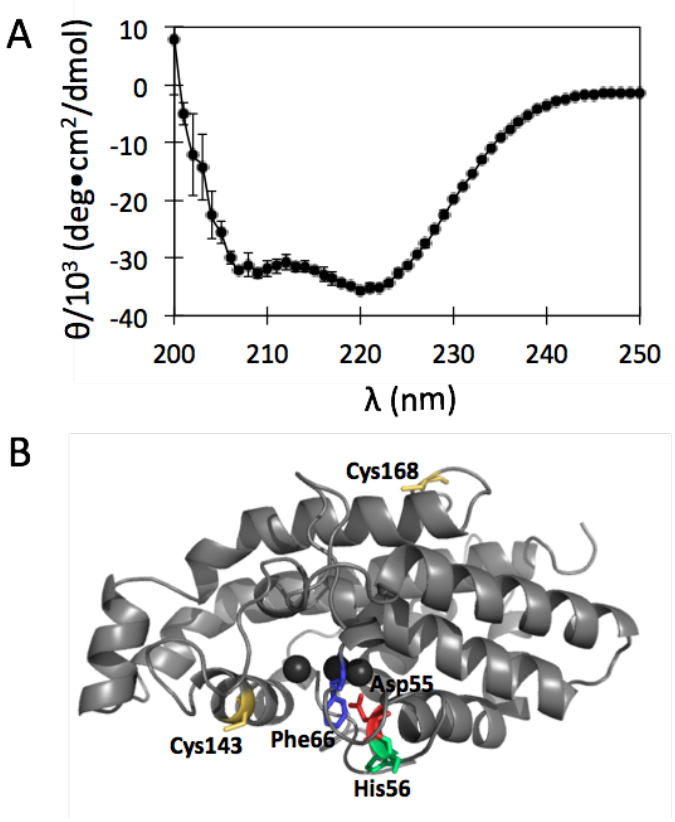

Figure 4.1 (A) Circular dichoism spectrum of PC-PLC in 20 mM HEPES buffer, 150 mM NaCl, pH 8.5; (B) Predicted structure of *L. monocytogenes* PC-PLC was modeled from structure of PLC_{Bc} [Hough et al., 1989] based on their sequence homology by SWISS-MODEL Alignment Mode. Residues that were mutated in this study are labeled in color: Asp55 (red), His56 (green), Phe66 (blue), Cys143 and Cys168 (yellow).

4.2 Metalloprotein PC-PLC

4.2.1 Zinc content

Throughout the protein expression and purification procedures, no zinc ions were added into protein samples. However, there still is the likelihood that the apo-PC-PLC could bind zinc ions from the growth medium or from trace amounts of zinc in water. Therefore, ICP-MS was used to measure the concentration of zinc under conditions where known concentrations of zinc were purposely added to the protein samples. Protein samples were set up in dialysis bags (Figure 4.2) for zinc loading. Two different zinc conditions were used, (A) non-zinc buffer (20 mM HEPES, 1 M NaCl, pH 8.0) and (B) zinc buffer (5 μM $ZnSO_4$, 20 mM HEPES, 1 M NaCl, pH 8.0). After equilibrium, protein

associated zinc ions increased the total zinc concentration of protein samples compared to that of the buffer. The results are summarized in Table 2.

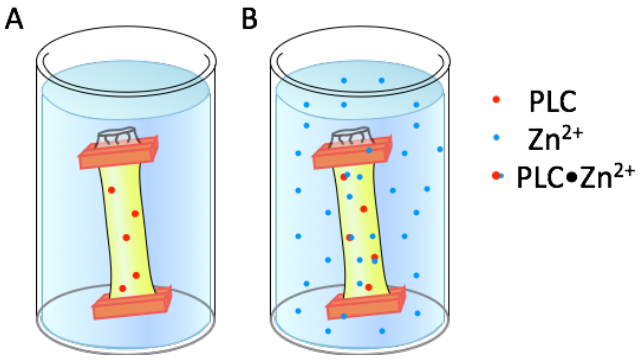

Figure 4.2 Schematic diagrams of ICP-MS samples dialyzed in (A) non-zinc buffer; (B) 5 μM Zn^{2+} buffer. After equilibrium, the difference of zinc concentrations between protein samples (yellow) and bulk solution (blue) is the zinc bound to protein.

Table 2. ICP-MS analysis of PC-PLC Zn^{2+} content under different conditions.

Sample	Free Zn^{2+} (μM)	Total Zn^{2+} (μM)	PLC-Zn^{2+} (μM)	PLC (μM)	Zn^{2+}/PLC
Non-Zn^{2+} buffer	0.040±0.003				
PLC in non-Zn^{2+} buffer	0.040±0.003	1.30±0.02	1.26±0.02	2.97±0.15	0.42
Zn^{2+}-buffer	5.04±0.06				
PLC in Zn^{2+}-buffer	5.04±0.06	8.73±0.07	3.69±0.07	1.78±0.09	2.08

In buffer without added Zn^{2+} (where free Zn^{2+} was measured at 0.040 μM), the PC-PLC had an average of 0.4 zinc ions. With 5 μM Zn^{2+} added, the ratio of Zn^{2+} to protein was 2.1. The number was smaller than the expected three zinc ions per protein from PLC_{Bc}, reflecting a relatively weaker affinity of the third zinc in *L. monocytogenes* PC-PLC. The equilibrium status of PC-PLC associated zinc is schematically represented in Figure 4.3. Assuming that the non-Zn^{2+} sample represents a single ion binding and that the 5 μM Zn^{2+} sample represents some occupation of the third site after the initial two sites are filled, the dissociation constants of these two zinc binding can be calculated with

the equations listed below: the lowest K_d is ~54 nM, the third Zn^{2+} would have a much higher K_d (~60 μM).

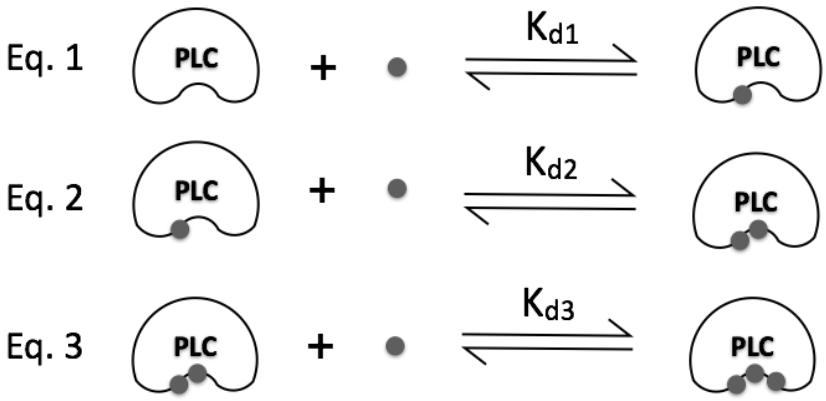

Figure 4.3 Schematic representation of multimeric zinc binding to PLC active site. And their specific affinities are measured by dissociation constants K_{d1}, K_{d2}, and K_{d3} of the equations.

$$K_{d1} = \frac{[PLC][Zn^{2+}]}{[PLC \bullet Zn^{2+}]}$$

$$K_{d3} = \frac{[PLC \bullet 2Zn^{2+}][Zn^{2+}]}{[PLC \bullet 3Zn^{2+}]}$$

For comparison with Zn^{2+} binding to PC-PLC as measured by ICP-MS, the dependence of enzyme activity on added Zn^{2+} was also measured. The enzyme assays were carried out with the monomeric substrate diC_6PC (5 mM) at pH 6.0 (chosen because optimal activity for this substrate occurred at the acidic pH, *vida infra*). The relation of enzyme specific activity to added zinc concentration is plotted in Figure 4.4. The data could be fit well with a hyperbolic function, resulting in an apparent dissociation constant ($^{app}K_d$) of zinc from PC-PLC in these reaction conditions of 1.94 ± 0.22 μM. If we assume that all three zinc ions are needed for PLC activity, then the dissociation

constant obtained from enzyme assays is much smaller than the one (K_{d3} ~ 60 μM) estimated from ICP-MS analysis in non-substrate containing solution. It could suggest that the third zinc ion might bind to active site cooperatively with substrate. There was a difference in the pH of the ICP-MS (pH 8) and enzyme activity (pH 6) studies, necessitated by keeping the protein at higher concentrations in solution for the MS work. However, zinc binding should be tighter at the more basic pH if histidine residues are involved.

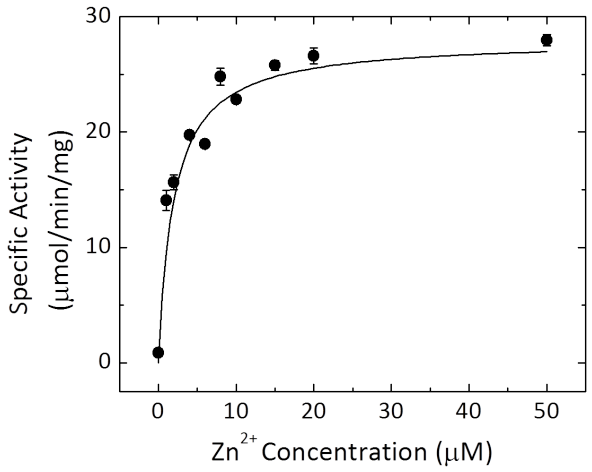

Figure 4.4 Zinc-dependence of *L. monocytogenes* PC-PLC activity towards 5 mM diC_6PC in 20 mM MES, 150 mM NaCl, 0.1 mg/mL BSA, pH 6.0. Data were fitted with hyperbolic function (curve) by Origin yielding $^{app}K_d$ of 1.94 ± 0.22 μM.

The need for less than expected Zn^{2+} under assay conditions could also be rationalized by the need for only two Zn^{2+} ions in the active site critical for activity. Regardless of the reason for the difference in the two methods to extract K_d values for Zn^{2+}, I used the result of the ICP-MS experiment to determine what concentration of Zn^{2+} would be adequate to fill all binding sites on the protein in subsequent kinetic studies: 50 μM Zn^{2+}.

4.3 Substrate specificity

The recombinant PC-PLC from *L. monocytogenes* can catalyze the hydrolysis of a range of phospholipid head groups including PC, PE, PS, PG, and sphingomyelin (SM) (all presented in Triton X-100 micelles). Of the phospholipids tested, only PI was not a substrate. PC is the substrate towards which the enzyme exhibits the highest activity, although the activity was fairly robust with PE, PS and sphoingomyelin as well.

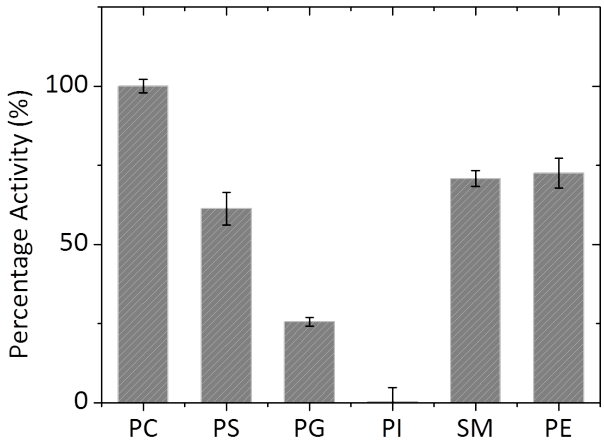

Figure 4.5 Specific activity of PC-PLC towards 6 mM substrates with different head groups 20 mM Triton X-100, 20 mM HEPES, 150 mM NaCl pH 6, in comparison with PC activity (100%). All the glycerol lipids used had dioleoyl acyl chains. SM was brain sphingomyelin (porcine).

Since PC was the best substrate, and since the aggregation state (monomer, micelle, or vesicles) of this phospholipid can be varied by acyl chain length, PC was used as the substrate for detailed kinetic studies.

4.4 pH profile

The pH profile for PC-PLC is an interesting characteristic, as the synthesis, activation, and release of this virulence factor is pH-sensitive [Marquis and Hager, 2000; Yeung et al., 2005; Forster et al., 2011]. Phospholipid substrates can be used in various physical states (monomer, micelle, or vesicle), which may also affect the pH profile. Towards POPC (6 mM) in 20 mM Triton X-100 micelles, PC-PLC exhibited an optimum pH that

was acidic – around pH 5 (Figure 4.6, black bars). In comparison, with the same assay and substrates, PLC_{Bc} exhibited maximal activity at neutral pH (Figure 4.6, grey bars).

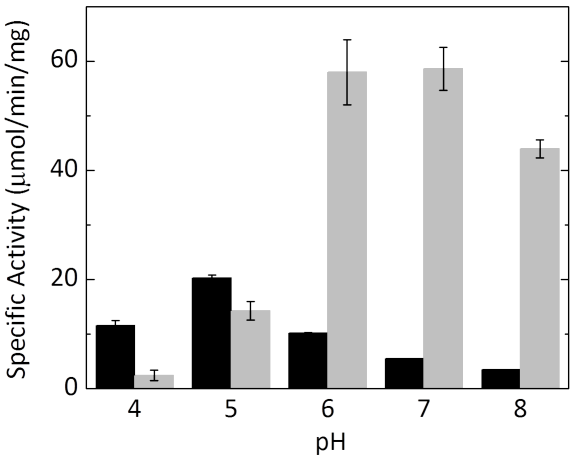

Figure 4.6 The pH-dependence of specific activity of *L. monocytogenes* PC-PLC (black) and *B. cereus* PLC_{Bc} (white) activities towards POPC (6 mM) in 20 mM Triton X-100 micelles, 150 mM NaCl, with 0.1 mg/mL BSA.

The specific activity of the PC-PLC was also examined towards long chain lipid POPC (4 mM) in small unilamellar vesicles (SUVs) in the absence or presence of cholesterol (2 mM) (Figure 4.7). In this experiment, cholesterol had no significant effect on enzyme activity. As with substrate in micelles, there was a very clear preference of PC-PLC for an acidic pH. The optimal pH for activity towards PC SUVs (pH 5) was similar to that observed for POPC mixed in Triton X-100 micelles.

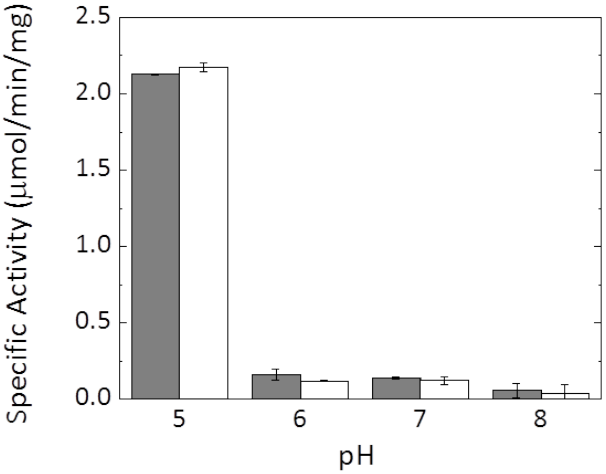

Figure 4.7 PC-PLC specific activity towards SUVs as a function of pH. Grey bars: 4 mM; white bars: POPC /cholesterol (4 mM /2 mM).

More insight into the acidic pH optimum of the enzyme was obtained from the detailed kinetic data with the mono-dispersed substrate, diC_6PC (Figure 4.8). Over the pH range tested (pH 5-8), the turnover rate, k_{cat}, of PC-PLC exhibited a relatively flat landscape (Figure 4.8 B), ranging from 4 to 7 s^{-1}. However, K_m (Figure 4.8 A), exhibited a marked minimum at pH 6 and 6.5. This led to a bell-shaped curve for the overall catalytic efficiency k_{cat}/K_m (Figure 4.8 C) with an optimal efficiency between pH 6-6.5. These results indicate that at least for monomers it is the K_m that modulates the enzyme efficiency, not the turnover rate. Furthermore, the much lower pH optimum for the PC micelle and vesicle systems suggests that this change is modulated by binding of a phospholipid in the active site or possibly bulk binding of the protein to the vesicles rather than a change in the environment of the catalytic residues.

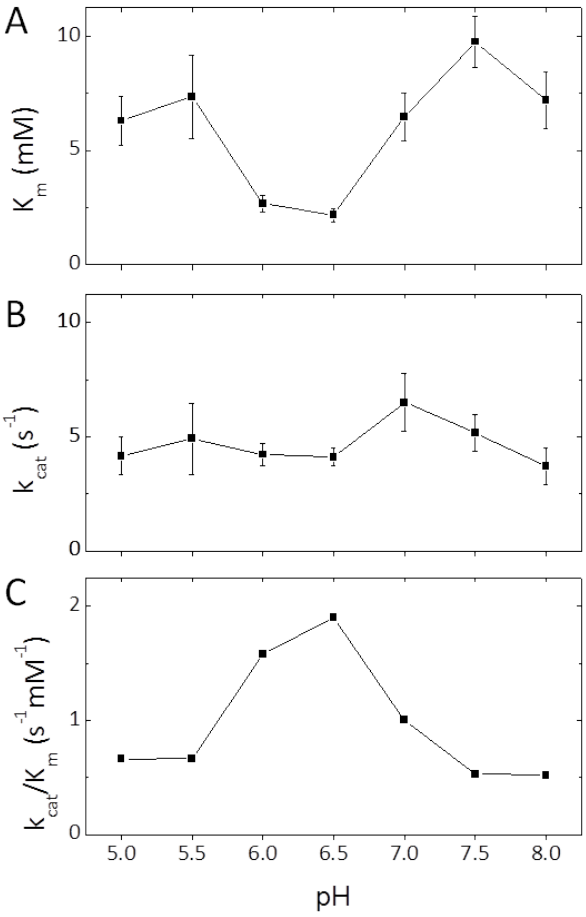

Figure 4.8 The pH dependence of kinetic parameters for *L. monocytogenes* PC-PLC-catalyzed diC_6PC hydrolysis: (A) K_m, (B) k_{cat}, and (C) k_{cat}/K_m. All assays were conducted in the presence of 50 μM $ZnSO_4$.

4.5 Micelle effect

PC-PLC activity was also examined with substrate diC_7PC (Figure 4.9). In the plot of activity versus substrate concentration, there are two distinct phases. The transition between these was at a diC_7PC concentration of 1.75 mM, a value very close to the published critical micelle concentration of the pure lipid (1.5 mM [Bian and Roberts, 1992]). Below that point, there was a hyperbolic increase in activity that followed Michaelis-Menten kinetics, from which K_m and k_{cat} for monomeric substrate diC_7PC could be extrapolated. Above that concentration, there was a very steep increase in enzyme activity. Thus, as soon as micelles were formed, the PC-PLC specific activity

increased and was 3-fold higher than what was observed for monomeric substrate. The steepness of the increase indicates that the apparent K_m for a micellar phospholipid is considerably lower. In other words, the micelle formation from monomer substrates enhances enzyme activity. As the catalytic mechanism remains identical, the enhanced activity is presumably caused by the micellar interface facilitating substrate binding to and/or product leaving the active site. Interestingly, the extent of the rate enhancement is comparable to what has been observed for PLC_{Bc} [El-Sayed et al., 1985].

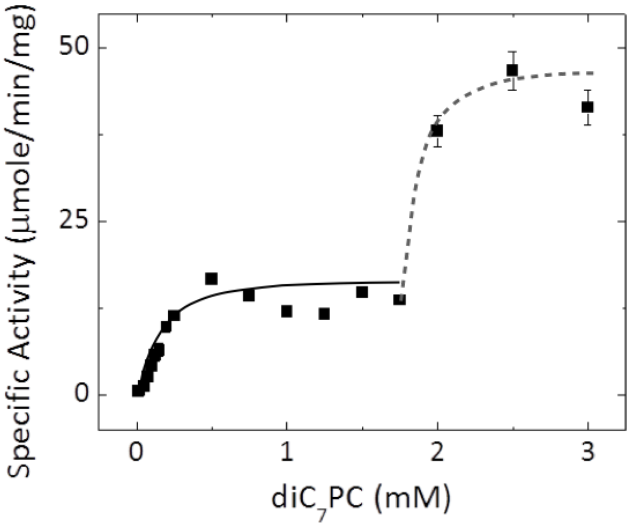

Figure 4.9 Specific activity of PC-PLC towards diC_7PC was measured with increasing substrate concentrations in 20 mM MES, 150 mM NaCl, 0.1 mg/mL BSA, pH 6. Black solid curve is the hyperbolic fit of monomer diC_7PC up to 1.75 mM; grey dotted curve is the hyperthetical hyperbolic fit of micelle diC_7PC substrates.

4.6 Acyl chain specificity

With the same head group, substrates with acyl chains of various lengths (diC_4PC, diC_6PC, and diC_7PC) were examined. A comparison of K_m, k_{cat}, and catalytic efficiency (k_{cat}/K_m) for the three monomeric short-chain PC substrates is shown in Table 3. Enzyme-catalyzed reactions were carried out with each substrate concentration below its critical micelle concentration (CMC). Therefore all the substrates should be monomers in the reactions. For all three monomers, it is the K_m of PC-PLC (which presumably reflects

substrate affinity) that exhibits a strong dependence on acyl chain length. Interestingly, the k_{cat} was quite similar for the three different short-chain PC molecules. This suggests that at least for monomeric substrate some degree of hydrophobicity is required for an isolated phospholipid to bind into the active site.

Table 3. Kinetic parameters of PC-PLC for substrates of short-chain phosphatidylcholine at pH 6.

substrate	CMC (mM) [a]	K_m (mM)	k_{cat} (s^{-1}) [b]	k_{cat}/K_m (mM^{-1} s^{-1})
diC_4PC	250	43.5±3.4	8.0±0.4	0.18
diC_6PC	14	2.8±0.8	12.8±1.5	4.6
diC_7PC	1.5	0.20±0.05	8.5±0.7	42.5

[a] CMC values for the short-chain PC molecules are from Bian and Roberts, 1992.
[b] The molecular mass of the protein was 29 kDa, and all assays were conducted in the presence of 50 μM $ZnSO_4$.

4.7 Binding of PC-PLC to liposomes

For monomer substrate, phospholipid binding, as reflected in K_m dictates overall enzyme catalytic efficiency over the pH range from 5-8.5. Therefore, it was of interest to assess the affinity of PC-PLC for phospholipid vesicles. The interaction of this peripheral membrane protein with vesicles was investigated using fluorescence correlation spectroscopy (FCS). Under the experimental conditions (POPC was presented in small unilamellar vesicles at 20 °C), the activity of PC-PLC towards the vesicles was sufficiently low so that less than 5 % (determined by NMR assays) of the total phospholipids would be hydrolyzed (assuming sufficient Zn^{2+} was present) over the time required for the FCS measurement. In the absence of added Zn^{2+} and with the chemical

reaction minimized, the association of PC-PLC to the vesicle membranes could be measured.

For FCS experiment, the protein must be fluorescently labeled. I generated the PC-PLC mutant C143S, which has a single cysteine (Cys168) available for modification with a fluorescent dye. This cysteine was labeled with a thiol-reactive reagent of the dye Alexa Fluor 488. Specific activities for C143S were comparable to that of the wild type enzyme (Figure 4.11). Thus, neither the mutation nor the labeling should affect the overall behavior of the protein.

Fluorophore-labeled protein in the solution was titrated with POPC/POPG (95/5) SUVs. A small amount of negatively charged lipid POPG was added to help prevent fusion of the vesicles. FCS detected and analyzed the fraction of protein bound on the vesicles. Measuring this for different PC concentrations could be used to derive the apparent dissociation constant (K_d). The final results, shown in Figure 4.10, show the effects of two variables: zinc concentration and pH. The apparent K_d at pH 7.4 was 65-85 μM with no significant change when excess Zn^{2+} was added. The same apparent K_d was observed at pH 5.5 when 50 μM Zn^{2+} was present. However, at the acidic pH without Zn^{2+}, the apparent K_d of the protein for the SUV was 2.5~3-fold higher. Distinct from the variation of K_m for monomeric substrate with pH, PC-PLC had weaker affinity towards PC vesicles at pH 5.5 (in the absence of Zn^{2+}). The addition of 50 μM zinc enhanced the affinity of PC-PLC for SUVs at pH 5.5 (the effect of Zn^{2+} at pH 7.4 was not statistically significant). Overall, similar binding of the protein to SUVs at pH 5.5 and 7.4 with 50 μM zinc indicates that bulk partitioning of the protein on vesicles is *not* responsible for the lower enzymatic activity observed at neutral pH.

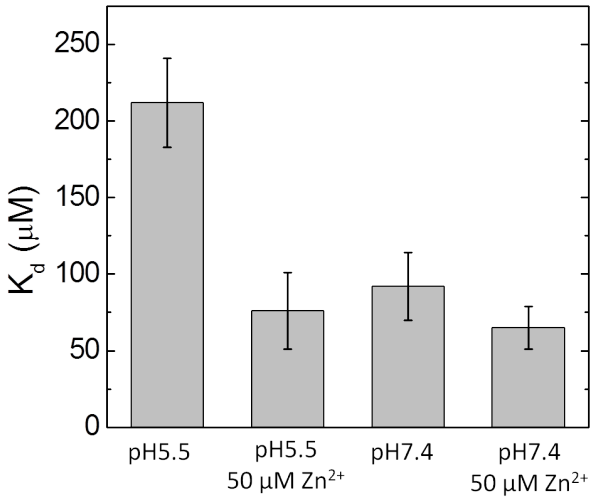

Figure 4.10 Apparent dissociation constant (K_d) for *L. monocytogenes* PC-PLC binding to POPC/POPG (95/5) SUVs at pH 5.5 (20 mM MES) or pH 7.4 (20 mM HEPES), with 150 mM NaCl, and 1 mg/mL BSA.

4.8 Predicted model for PC-PLC and mutation of active site residues

The high sequence homology of PC-PLC to the PLC_{Bc} allowed me to generate a hypothetical structure for the *L. monocytogenes* enzyme (Figure 4.1 B) based on the crystal structures of PLC_{Bc} [Hough et al., 1989]. The simulated structure, not surprisingly, is very similar to that for PLC_{Bc} showing a helical single domain protein. Work by Martin and coworkers had explored the relevance of residues in the active site to catalytic activity, and in PLC_{Bc} the residues Asp55, Tyr56, and Phe66 are part of the active site and important for enzymatic activity [Martin and Hergenrother, 1998; Martin et al., 2000]. *L. monocytogenes* PC-PLC conserves the same amino acids at these positions with the exception of His56 (which is Tyr in PLC_{Bc}).

In studies of PLC_{Bc}, Asp55 was suggested as the putative general base that aids in activating the nucleophilic water for attack on the phosphodiester since alterations at this position reduced enzymatic activity 10^4~10^6-fold [Martin and Hergenrother, 1998]. In my experiment, replacement of Asp55 in PC-PLC with Asn also diminished the enzyme

activity. However, the loss of enzymatic activity was not as dramatic as that for the Bacillus enzyme (100-fold decrease as shown in Figure 4.11). Nonetheless, this does suggest that Asp55 is likely to have a similar role in PLC catalysis where it helps to polarize the water molecule that will attack the phosphorus. In the structure of the PLC_{Bc}-inhibitor complex, the choline moiety of the analogous inhibitor could form a cationic complex with the π-system of one or both Tyr56 and Phe66 [Hansen et al., 1993a]. These two residues were shown to be involved in substrate recognition and enzyme specificity [Martin et al., 2000]. In PC-PLC, the activity of mutant H56Y was basically comparable to unaltered enzyme, indicating it was a conservative and innocent mutation between the two homologous enzymes. However, F66Y, a mutation that might be thought of as conservative, caused a dramatic loss of activity. The difference in the significance of these two mutations indicated H56 and F66 might not have entirely overlapping roles in the two enzymes. In *L. monocytogenes* mutant F66Y, it is possible that the added hydroxyl group may form a hydrogen bond with other active site residues so that this residue is no longer aligned for cation-π interactions with the choline.

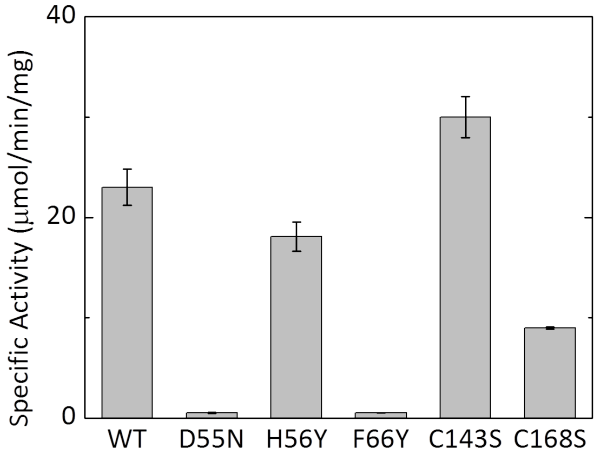

Figure 4.11 Specific activity of the PC-PLC mutants towards 5 mM diC_6PC in 20 mM MES, 150 mM NaCl, 0.1 mg/mL BSA, pH 6.

A unique feature of PC-PLC is that it has two cysteine residues that are absent in the PLC_{Bc} sequence, Cys143 and Cys168. Both cysteine residues, on the surface of the protein, were changed to serine to see if that substitution had any effect on PC-PLC activity. C143S actually exhibited higher diC_6PC hydrolysis activity than the recombinant wild type enzyme, while the activity of C168S was reduced. These results suggest that the two free cysteine residues are not essential for catalysis. Neither are they critical for disulfide interactions since the protein is a monomer.

4.9 Is there synergism of PC-PLC with LLO in in vitro assays?

Since the kinetic results suggest that PC-PLC prefers acidic pH values with bilayers as substrates and since LLO is activated upon solution acidification [Glomski et al., 2002; Schuerch et al., 2005], I examined the effect of the recombinant PC-PLC on LLO in hemolysis of red blood cells and the effect of added LLO on the enzyme activity of PC-PLC towards POPC/cholesterol (2/1) LUVs. The presence of PC-PLC (up to a maximum concentration of 20 nM) had little to no impact on hemolysis caused by LLO (Figure 4.12). Furthermore, adding LLO to LUVs to disrupt the vesicle structures did not dramatically enhance PC hydrolysis by PC-PLC (Figure 4.13), although there was a slight improvement in total amount of PC hydrolyzed and perhaps a slightly faster rate after the lag phase. At least in these in vitro experiments, there was no significant dramatic interplay between the two virulence factors.

One should also notice that instead of a linear slope for initial velocity, the reaction with substrates in LUVs proceeded through a sigmoidal trajectory (Figure 4.13). This curve was unique for substrate presented in LUVs; for substrates in all other conditions

(monomer, micelle, or SUV) PC-PLC consistently exhibited an initial rate with a linear amount of product formed. The distinct sigmoidal reaction curve of LUVs is likely related to the high lateral pressure of vesicles where long chain substrates are ordered when packed in a relative flat surface [Traikia et al., 2002]. This type of flat surface should be relatively defect-free. In the early stage, the membrane penetration of enzyme is infrequent and limited; therefore the initial reaction rate was extremely slow. As the reaction proceded, diacylglycerol (DAG), a typical membrane-destabilizing agent, was produced and accumulated in the membrane bilayer. Because of its small polar head group and large aliphatic acyl chains, DAG increased membrane-packing defects [Vamparys, et al., 2013], which accelerated PC-PLC catalyzed reaction. Finally, the reaction reached a plateau when DAG built up in the membrane and inhibited the enzyme, possibly by causing fusion of vesicles and trapping the enzyme.

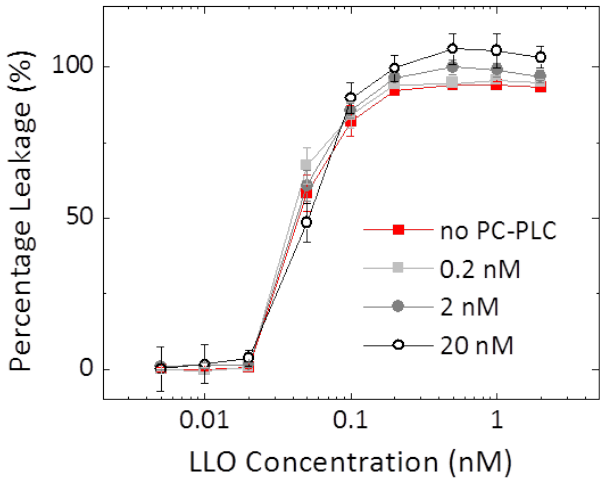

Figure 4.12 Hemolytic assay of LLO with addition of PC-PLC at indicated concentrations.

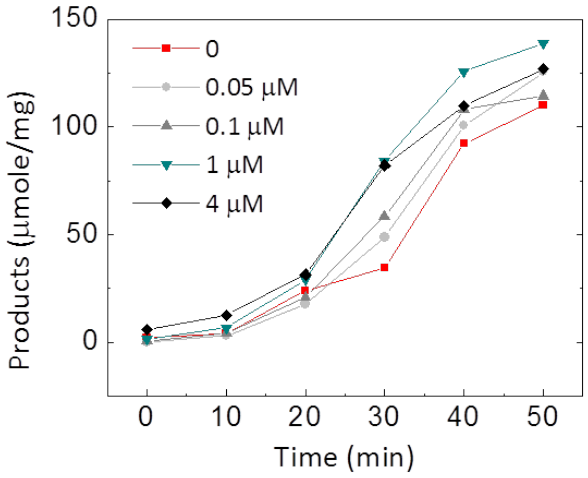

Figure 4.13 Time-course of PC-PLC hydrolysis of 5 mM POPC/Cholesterol (2/1) LUVs in 20 mM MES buffer, 150 mM NaCl, pH 5.5, 0.1 mg/mL BSA. LLO was added to the final concentration indicated for the different curves.

4.10 Catalytic cycle of PC-PLC

Enzymatic reactions proceed through a catalytic cycle involving substrate binding, reaction, and product release. The rate-determining step (RDS) of PC-PLC catalyzed hydrolysis in the catalytic cycle was investigated by the following experiments, which investigated viscosity and proton inventory effects on enzymatic efficiency of PC-PLC, respectively.

4.10.1 Viscosity effects

Hydrolysis by PLC_{Bc} was found inhibited by its reaction product diacylglycerol (DAG) [Tan and Roberts, 1996]. This suggests the possibility that the reaction rate might be limited by the release of the product. If this is the case, solvent viscosity should influence the catalytic activity of this non-specific phospholipase. Different sucrose viscosities were used to test the effects of solvent microviscosity on PC-PLC activity towards diC_6PC monomers. The results (Figure 4.14) showed that the activity of *L. monocytogenes* PC-PLC is independent of solvent viscosity. For comparison, the dashed

line shows the expected relationship of enzyme efficiency for a diffusion-controlled reaction. Therefore in the reaction of water-soluble substrate, product release is not the rate-limiting step. The viscosity values used in the study were taken from Iscotables, 7th edition.

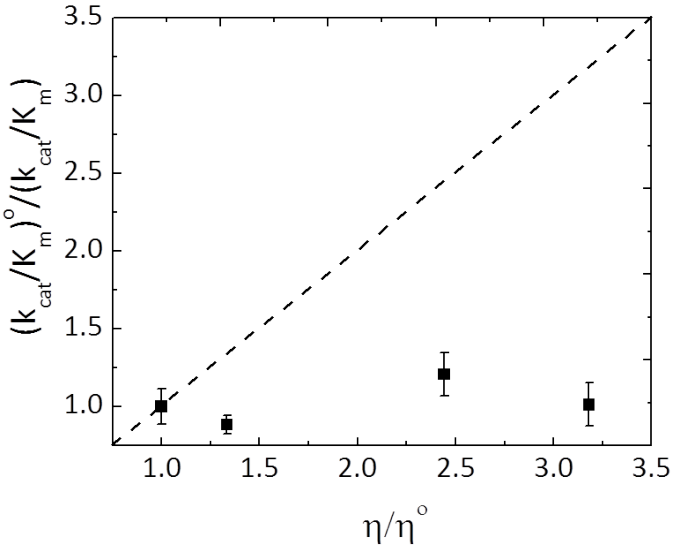

Figure 4.14 Plot of relative activity as function of relative viscosity of the assay solution. η is the viscosity of the sucrose added solution, η^o is the viscosity of the original solution, in the absence of sucrose. k_{cat}/K_m is the activity of PC-PLC on diC_6PC in the solution at pH 6, (K_{cat}/K_m) is the activity without sucrose.

4.10.2 Proton inventory effects

Solvent isotopic effects on PC-PLC activity were also tested. If proton transfer is involved in the rate-limiting step of the reaction, the content of D_2O in the solution should affect the reaction rate. Indeed, correlation was observed when D_2O was added to the reaction buffer, and the activity decreased proportionally with increasing D_2O mole fraction with a slope of -0.47 (R^2=0.90). The linear fit also indicates one (instead of multiple) proton is transferred during the rate-determining step [Kresge, 1964]. Both the solvent viscosity effect and isotopic effects of *L. monocytogenes* PC-PLC are consistent with those for PC-PLC$_{Bc}$ [Martin and Hergenrother, 1999], demonstrating the converging catalytic features of PC-PLC enzymes and in particular that one proton transfer in the

hydrolysis is rate-limiting. pD values in this study were determined by adding 0.4 to the reading of the pH meter (pD = pH + 0.4) [McKay and Wright, 1996].

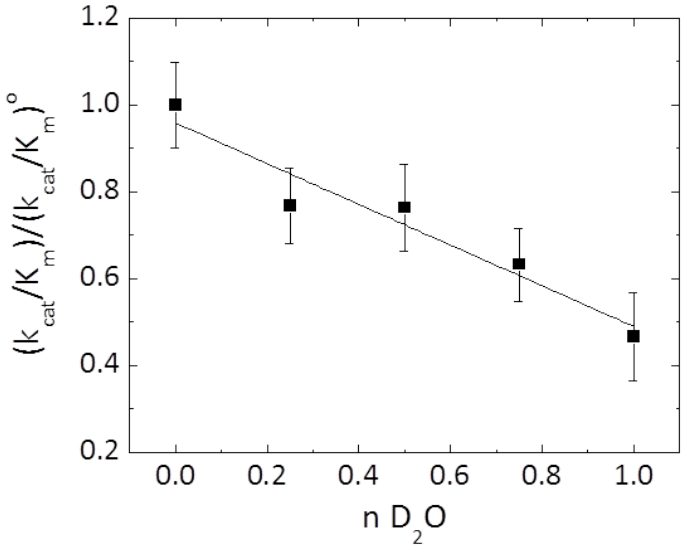

Figure 4.15 Plot of relative activity *vs* mole fraction of D_2O in the assay solution. n is the mole fraction of D_2O in the solution. k_{cat}/K_m is the enzymatic efficiency of PC-PLC towards monomeric diC_6PC at pH 6 $(k_{cat}/K_m)°$ is the activity without sucrose.

4.11 Discussion

L. monocytogenes PC-PLC is considered a virulence factor of that microorganism. While it has significant sequence homology and a structure that is likely similar to the PLC from *B. cereus*, it does have significant differences in activity and other behavior. The purified protein PC-PLC preferred more basic pH and concentrated salt for stability in the solution. From circular dichroism its secondary structure exhibited a largely α-helical content that was not sensitive to the presence of zinc ions. Even though pivotal for enzyme activity, zinc ions had little influence over the secondary structure of PC-PLC suggesting the protein folds well on its own without Zn^{2+}.

Zinc in proteins may be important for structural reasons but when in the active sites of metalloenzymes it is crucial for activity [McCall et al., 2000], as is the case for PC-PLC.

Based on the sequence alignment, the nonspecific PLC enzyme synthesized by *L. monocytogenes* should be similar to PLC_{Bc} and the N-terminal domain of α-toxin from *C. perfringins*. Both of them bind three zinc ions in the active site, of which the co-catalytic roles of the three zinc ions been well established [Hough et al., 1989; Neylor et al., 1998]. ICP-MS analysis in our study suggests that with the presence of 5 μM of zinc, PC-PLC contains 2.1 atoms of zinc/molecule. The result was less than the expected three atoms of zinc per protein. However, it was not entirely surprising. For both PLC_{Bc} and alpha-toxin from *C. perfringens*, prior to the solution of protein structures [Hough et al., 1989; Neylor et al., 1998], all assays (atomic absorption spectrometry, EXAFS, EPR, magnetic circular dichroism, and ion exchange) showed two zinc ions for each protein instead of three [Little and Otnaess, 1975; Little, 1981; Bicknell et al., 1986; Krug and Kent, 1984; Nagahama et al., 1997]. This discrepancy indicates that the third metal site might be only partially occupied in buffer with 5 μM Zn^{2+} but without substrate. From my experiment, the affinity of the three zinc ions for PC-PLC was estimated to be 54 nM ~ 60 μM when no substrate was present. The low affinity of the last zinc ion lends further support to the hypothesis that the last zinc is loosely bound in the absence of substrate. More importantly, what we see in comparing affinities measured by ICP-MS for Zn^{2+} binding to protein and the K_d extracted from enzymatic studies where monomeric substrate is present (at the same pH) strongly suggests that when the protein binds to substrate, binding of the third Zn^{2+} is facilitated.

One of the more intriguing kinetic results for this recombinant enzyme is its preference for an acidic pH. As a virulence factor PC-PLC is expressed, secreted, and activated upon the acidification of the environment [Marquis et al., 1997]. This is a

marked contrast to the preference of PLC_{Bc} for pH > 6. PLC_{Bc} maintains high activity at pH 8, where the activity of PC-PLC is fairly low. The difference might be expected as the two phospholipases are secreted by bacteria of different life styles. *L. monocytogenes* is an intracellular pathogen, whereas *B. cereus* is not. The PC-PLC, as a virulence factor of *L. monocytogenes*, works in phagosomes/endosomes, where the environmental pH progressively drops after vacuole formation. The activity of LLO, the major virulence factor of *L. monocytogenes*, has also been found with profound acidic pH optimum [Glomski et al., 2002]. Coordination of the two discrete activities, LLO and PC-PLC, to work under the same conditions would be a reasonable strategy to allow the bacterium to escape the vacuole and enter the cytosol.

Goldfine et al. [1993] reported PC-PLC, isolated from Listeria culture supernatant, exhibited a broad pH profile over from pH 5.5-8.0 with micellar substrates. However, it should be mentioned that the non-specific phospholipase C activity is sensitive to ions that are present in most of biochemical buffers (e.g., phosphate, Tris, acetate, and citrate) [Aakre and Little, 1982; Hansen et al., 1992; Hansen et al., 1993b; Goldfine et al., 1993]. When the activity was measured in low pHs, the buffering agent acetate might compromise the overall activity measured. MES was used to buffer acidic buffers in my study; that molecule has little to no effects on PC-PLC activity.

The preference of PC-PLC for acidic pH for optimal activity was consistent whether substrates were present as monomers, or in micelles vesicles, although it is much more pronounced for aggregated substrates. For diC_6PC mono-dispersed in solution optimal enzyme activity is observed at pH 6.5, where the specific activity is about 3-fold that measured at pH 7.5 (Figure 4.8 C). For long chain substrate POPC in either Triton X-100

micelles or in SUVs, PC-PLC was most active at pH 5. For the SUVs, the ratio of activity at acidic pH to that at neutral pH was as high as 10-fold (Figure 4.7). Nonetheless, the active site chemistry catalyzed by the enzyme is the same for all substrates. As observed with monomeric diC_6PC, k_{cat} exhibited little variation with pH (Figure 4.8 B). The most likely explanation for the activity towards vesicles exhibiting a pronounced acidic pH optimum lies in the substrate binding as in the case of diC_6PC. However, this is not bulk partitioning of the enzyme on vesicles (as measured by FCS), which is relatively pH-insensitive. The apparent K_d values with 50 mM Zn^{2+} showed little sensitivity to pH and had a moderately low value, 65-90 μM. Thus, under POPC vesicle assay conditions, the bulk of the protein is at least transiently partitioned onto the vesicle. However, most of these initial binding complexes are not catalytically productive when no excess Zn^{2+} is present. Therefore, even when the enzyme is already membrane associated, the successful entry of substrate into the enzyme active site from the two-dimensional membrane interface might still be challenging, and be affected by altering pH. An example of that was seen in a recent study that showed vesicle membrane fusion induced by low pH facilitated the enzymatic activity of PLC_{Bc} [Shimanouchi et al., 2013]. Of course we cannot exclude that when the protein is transiently anchored at a bilayer, product release (in this case, release of diacyglycerol into the membrane bilayer [El-Sayed and Roberts, 1985]) may be facilitated at acidic pH.

Even though lipid hydrolysis of PC-PLC occurred at the polar the head group, the acyl chain length had considerable effects on PC-PLC activity, at least for monomeric substrates. The effect was on K_m, the affinity for the substrate, rather than the turnover rate (k_{cat}). Similar effects were also found for PLC_{Bc} [Little, C., 1977; El-Sayed et al.,

1985]. This may represent a general way for the phospholipases to engage their amphiphilic substrates. Besides the direct contacts with the hydrophilic head group region [Hansen et al., 1993a], the potential hydrophobic interaction with the hydrocarbon chain of phospholipids from PC-PLC is also important for efficient substrate recognition. The micellar effects on PC-PLC activity lend further support for the hypothesis. When substrate was packed in aggregates, its diffusion into the enzyme active site was facilitated by hydrophobic interaction with enzyme when solvation of the alkyl fatty acids was prevented. Such hydrophobic interaction has also been found in the interfacial catalysis of phospholipase A_2 [Scott et al., 1990]. If one was to design an inhibitor for PC-PLC, the moieties extending out of enzyme active site should not be underestimated.

Selected mutations introduced into PC-PLC are consistent with a mechanism similar to that of PLC_{Bc}. Asp55 and Phe66 are two of the most critical residues for PLC_{Bc} activity [Martin and Hergenrother, 1998; Martin et al., 2000; Hansen et al., 1993a]. They are also extremely important for PC-PLC. The two cysteines of PC-PLC seemed to have no obvious roles in activity, where mutations did not cause catastrophe in catalysis. However, the redox ability of cysteines allows potential *in vivo* regulation, especially for Cys143 because it is close to the active site.

Chapter 5 Future Directions

5.1 Investigation into LLO cysteine glutathionylation

The conserved cysteine residue in domain 4 of LLO has been found to be glutathionylated *in vivo* (unpublished results from Portnoy Laboratory, University of California at Berkeley). Mutagenesis studies replacing Cys with Ala or Ser consistently found it was not essential for either hemolytic activity or virulence *in vivo* [Michel et al., 1990]. The fact that this Cys is not critical for CDC activity is interesting, as the Cys is preserved in most of the CDC member sequences. Thus, the finding of glutathionylation suggests the real function of the Cys has yet to be found.

To pursue this investigation, one should first establish the activity of glutathionylated LLO. Specifically, one can prepare glutathionylated LLO and test the activity of it *in vitro* through liposome leakage and hemolytic assay.

5.2 Crystallography of PC-PLC

Before my work, there was no recombinant *L. monocytogenes* PC-PLC. Furthermore, the purification of the enzyme from cultures of *L. monocytogenes* provided very little protein with modest purity. The expression system I used is capable of generating clean and active enzyme, potentially good enough for crystallization trials. One difficulty I experienced with this protein was the stability issue upon the addition of zinc. Zinc ions are critical for enzyme activity, however, they were no help in terms of stabilizing the protein. My hypothesis is that there might be other weak zinc binding sites on the surface of the protein and occupation of these sites would disrupt the normal distribution of

surface charge and end up destabilizing the protein. Therefore, before any crystallization attempts, the PC-PLC needs to be stabilized in the solution with a minimum of zinc.

One way to do that is to deliver zinc ions with a moderate metal binder. For example, researchers from the Drennan Laboratory at from MIT used a Zn-NTA (nitrilotriacetic acid) complex to avoid protein precipitation [Phillips, C. M., et al., 2008]. The complex has been tried on PC-PLC in my study. However, the affinity of NTA for zinc (K_d ~ 3.98×10^{-11} M [Dawson, R. M. C., et al., 1989]), which was not competitive against with the tightly bound Zn^{2+} in the metalloprotein NikR ($K_d < 10^{-12}$ M [Wang et al., 2004]) in the previous-mentioned study, was an issue for PC-PLC activity. Therefore the proper zinc-chelator candidate needs to be identified first.

Another issue of current preparation of PC-PLC is the low protein yield. About 1 mg of PC-PLC was purified from 1 L of culture media. To make adequate protein for crystallography there is a lot of space for improvement.

I think an essential issue lies in a tendency of PC-PLC to aggregate in the solution and the relatively long time needed for the purification process. Every protein is unique in the tendency and extent of misfolding or aggregation. Adding a fusion module could help prevent or slow down the aggregation process. The N-terminal intein tag used in current protocol is a relatively large (56 kDa) and fairly soluble on its own. There still might be better candidate to solubilize PC-PLC. As one example, maltose-binding protein (MBP) has been known to increase solubility and prevent aggregation of proteins of interest. However, after the affinity chromatography, intein, or any other fusion tag would usually be cleaved off PC-PLC. So the aid in solubility from fusion tag will be limited.

Formulation strategies could also be explored to further improve protein stability. In my work, salt concentration (1 M or 150 mM NaCl) and pH (pH 6.0 or 8.5) were briefly tested. To keep PC-PLC from aggregating, 1 M NaCl at pH 8.5 was optimal. Various additives, such as inorganic phosphate or other enzyme inhibitors might be used to help maintain PC-PLC in solution.

Mutagenesis might be anther approach. For example, the two cysteine mutants C143A and C168A exhibited no significant defects in enzymatic behavior in our model systems. Potentially a double mutant C143A/C168A could yield a non-thiol protein that has no covalent variants (-S-S- bonds). More importantly, the need for reducing agents, which can also form complexes with Zn^{2+}, would be abolished.

With protocols optimized for protein stability and preparation yield, crystallization of PC-PLC could occur with relative ease.

References

Aakre, S. E., and Little, C., (1982) Inhibition of *Bacillus cereus* phospholipase C by univalent cation. *Biochem. J.* 203, 799-801.

Alberti-Segui, C., Goeden, K. R., and Higgins, D. E., (2007) Differential function of *Listeria monocytogenes* listeriolysin O and phospholipases C in vacuolar dissolution following cell-to-cell spread. *Cell. Microbiol.* 9, 179-195.

Alouf, J. E., Billington, S. J., and Jost, B. H. (2005) Repertoire and general features of the family of cholesterol-dependent cytolysins, in The Comprehensive Sourcebook of Bacterial Protein Toxins (Alouf, J. E., and Popoff, M. R., Eds.) pp 643-658, Academic Press: Oxford, England.

Alving, C. R., Habig, W. H., Urban, K. A., and Hardegree, M. C., (1979) Cholesterol-dependent tetanolysin damage to liposomes. *Biochim. Biophys. Acta,* 551, 224-228.

Arnold K., Bordoli L., Kopp J., and Schwede T. (2006). The SWISS-MODEL Workspace: A web-based environment for protein structure homology modelling. *Bioinformatics 22,* 195-201.

Bavdek, A., Kostanjsek, R., Antonini, V., Lakey, J. H., Dalla Serra, M., Gilbert, R. J., and Anderluh, G. (2012) pH dependence of listeriolysin O aggregation and pore-forming ability. *FEBS J. 279,* 126-141.

Bayley, H. (1997) Toxin structure: part of a hole? *Curr. Biol.* 7, R763-R767.

Beauregard, K., Lee, K., Collier, R., Swanson, J., (1997) pH-dependent perforation of macrophage phagosomes by listeriolysin O from Listera monocytogenes, J. Exp. Med. 186, 1159-1163.

Bian, J. and Roberts, M.F. (1992) Thermodynamic comparison of lyso- and diacylphosphatidylcholines. *J. Colloid Interface Sci.* 153, 420–428.

Bicknell, R., Hanson, G. R., Holmquist, B., and Little, C. (1986) A Spectral Study of Cobalt(II)-Substituted *Bacillus cereus* Phospholipase C. *Biochemistry* 25, 4219−4233.

Birmingham, C. L., Canadien, V., Gouin, E., Troy, E. B., Yoshimori, T., Cossart, P., Higgins, D. E., Brumell, J. H., (2007) *Listeria monocytogenes* evades killing by autophagy during colonization of host cells. *Autophagy*, 3, 442-451.

Bitar, A. P., Cao, M., and Marquis, H., (2008) The metalloprotease of *Listera monocytogenes* is activated by intramolecular autocatalysis. *J. Bacteriol.* 190, 107-111.

Bourdeau, R. W., Malito, E., Chenal, A., Bishop, B. L., Musch, M. W., Villereal, M. L., Chang, E. B., Mosser, E. M., Rest, R. F. and Tang, W. J. (2009) Cellular functions and x-ray structure of anthrolysin O, a cholesterol-dependent cytolysin secreted by *Bacillus anthracis*. *J. Biol. Chem. 284,* 14645–14656.

Cabanes, D., Dehoux, P., Dussurget, O., Frangeul, L., and Cossart, P., (2002) Surface proteins and the pathogenic potential of *Listeria monocytogenes. Trends Microbiol*, 10, 238-245.

Cameron, L. A., Footer, M. J., van Qudenaarden, A., Theriot, J. A., (1999) Motility of ActA protein-coated microspheres driven by actin polymerization, Proc. Natl. Acad. Sci. USA, 96, 4908-4913.

Camilli, A., Goldfine, H., and Portnoy, D. A. (1991) *Listeria monocytogenes* mutants lacking phosphatidylinositol-specific phospholipase C are avirulent. *J. Exp. Med.* 173, 751-754.

Camilli, A., Tilney, L. G., and Portnoy D. A., (1993) Dual roles of plcA in *Listeria monocytogenes* pathogenesis. *Mol. Microbiol*. 8, 143-157.

Carrero J. A., Calderon, B., Unanue, E. R., (2004) Listeriolysin O from *Listeria monocytogenes* is a lymphocyte apoptogenic molecule. *J. Immunol.* 172, 4866-4874.

Carrero J. A., Vivanco-Cid H., and Unanue E. R. (2008) Granzymes Drive a Rapid Listeriolysin O-induced T Cell Apoptosis, *J Immunol. 181,* 1365–1374.

Chen, W., Goldfine, H., Ananthanarayanan, B., Cho, W., and Roberts, M. F., (2009) *Listeria monocytogenes* phosphatidylinositol-specific phospholipase C: kinetic activation and homing in on different interfaces, *Biochemistry*, 48, 3578-3592.

Chong, S., Williams, K.S., Wotkowicz, C., and Xu, M. Q. and Perler, F.B. (1999) Modulation of protein splicing of the *Saccharomyces cerevisiae* vacuolar membrane ATPase intein. *J. Biol. Chem.,* 273, 10567-10577.

Colombo, M. I., (2007) Autophagy: a pathogen driven process. *IUBMB Life,* 59, 238-242.

Cossart, P., Vincente, M. F., Mengaud, J., Baquero. F., Perez-Diaz, J. C., and Berche, P., (1989) Listeriolysin O is essential for virulence of *Listeria monocytogenes*: direct evidence obtained by gene complementation. *Infect. Immun.* 57, 3629-3636.

Cossart, P., Bierne, H., (2001) The use of host cell machinery in the pathogenesis of *Listeria monocytogenes, Curr. Opin. Immunol.* 13, 96-103.

Cowell, J. L., and Bernheimer, A. W., (1978) Role of cholesterol in the action of cereolysin on membranes. *Arch. Biochem. Biophys.* 190, 603-610.

Czajkowsky, D. M., Hotze, E. M., Shao, Z., and Tweten, R. K. (2004) Vertical collapse of a cytolysin prepore moves its transmembrane β-hairpins to the membrane. *EMBO J. 23,* 3206–3215.

Dancz, C. E., Haraga, A., Portnoy, D. A., and Higgins, D. E. (2002) Inducible control of virulence gene expression in Listeria monocytogenes: temporal requirement of listeriolysin O during intracellular infection. *J Bacteriol* 184, 5935-5945.

Dang, T. X., Hotze, E. M., Rouiller, I., Tweten, R. K., and Wilson-Kubalek, E. M. (2005) Prepore to pore transition of a cholesterol dependent cytolysin visualized by electron microscopy. *J. Struct. Biol. 150,* 100–108.

Dawson R. M. C., Elliot, D. C., Elliot, W. H., and Jones, K. M., (1989) Data for Biochemical Research, 3rd edit. Oxford University Press, New York.

Decatur, A. L., and Portnoy, D. A. (2000) A PEST-like sequence in listeriolysin O essential for *Listeria monocytogenes* pathogenicity. *Science* 290, 992-995.

Di Tommaso, P., Moretti, S., Xenarios, I., Orobitg, M., Montanyalo, A., Chang, J. M., Taly, J. F., Notredame, C., (2011) T-Coffee: a web server for the multiple sequence alignment of protein and RNA sequences using structural information and homology extension. Nucl. Acids Res. 39, W13-W17.

Duncan, J. L., and Schlegel. R., (1975) Effect of streptolysin O on erythrocyte membranes, liposomes, and lipid dispersions A protein-cholesterol interaction. *J. Cell Biol.* 67, 160-174.

El-Sayed, and Roberts, M. F., (1985) Charged detergents enhance the activity of phospholipase C (*Bacillus cereus*) towards micellar short-chain phosphatidylcholine. *Biochim. Biophys. Acta.* 831, 133-141.

El-Sayed, M. Y., DeBose, C. D., Coury, L. A., Roberts, M. F., (1985) Sensitivity of phospholipase C (Bacillus cereus) activity to phosphatidylcholine structural modifications. Biochim. Biophys. Acta. 837, 325-335.

Forster, B. M., Bitar, A. P., Slepkov, E. R., Kota, K. J., Sondermann, H., and Marquis, H., (2011) The metalloprotease of *Listeria monocytogenes* is regulated by pH. 193, 5090-5097.

Farranda, A. J., LaChapellea, S., Hotzea, E. M., Johnson, A. E., and Tweten R. K., (2010) Only two amino acids are essential for cytolytic toxin recognition of cholesterol at the membrane surface. *Proc. Natl. Acad. Sci. U. S. A.* 107, 4341-4346.

Feng, J., Wehbi, H., Roberts, M. F., (2002) Role of tryptophan residues in interfacial binding of phosphatidylinositol-specific phospholipase C. *J. Biol. Chem.* 277, 19867-19875.

Gasteiger E., Hoogland C., Gattiker A., Duvaud S., Wilkins M. R., Appel R. D., Bairoch A. (2005) Protein Identification and Analysis Tools on the ExPASy Server; (In) John M. Walker (ed): The Proteomics Protocols Handbook, Humana Press. pp. 571-607.

Geddi, M. M., Higgins, D. E., Tilney, L. G., and Portnoy, D. A. (2000) Role of listeriolysin O in cell-to-cell spread of Listeria monocytogenes. *Infect Immun* 68, 999-1003.

Geoffroy, C., Gaillard, J. L., Alouf, J. E., and Berche, P., (1987) Purification, characterization, and toxicity of the sulfhydryl-activated hemolysin listeriolysin O from *Listeria monocytogenes*. *Infect. Immun.* 55, 1641-1646.

Geoffroy, C., Raveneau, J., Beretti, J., Lecroisey, A., Vazquez-Boland, J., Alouf, J. E., and Berche, P., (1991) Purification and characterization of an extracellular 29-kilodalton phospholipase C from *Listeria monocytogenes*. *Infect. Immun.* 59, 2382-2388.

Giddings, K. S., Johnson, A. E., and Tweten, R. K. (2003) Redefining cholesterol's role in the mechanism of the cholesterol-dependent cytolysins. *Proc. Natl. Acad. Sci. U. S. A.* 100, 11315–11320.

Giddings, K. S., Zhao, J., Sims, P. J., and Tweten, R. K. (2004) Human CD59 is a receptor for the cholesterol-dependent cytolysin intermedilysin. *Nat. Struct. Mol. Biol.* 11, 1173–1178.

Giddings, K. S., Johnson, A. E., and Tweten, R. K. (2005) Perfringolysin O and intermedilysin: Mechanisms of pore formation by the cholesterol-dependent cytolysins, in *The Comprehensive Sourcebook of Bacterial Protein Toxins* (Alouf, J. E., and Popoff, M. R., Eds.), Academic Press, Oxford, England, pp. 671-679.

Gilbert, R. J., (2005) Inactivation and activity of cholesterol-dependent cytolysins: what structural studies tell us, Structure 13, 1097-1106.

Gilmore, M. S., Cruz-Rodz, A. L., Leimester-Wachter, M., Kreft, J., and Goebel, W., (1989) A *Bacillus cereus* cytolytic determinant, cereolysin AB, which comprises the phospholipase C and sphingomyelinase genes: nucleotide sequence and genetic linkage. *J. Bacteriol*. 171, 744-753.

Glomski, I. J., Geddi, M. M., Tsang, A. W., Swanson, J. A., and Portnoy, D. A., (2002) The *listeria monocytogenes* hemolysin has an acidic pH optimum to compartmentalize activity and prevent damage to infected host cells. *J Cell Biol* 6, 1029-1038.

Goldfine H., Johnston N. C., and Knob C. (1993) Nonspecific phospholipaseC of *Listeria monocytogenes*: activity on phospholipids in Triton X-100-mixed micelles and in biological membranes. *J. Bacteriol.,* 175, 4298-4306.

Goldstein, R., Cheng, J., Stec, B., Roberts, M. F., (2012) Structure of the S. aureus PI-specific phospholipase C reveals modulation of active site access by a titratable π-cation latched loop. *Biochemistry*, 51, 2579-2587.

Gründling A., Gonzalez, M. D., Higgins, D. E., (2003) Requirement of the *Listeria monocytogenes* broad-range phospholipase PC-PLC during infection of human epithelial cells. *J. Bacteriol.* 185, 6295-6307.

Hadders, M. A., Beringer D. X., and Gros, P. (2007) Structure of C8a-MACPF Reveals Mechanism of Membrane Attack in Complement Immune Defense. *Science 317,* 1552-1554.

Hansen, S., Hansen, L. K., Hough. E., (1992) Crystal structures of phosphate, iodide and iodate-inhibited phospholipase C from *Bacillus cereus* and structural investigations of the binding of reaction products and a substrate analogue. *J. Mol. Biol.* 225, 543-549.

Hansen, S., Hough, E., Svensson, L. A., Wong, Y. L., Martin, S. F., (1993a) Crystal structure of phospholipase C from *Bacillus cereus* complexed with a substrate analog. *J. Mol. Biol.* 234, 179-187.

Hansen, S., Hansen, L. K., and Hough, E., (1993b) The crystal structure of tris-inhibited phospholipase C from Bacillus cereus at 1.9 Å resolution; nature of the metal ion in site 2. *J. Mol. Biol.* 231, 870-876.

Hase, C. C., and Finkelstein, R. A., (1993) Bacterial extracellular zinc-containing metalloproteases. *Microbiol. Rev.* 57, 823-837.

Henry, R., Shaughnessy, L., Loessner, M. J., Alberti-Segui, C., Higgins, D. E., Swanson, J. A., (2006) Cytolysin-dependent delay of vacuole maturation in macrophages infected with *Listeria monocytogenes, Cell. Microbiol.* 8, 107-119.

Hergenrother, P. J., Martin, S. F., (1997) Determination of the kinetic parameters for phospholipase C (*Bacillus cereus*) on different phospholipid substrates using a chromogenic assay based on the quantitation of inorganic Phosphate. *Anal. Biochem.,* 251, 45-49.

Hergenrother, P. J., Martin, S. F., (2001) Phosphatidylcholine-preferring phospholipase C from *B. cereus*. function, structure, and mechanism. *Top. Curr. Chem.*, 211, 131-167.

Hermanson, G., (1996) *Bioconjugate Techniques*, Academic Press.

Heuck, A. P., Hotze, E., Tweten, R. K., and Johnson, A. E., (2000) Mechanism of membrane insertion of a multimeric β-barrel protein: perfringolysin O creates a pore using ordered and coupled conformational changes. *Mol. Cell*, 6, 1233-1242.

Hough, E., Hansen, L. K., Birknes, B., Jynge, K., Hansen, S., Hordvik, A., Little, C., Dodson, E., and Derewenda, Z., (1989), High-resolution (1.5 Å) crystal structure of phospholipase C from *Bacillus cereus*, *Nature*, 338, 357-360.

Howard, J. G., Wallace, K. R., and Wright, G. P., (1953) The inhibitory effects of cholesterol and related sterols on haemolysis by streptolysin. *Br. J. Exp. Pathol.* 34, 174-180.

Iwamoto, M., Ohno-Iwashita, Y., and Ando, S. (1987) Role of the essential thiol group in the thiol-activated cytolysin from Clostridium perfringens. *Eur. J. Biochem.* 167, 425-430.

Johansen, T., Holm, T., Guddal, P. H., Sletten, K., Hougli, F. B., and Little, C., (1988) Cloning and sequencing of the gene encoding the phsophatidylcholine-preferring phospholipase C from *Bacillus cereus. Gene* 65, 293-304.

Johnson, M. K., Geoffroy, C., and Alouf, J. E., (1980) Binding of cholesterol by sulfhydryl-activated cytolysins. *Infect. Immun.* 27, 97-101.

Jones, S., and Portnoy, D. A., (1994) Characterization of *Listeria monocytogenes* pathogenesis in a strain expressing perfringolysin O in place of listeriolysin O. *Infect. Immun.* 62, 5608-5613.

Kayal, S. and Charbit, A., (2006) Listeriolysin O: a key protein of *Listeria monocytogenes* with multiple functions, *FEMS Microbiol Rev*, 30, 514-529.

Kresge A. J., (1964) Solvent isotope effect in H_2O-D_2O mixtures. *Pure Appl. Chem.,* 8, 243-258.

Lang, P. A, Schenck, M., Nicolay, J. P., Becker, J. U., Kempe, D. S., Lupescu, A., Koka, S., Eisele, K., Klarl, B. A., Rubben, H., Schmid, K. W., Mann, K., Hildenbrand, S., Hefter, H., Huber, S. M., Wieder, T., Erhardt, A., Haussinger, D., Gulbins, E., and Lang, F. (2007) Liver cell death and anemia in Wilson disease involve acid sphingomyelinase and ceramide. *Nat. Med*. *13,* 164-170.

Lanzetta, P. A., Alvarez, L. J., Reinach, P. S., Candia, O. A., (1979) An improved assay for nanomole amounts of inorganic phosphate. *Anal. Biochem.* 100, 95-97.

Leimeister-Wachter, M., Domann, E., and Chakraborty, T., (1991) Detection of a gene encoding a phosphatidylinositol-specific phospholipase C that is coordinately expressed with listeriolysin in *Listeria monocytogenes. Mol. Microbiol*. 5, 361-366.

Lety, M.-A., Frehel, C., Dubail, I., Beretti, J.-L., Kayal, S., Berche, P., and Charbit, A., (2001) Identification of a PEST-like motif in listeriolysin O required for phagosomal escape and for virulence in *Listeria monocytogenes. Mol. Microbiol.* 39, 1124–1139.

Levine, B., Kroemer, G., (2008) Autophagy in the pathogenesis of disease, *Cell*, 132, 27-42.

Little, C. and Otnaess, A.-B. (1975) Metal ion dependence of phospholipase C from *Bacillus cereus, Biochim. biophys. Acta.* 391, 326−333.

Little, C., (1977) Phospholipase C from *Bacillus cereus*. Action on some artificial lecithins. *Acta. Chem. Scand*. B31, 267-272.

Little, C. (1981) Effect of some divalent metal cations on phospholipase C from *Bacillus cereus. Acta chem. scand.* B35, 39−44.

Ma, B., Tsai, C. J., Haliloğlu, T., and Nussinov, R. (2011) Dynamic allostery: linkers are not merely flexible. *Structure 19*, 907–917

Magde D., Elson E. L., and Webb W. W. (1974) Fluorescence correlation spectroscopy II. An experimental realization, *Biopolymers 13,* 29–61.

Marquis, H., Doshi, V., and Portnoy, D. A., (1995) The broad-range phospholipase C and a metalloprotease mediate listeriolysin O-independent escape of *Listeria*

monocytogenes from a primary vacuole in human epithelial cells. *Infect. Immun.* 63, 4531-4534.

Marquis, H., Goldfine, H., and Portnoy, D. A., (1997) Proteolytic pathways of activation and degradation of a bacterial phospholipase C during intracellular infection by *Listeria monocytogenes. J. Cell Biol.* 137, 1381-1392.

Martin S. F., Hergenrither P. J. (1998) General base catalysis by the phosphatidylcholine-preferring phospholipase C from *Bacillus cereus*: the role of Glu4 and Asp55. *Biochemistry*, 37, 5755-5760.

Martin S. F., Hergenrither P. J. (1999) Catalytic Cycle of the Phosphatidylcholine-Preferring Phospholipase C from *Bacillus cereus*. Solvent Viscosity, Deuterium Isotope Effects, and Proton Inventory Studies. *Biochemistry*, 38, 4403-4408.

Martin S. F. Follows B. C., Hergenrother P. J., Trotter B. K., (2000) The choline binding site of phospholipase C (*Bacillus cereus*): insights into substrate specificity. *Biochemistry*, 39, 3410-3415.

McCall, K. A., Huang, C. C., and Fierke, C. A., (2000) Function and mechanism of zinc metalloenzymes. *J. Nutr.* 130, 1437S-1446S.

McKay, G. A., Wright, G. D., (1996) Catalytic mechanism of enterococcal kanamycin kinase (APH(3')-IIIa): viscosity, thio, and solvent isotope effects support a Theorell-Chance mechanism. *Biochemistry*, 35, 8680-8685.

Mengaud, J., Vicente, M. F., Chenevert, J., Moniz Pereira, J., Geoffroy, C., Gicquel-Sanzey, B., Baquero, F., Perez-Diaz, J. C., and Cossart, P., (1988) Expression in *Escherichia coli* and sequence analysis of the listeriolysin O determinant of *Listeria monocytogenes. Infect. Immun.* 56, 766-772.

Mengaud, J., Braun-Breton, C., and Cossart, P., (1991) Identification of a phosphatidylinositol-specific phospholipase C in *Listeria monocytogenes*: a novel type of virulence factor? *Mol. Microbiol.* 5, 367-372.

Mengaud, J., Geoffroy, C., and Cossart, P., (1991a) Identification of a new operon involved in *Listeria monocytogenes* virulence: its first gene encodes a protein homolyogous to bacterial metalloproteases. *Infect. Immun.* 59, 1043-1049.

Meyer-Morse, N., Robbins, J. R., Rae, C. S., Mochegova, S. N., Swanson, M. S., Zhao, Z., Virgin, H. W., Portnoy D. A., (2010) Listeriolysin O is necessary and sufficient to induce autophagy during *Listeria monocytogenes* infection, *PLos One*, 5, e8610.

Michel, E., Reich, K. A., Favier, R., Berche, P., and Cossart. P., (1990) Attenuated mutants of the intracellular bacterium Listeria monocytogenes obtained by single amino acid substitutions in listeriolysin O. *Mol. Microbiol.* 4, 3609–3619.

Milohanic E., Glaser, P., Coppee, J. Y., Frangeul, L., Vega, Y., Vazquez-Boland, J. A., Kunst, F., Cossart, P., Buchrieser, C., (2003) Transcriptome analysis of *Listeria monocytogenes* identifies three groups of genes differently regulated by PrfA. *Mol Microbiol,* 47, 1613-1625.

Mizushima, N., Ohsumi, Y., Yoshimori, T., (2002) Autophagosome formation in mammalian cells. *Cell Struct. Funct*. 27, 421-429.

Moser, J., Gerstel, B., Meyer, J. E. W., Chakraborty, T., Wehland, J., Heinz, D. W., (1997) Crystal structure of the phosphatidylinositol-specific phospholipase C from the human pathogen *Listeria monocytogenes. J. Mol. Biol*. 273, 269-282.

Nakamura, M., Sekino-Suzuki, N., Mitsui, K., and Ohino-Iwashita. (1998) Contribution of tryptophan residues to the structural changes in Perfringolysin O during interaction with liposomal membranes. *J. Biochem. 123*, 1145- 1155.

Nakamura, M., Kondo, H., Shimada, Y., Waheed, A. A., and Ohno-Iwashita, Y., (2003) Cellular aging-dependent decrease in cholesterol in membrane microdomains of human diploid fibroblasts. *Exp. Cell Res.* 290, 381-390.

Nomura, T., Kawamura, I., Kohda, C., Baba, H., Ito, Y., Kimto, T., Watanabe, I., Mitsuyama, M., (2007) Irreversible loss of membrane-binding activity of Listeria-derived cytolysins in non-acidic conditions: a distinct difference from allied cytolysins produced by other Gram-positive bacteria. *Microbiol*. 153, 2250-2258.

Ohno-Iwashita, Y., Iwamoto, M., Ando, S., and Iwashita, S., (1992) Effect of lipidic factors on membrane cholesterol topology-mode of binding of theta-toxin to cholesterol in liposomes. *Biochim. Biophys. Acta,* 1109, 81-90.

Olofsson, A., Hebert, H., and Thelestam, M. (1993) The projection structure of perfringolysin O (*Clostridium perfringens* θ-toxin). *FEBS Lett. 319,* 125–127.

O'Neil, H. S., Forster, B. M., Roberts, K. L., Chambers, A. J., Bitar, and Marquis, H., (2009), The propeptide of the metalloprotease of *Listeria monocytogenes* controls compartmentalization of the zymogen during intracellular infection, *J. Bacteriol.* 191, 3594-3603.

Ortega, A., Amoros, D., and de la Torre, J. G. (2011) Prediction of hydrodynamic and other solution properties of rigid proteins from atomic- and residue-level models. *Biophys. J. 101,* 892-898.

Orvedahl, A., Lavine, B., (2009) Eating the enemy within: autophagy in infectious diseases. *Cell Death Differ.* 16, 57-69.

Palmer, M. (2004) Cholesterol and the activity of bacterial toxins. *FEMS Microbiol. Lett.* 238, 281–289.

Perez-Iratxeta, C., Andrade-Navarro, M. A., (2008), K2D2: Estimation of protein secondary structure from circular dichroism spectra, *BMC struct. Biol.,* 8, 25.

Pinkney, M., Beachey, E., and Kehoe, M., (1989) The thiol-activated toxin streptolysin O does not require a thiol group for cytolytic activity. *Infect. Immun.* 57, 2553–2558.

Polekhina, G., Giddings, K. S., Tweten, R. K. and Parker, M. W. (2005) Insights into the action of the superfamily of cholesterol-dependent cytolysins from studies of intermedilysin. *Proc. Natl. Acad. Sci. USA, 102,* 600–605.

Portnoy, D. A., Jacks, P. S., and Hinrichs, D. J., (1988) Role of hemolysin for the intracellular growth of Listeria monocytogenes. *J Exp Med* 167, 1459-1471.

Portnoy, D. A., Tweten, R. K., Kehoe, M., and Bielecki. J., (1992) Capacity of listeriolysin O, streptolysin O, and perfringolysin O to mediate growth of *Bacillus subtilis* within mammalian cells. *Infect. Immun*. 60, 2710-2717.

Poyart, C., Abachin, E., Razafimanantsoa, I., and Berche, P., (1993) The zinc metalloprotease of *Listeria monocytogenes* is required for maturation of phosphatidylcholine phospholipase C: direct evidience obtained by gene complementation. *Infect. Immun.* 61, 1576-1580.

Pu M., Roberts M. F., and Gershenson A. (2009) Fluorescence correlation spectroscopy of phosphatidylinositol-specific phospholipase C monitors the interplay of substrate and activator binding sites. *Biochemistry 48,* 6835–6845.

Pu M., Fang X., Redfield A. G., Gershenson A., and Roberts M. F. *(*2009*)* Correlation of vesicle binding and phospholipid dynamics with phospholipase C activity. Insights into phosphatidylcholine activation and surface dilution inhibition. *J. Biol. Chem. 284,* 16099–16107.

Py, B. F., Lipinski, M. M. Yuan, J., (2007) Autophagy limits Listeria monocytogenes intracellular growth in the early phase of primary infection. Autophagy, 3, 117-125.

Qian, X., Zhou, C., and Roberts, M. F. (1998) Phosphatidylcholine activation of bacterial phosphatidylinositiol phospholipase C toward PI vesicles. Biochemistry 37, 6513-6522.

Ramachandran, R., Heuck, A. P., Tweten, R. K., and Johnson, A.E. (2002) Structural insights into the membrane-anchoring mechanism of a cholesterol-dependent cytolysin. *Nat. Struct. Mol. Biol.* 9, 823–827.

Ramachandran, R., Tweten, R. K., and Johnson, A. E. (2004) Membrane-dependent conformational changes initiate cholesterol dependent cytolysin oligomerization and intersubunit beta-strand alignment. *Nat. Struct. Mol. Biol.* 11, 697–705.

Raveneau, J., Geoffroy, C., Beretti, J. L. Gaillard, J. L., Alouf, J. E., Berche, P., (1992) Reduced virulence of a *Listeria monocytogenes* phospholipase deficient mutant obtained by transposon insertion into the zinc metalloprotease gene. *Infect. Immun.* 60, 916-921.

Rich, K. A., Burkett, C., Webster, P., (2003) Cytoplasmic bacteria can be targets for autophagy. *Cell Microbiol.,* 5, 455-468.

Rosado C. J., Kondos S., Bull T. E., Kuiper M. J., Law R. H. P., Buckle A. M., Voskoboinik I., Bird P. I., Trapani J. A., Whisstock J. C., and Dunstone M. A. (2008) The MACPF/CDC family of pore-forming toxins, *Cell. Microbiol. 10,* 1765–1774.

Rosenqvist, E., Michaelsen, T. E., and Vistnes, A. I., (1980) Effect of streptolysinO and digitonin on egg lecithin/cholesterol vesicles. *Biochim. Biophys. Acta,* 600, 91-102.

Rossjohn, J., Feil, S. C., Mckinstry, W. J., Tweten, R. K. and Parker, M. W. (1997) Structure of a cholesterol-binding, thiol-activated cytolysin and a model of its membrane form. *Cell, 89,* 685–692.

Rossjohn, J., Polekhina, G., Feil, S. C., Morton, C. J., Tweten, R. K., and Parker, M. W. (2007) Structures of perfringolysin O suggest a pathway for activation of cholesterol-dependent cytolysins. *J. Mol. Biol.* 367, 1227–1236.

Rottem, S., Cole, R. M., Habig, W. H., Barile, M. F., and Hardegree, M. C., (1982) Structural characteristics of tetanolysin and its binding to lipid vesicles. *J. Bacteriol.* 152, 888-892.

Saunders, F. K., Mitchell, T. J., Walker, J. A., Andrew, P. W., and Boulnois, G. J., (1989) Pneumolysin, the thiol-activated toxin of *Streptococcus pneumoniae*, does not require a thiol group for in vitro activity. *Infect. Immun.* 57, 2547–2552.

Scott, D. L., White, S. P., Otwinowski, Z., Yuan, W., Gelb, M. H., and Sigler, P. B., (1990) Interfacial catalysis: the mechanism of Phospholipase A_2. *Science*, 250, 1541-1546.

Schnupf, P., and Portnoy, D. A., (2007) Listeriolysin O: a phagosome-specific lysine, Microbes Infect, 9, 1176-1187.

Schuerch, D. W., Wilson-Kubalek, E. M., and Tweten, R. K., (2005) Molecular basis of listeriolysin O pH dependence. *Proc. Natl. Acad. Sci. USA*, 102, 12537-12542.

Shany, S., Bernheimer, A. W., Grushoff, P. S., and Kim, K. S., (1974) Evidence for membrane cholesterol as the common binding site for cereolysin, streptolysin O and saponin. *Mol. Cell. Biochem.* 3, 179-186.

Shimada, Y., Maruya, M., Iwashita, S., and Ohno-Iwashita, Y., (2002) The C-terminal domain of perfringolysinO is an essential cholesterol-binding unit targeting to cholesterol-rich microdomains. Eur. J. Biochem., 269, 6195-6203.

Shimanouchi, T., Kawasaki, H., Fuse, M., Umakoshi, H., and Kuboi, R., (2013) Membrane fusion mediated by phospholipase C under endosomal pH conditions. Colloids Surf. B. 103, 75-83.

Simons, K., and Ehehalt, R., (2002) Cholesterol, lipid rafts, and disease. J. Clin. Invest. 110, 597-603.

Smith, G. A., Marquis, H., Jones, S., Johnston, N. C., Portnoy, D. A., and Goldfine, H., (1995) The two distinct phospholipases C of *Listeria monocytogenes* have overlapping roles in escape from a vacuole and cell-to-cell spread. *Infect. Immun.* 63, 4231-4237.

Smyth, J., and Duncan, J. L., (1978) Thiol-activated (oxygen labile) cytolysins, p. 129–183. In J. Jeljaszewicz and T. Wadstro¨m (ed.), Bacterial toxins and cell membranes. Academic Press Ltd., London, England.

Soltani, C. E., Hotze, E. M., Johnson, A. E., and Tweten, R. K. (2007a) Specific protein-membrane contacts are required for prepore and pore assembly by a cholesterol-dependent cytolysin. *J. Biol. Chem.* 282, 15709–15716.

Soltani, C. E., Hotze, E. M., Johnson, A. E., and Tweten, R. K. (2007b) Structural elements of the cholesterol-dependent cytolysins that are responsible for their cholesterol-sensitive membrane interactions. *Proc. Natl. Acad. Sci. U. S. A.* 104, 20226–20231.

Stewart, J. C. (1980) Colorimetric determination of phospholipids with ammonium ferrothiocyanate. *Anal. Biochem. 104,* 10-14.

Swanson, M. S., (2006) Autophagy: eating for good health. *J. Immunol.* 177, 4945-4951.

Tan, C. A., Roberts, M. F., (1996) Vanadate is a potent competitive inhibitor of phospholipase C from *Bacillus cereus*. *Biochim. Biophys. Acta*, 1298, 58-68.

Thompson, J. R., Cronin, B., Bayley, H., and Wallace,M. I. (2011) Rapid assembly of a multimeric membrane protein pore. *Biophys. J. 101,* 2679–2683.

Tilley, S. J., Orlova, E. V., Gilbert, R. J., Andrew, P. W., and Saibil, H. R. (2005) Structural basis of pore formation by the bacterial toxin pneumolysin. *Cell 121,* 247–256.

Tilney, L. G., Portnoy, D. A., (1989) Actin filaments and the growth, movement, and spread of the intracellular bacterial parasite, *Listeria monocytogenes, J. Cell Biol.* 109, 1597-1608.

Titball, R. W., Hunter, S. E., Martin, K. L., Morris, B. C., Shuttleworth, A. D., Rubidge, T., Anderson, D. W., Kelly, D. C., (1989) Molecular cloning and nucleotide sequence of the alpha-toxin (phospholipase C) of *Clostridium perfringens*. *Infect. Immun*. 57, 367-376.

Titball, R. W., Naylor C. E., Basak, A. K., (1999) The *Clostridium perfringens* α-toxin, *Anaerobe*, 5, 51-64.

Titball, R. W., (1993) Bacterial phospholipase C. *Microbiol. Rev.* 57, 347-366.

Traikia, M., Warschawski, D. E., Lambert, O., Rigaud, J. L., and Devaux, P. F., (2002) Asymmetrical membranes and surface tension. *Biophys. J.* 83, 1443-1454.

Tweten, R. K., Parker, M. W., Johnson, A. E., (2001) The cholesterol-dependent cytolysins. *Curr. Top. Microbiol. Immunol.* 257, 15-33.

Umashankar, M., Sanchez San Martin, C., Liao, M., Reilly, B., Guo, A., Taylor, G., and Kielian, M. (2008) Differential cholesterol binding by class II fusion proteins determines membrane fusion properties. *J. Virol.* 82, 9245–9253.

Vamparys, L., Gautier, R., Vanni, S., Drew Bennett, W. F., Peter Tieleman, D., Antonny, B., Etchebest, C., and Fuchs, P. F. J., (2013) Conical lipids in flat bilayers induce packing defects similar to that induced by positive curvature, *Biophys. J.,* 104, 585-593.

van Engeland, M., Nieland, L.J., Ramaekers, F.C, Schutte, B., and. Reutelingsperger, C.P. (1998) Annexin V-affinity assay: a review on an apoptosis detection system based on phosphatidylserine exposure. *Cytometry 31,* 1-9.

Vazquez-Boland, J., Kocks, C., Dramsi, S., Ohayon, H., Geoffroy, C., Mengaud, J., and Cossart, P., (1992) Nucleotide sequence of the lecithinase operon of *Listeria monocytogenes* and possible role of lecithinase in cell-to-cell spread. *Infect. Immun.*, 60, 219-230.

Vazquez-Boland, J. A., Kuhn, M., Berche, P., Chakraborty, T., Dominquez-Bernal, G., Goebel, W., Gonzalez-Zorn, B., Wehland, J., and Kreft, J., (2001) *Listeria* pathogenesis and molecular virulence determinants. *Clin, Microbiol. Rev.* 14, 584-640.

Waheed, A. A., Shimada, Y., Heijnen. H. F., Nakamura, M., Inomata, M., Hayashi, M., Iwashita, S., Slot, J. W., and Ohno-Iwashita, Y., (2001) Selective binding of perfringolysin O derivative to cholesterol-rich membrane microdomains (rafts). Proc. Natl. Acad. Sci. USA, 98, 4926-4931.

Wang, S. C., Dias, A. V., Bloom, S. L., and Zamble, D. B., (2004) Selectivity of metal binding and metal-induced stability of *Escherichia coli* NikR, *Biochemistry*, 43, 10018-10028.

Yeung, P. S., Zagorski, N., Marquis, H., (2005) The metalloprotease of *Listeria monocytogenes* controls cell wall translocation of the broad-range phospholipase C. *J. Bacteriol.* 187. 2601-1608.

Zhou, C., Qian, X., and Roberts M. F. (1997) Allosteric activation of phosphatidylinositol specific phospholipase C: specific phospholipid binding anchors the enzyme to the interface. Biochemistry 36, 10089-10097.

Ziegler, U., and Groscurth, P. (2004) Morphological features of cell death. News Physiol. Sci. 19, 124-128.